JGR Solid Earth

FEATURE ARTICLE
10.1029/2018JB016463

GRAND CHALLENGES
CENTENNIAL COLLECTION
AGU100 ADVANCING EARTH AND SPACE SCIENCE

The Nature of the Lithosphere-Asthenosphere Boundary

Catherine A. Rychert[1], Nicholas Harmon[1], Steven Constable[2], and Shunguo Wang[2]

[1]Ocean and Earth Science, University of Southampton, National Oceanography Centre, Southampton, UK, [2]Institute of Geophysics and Planetary Physics, Scripps Institution of Oceanography, University of California, San Diego, La Jolla, CA, USA

Abstract Plate tectonic theory was developed 50 years ago and underpins most of our understanding of Earth's evolution. The theory explains observations of magnetic lineations on the seafloor, linear volcanic island chains, large transform fault systems, and deep earthquakes near deep sea trenches. These features occur through a system of moving plates at the surface of the Earth, which are the surface expression of mantle convection. The plate consists of the chemically distinct crust and some amount of rigid mantle, which move over a weaker mantle beneath. However, exactly where the transition between stronger and weaker mantle occurs and what determines and defines the plate are still debated. In the classic definition the plate is defined thermally, by the geotherm-adiabat intersection, where the plate is the conductively cooling part of the mantle convection system. Many observations such as heat flow, seafloor bathymetry, seismic imaging, and magnetotelluric (MT) imaging are consistent with general lithospheric thickening with age, which suggests that temperature is an important factor in determining lithospheric thickness. However, while age averages give a good indication of overall properties, the range of lithospheric thicknesses reported is large for any given tectonic age interval, suggesting greater complexity. A number of observations including sharp discontinuities from teleseismic scattered waves and active source reflections and also strong anomalies from surface and body wave tomography and MT imaging cannot be explained by a purely thermal model. Another property or process is required to explain the anomalies and sharpen the boundary. Many subsolidus models have been proposed, although none can universally explain the variety of independent global observations. Alternatively, a small amount of partial melt can easily satisfy a range of observations. The presence of melt could also weaken the mantle over geologic timescales, and it would therefore define the lithosphere-asthenosphere boundary (LAB). The location of melt is important to mantle dynamics and the LAB, although exactly where and exactly how much melt exists in the mantle are debated. Asthenospheric melt interpretations include a variety of forms: in small or large melt triangles beneath spreading ridges, in channels, in layers, along a permeability boundary leading to the ridge, at a depth of neutral buoyancy, punctuated, or pervasively over broad areas and either sharply or gradually falling off with depth. This variability in melt character or geometry may explain the previously described variability in LAB depths. The LAB is likely highly variable laterally as are the locations, forms, and amounts of melt, and the LAB is likely dynamic, dictated by small-scale convection and the dynamics of melt generation and migration. A melt-defined, dynamic LAB and a weak asthenosphere have broad implications for our understanding of Earth systems and planetary habitability. A weak asthenosphere caused by volatiles or melt could enable plate tectonic style convection, allow multiple scales of convection, and dictate the driving forces of the system. A better understanding of plate tectonics has broad implications for life on Earth. These include mitigating natural disasters caused by plate motions including volcanoes, earthquakes, and tsunamis. In addition, uplift and subsidence of the tectonic plates affects the sea level, impacting the level of the paleo-oceans and potentially affecting climate change estimates through geologic time. Finally, plate tectonic processes shape the surface morphology of the planet, making continents that enable our existence on land and the ocean basins that hold our free-surface water. Remarkably, despite large amounts of material transfer into and out of the mantle, and multiple scales of convection, plate tectonics has maintained a hydrosphere over billions of years that is favorable for life.

Plain Language Summary Plate tectonic theory is the framework that describes everything from the formation of the continents billions of years ago to natural disasters such as volcanoes, earthquakes, and tsunamis today. Even climate change estimates over geologic timescales rely on accurate plate tectonic reconstructions to understand the paleo-oceans. Despite the intricate links between plate tectonics and life on Earth, exactly what makes a plate “plate-like” is debated. In other words, what properties define the

Key Points:
- Temperature determines the LAB depth to first order, but the LAB is laterally variable in depth and possibly also in character
- Sharp discontinuities overlying strong seismic and magnetotelluric anomalies suggest a melt-defined LAB, at least in many locations
- The LAB is dynamic and dictated by mantle dynamics including melt generation and migration with broad implications for Earth's evolution

Correspondence to:
C. A. Rychert,
c.rychert@soton.ac.uk

Citation:
Rychert, C. A., Harmon, N., Constable, S., & Wang, S. (2020). The nature of the lithosphere-asthenosphere boundary. *Journal of Geophysical Research: Solid Earth*, *125*, e2018JB016463. https://doi.org/10.1029/2018JB016463

Received 4 NOV 2019
Accepted 10 SEP 2020
Accepted article online 15 SEP 2020

transition from the rigid plate, or lithosphere, to the weaker, convecting asthenosphere, and where does this transition occur? Classically, the lithosphere-asthenosphere boundary is defined thermally, with a gradual transition from the cold conductively cooling lithosphere to the warmer, convecting asthenosphere beneath. Overall, lithospheric thickening with age is observed beneath the oceans and toward the continental interiors suggesting that temperature and conductive cooling play a first-order role in controlling lithospheric thickness. However, within any given tectonic age interval a wide range of lithospheric thicknesses have been reported. Observations of sharp changes with depth in seismic wave speed and strong anomalies in seismic wave speed and electrical resistivity are similarly inconsistent with the smooth variations predicted by simple conductive cooling. Other properties or processes must define the tectonic plate. The lithosphere may be relatively dehydrated, which would enhance its strength. In contrast, asthenospheric hydration could make it relatively weak and also reduce its melting temperature. A small amount of partial melt beneath the plate in the asthenosphere may exist, which could further ease convection and therefore define the plate. Melt provides a simple explanation for a host of observations with large implications for plate tectonics, mantle dynamics, and Earth's evolution. So far reports of melt are variable in location and character. The variability in lithospheric thickness and also melt location and character suggests that the lithosphere-asthenosphere boundary is likely dynamic and dictated by mantle dynamics including melt generation and migration.

The Earth's lithosphere is defined as its rigid outer layer including both the crust and a part of the upper mantle that moves coherently over the weaker, convecting asthenosphere. The thickness of the lithosphere and also the physical and chemical properties that distinguish the lithosphere from the asthenosphere have implications for natural hazard mitigation, climate change over geologic timescales, and our understanding of plate tectonics and the habitability and evolution of the planet. However, the exact thickness of the lithosphere and the properties that distinguish the lithosphere from the asthenosphere are debated. Despite its importance, the lithosphere-asthenosphere boundary (LAB) has remained elusive.

The concept of a plate, or lithosphere, was developed in the beginning of the twentieth century to explain the existence of topography, in other words a rigid outer layer floating over a weaker one. A variety of seismic observations suggested the existence of a seismically fast layer that overlay a deeper, slower layer, and the layers were equated with the lithosphere and the asthenosphere, respectively. However, 1-D seismic velocity models of the Earth did not include an asthenospheric low-velocity zone (LVZ). This was probably the beginning of the elusive nature of the LAB. Plate tectonic theory, as we know it today, was then developed, and the lithosphere and the asthenosphere were discussed in a new framework involving several distinct plates that dynamically interact with the asthenosphere. The plates were modeled as a conductively cooling boundary layer of mantle convection, where the plate was defined by cooler temperatures. In the thermal model there is a very gradual transition from the lithosphere to the asthenosphere, occurring over tens of kilometers. A wide variety of observations and approaches generally support lithospheric thickening with age beneath the oceans with continued thickening toward the oldest continental interiors. This suggests that temperature plays a dominant role in dictating the thickness of the lithosphere. However, there are also large variations in reported LAB depths within any age interval. Our analysis suggests that these variations represent Earth structure, and therefore, other properties or processes also play a role.

Key observations about the nature of the LAB come from scattered waves such as *P*-to-*S* and *S*-to-*P* receiver functions and *SS* precursors, which image velocity discontinuities that require sharp velocity gradients in depth, sharper than can be explained by temperature alone. The depths of the sharp velocity discontinuities coincide with the gradual drop in velocity at the base of the plate in seismic tomography studies, which have relatively broad depth resolution. The depths also correspond to the depths of a predicted strong decrease in viscosity and the solidus for mildly hydrated mantle. The agreement suggests that the discontinuities from scattered waves likely represent real Earth structure and also the LAB in all locations except for shallow discontinuities (60–110 km depth) beneath continental interiors, which are equated with internal layering. Similarly, observations of slow seismic velocity anomalies and low resistivities beneath the plate are difficult to explain with temperature alone. Hundreds of observations have now been equated with the LAB as a sharp discontinuity defined by a property besides temperature.

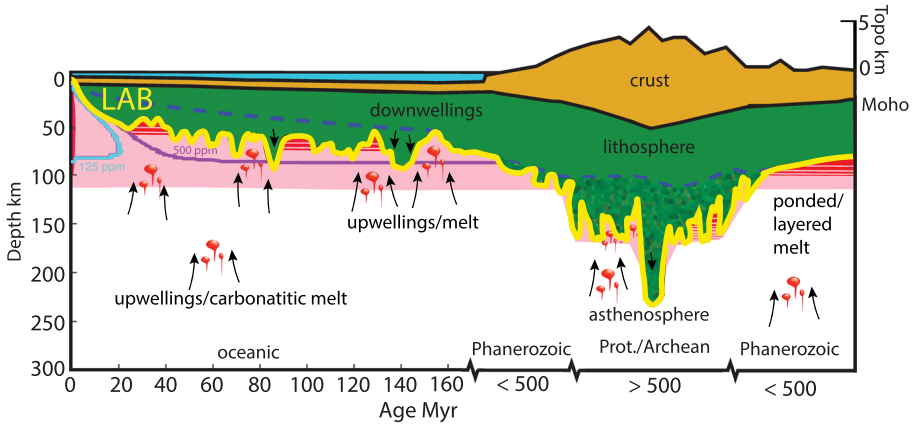

Figure 1. Synthesis. The lithospheric mantle is green, with a mottled green layer representing the possible compositional change (from green to mottled) at the MLD. Blue dashed line indicates the effective elastic thickness depth. The lithosphere-asthenosphere boundary (LAB) is shown by the thick yellow line, as determined by scattered wave observations, but also in agreement with the general trends from other observables such as *SS* precursors, deepest diamond origin depth, heat flow, surface waves, and magnetotelluric imaging. Regions potentially containing partial melt possibly enhanced by thermal upwellings and/or a hydrated mantle are shown in pink, with red regions showing areas of greater melt concentrations in a variety of forms: deep ascending carbonatitic melt, in thin channels or multiple channels at a depth of neutral buoyancy or beneath a permeability boundary, and in focused region beneath the ridge axis. The solidus for 125 ppm (cyan) and 500 ppm (purple) water concentrations assuming a 90 km thick plate model and potential temperature 1350°C are shown.

Many models have been proposed to explain the observations of sharp discontinuities and strong anomalies such as elastically accommodated grain boundary sliding, near melt conditions, anisotropy, composition, and grain size. Subsolidus factors are probably required to explain discontinuities at 60–110 km depth beneath continental interiors. However, none of the subsolidus models easily explain the wide range of independent observations for a sharp LAB, slow seismic velocity anomalies, and low electrical resistivity anomalies. Melt is the most straightforward explanation. The presence of a small percentage of melt that would explain the seismic wave velocities and electrical resistivities, would also reduce the viscosity of the mantle over geologic timescales, and therefore define the LAB.

Whether or not melt can exist in the mantle over length and timescales imageable by geophysical methods, and also the exact form, location, and amount of melt that exists are debated, despite important implications. Melt has been proposed to exist in a focused melt triangle, in a much wider triangle beneath the ridge, in ephemeral and intricate vertical and subvertical veins beneath the ridge, beneath a permeability boundary along the base of the plate connecting to the ridge, concentrated in a thin channel, in multiple layers, at a depth of neutral buoyancy, in punctuated upwellings, beneath older lithosphere, and even beneath continental interiors. Our analysis suggests that the form location and amount of melt are likely highly variable (Figure 1). Given that the presence of melt would define the plate, this implies that the LAB is dynamic, and variations in melt generation and migration determine the thickness of the plate.

There are profound implications of a dynamic LAB underlain by a low-viscosity asthenosphere as facilitated by volatiles and/or melt and melt dynamics. A low-viscosity asthenosphere is essential for plate tectonic style convection. It also allows for multiple scales of convection in the planet, explaining a range of observations. Smaller-scale convection and other complex mantle flows may cause upwellings that promote partial melting of the asthenosphere and explain numerous intraplate volcanic centers. These flows also limit the thickness of the tectonic plates. Low viscosities in the asthenosphere can also enhance or weaken the driving forces of plate tectonics. At relatively short geologic timescales, the low-viscosity asthenosphere promotes rebound of the tectonic plates owing to lake level changes, deglaciation, and large earthquake events. This rebound controls the level of the plates and thus the apparent sea level, important to our understanding of climate change over geologic timescales. Similarly, the viscous relaxation of stresses in faults zones is

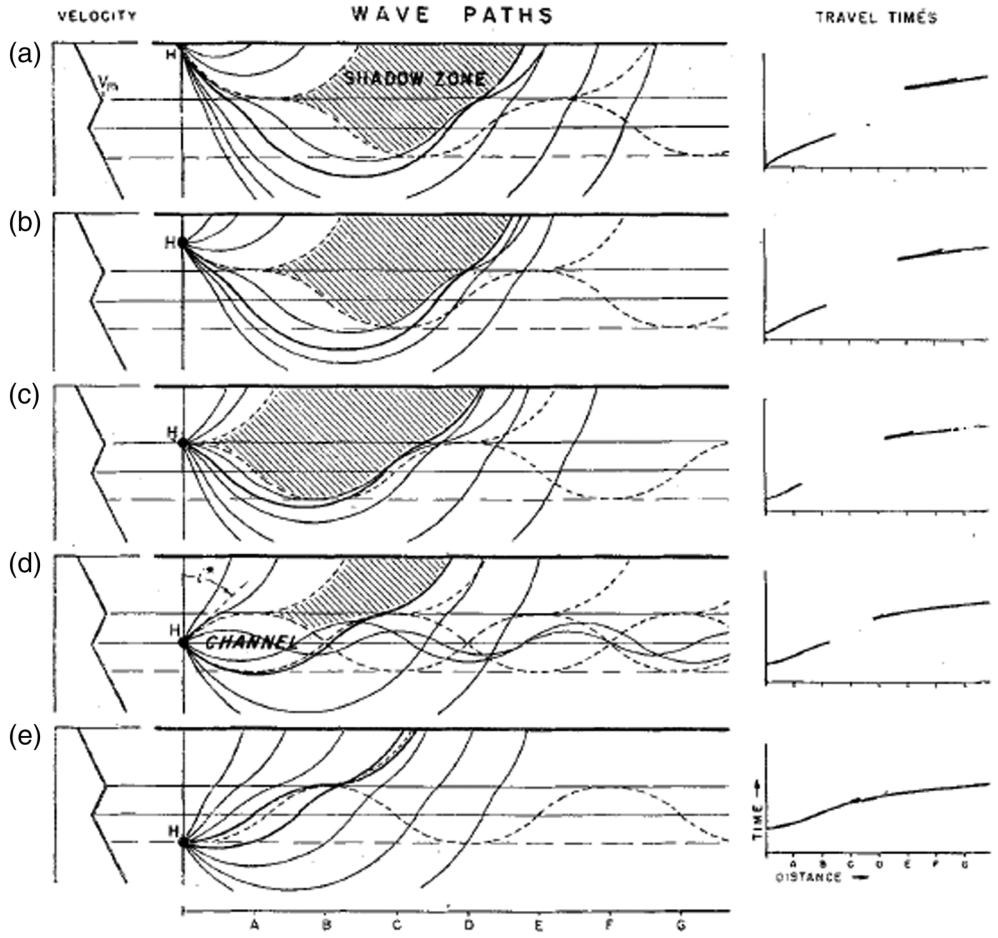

Figure 2. (a–e) Example of a shadow zone (Gutenberg, 1948). Some of the first seismic observations interpreted as a higher-velocity lithosphere above a slower asthenosphere came from Beno Gutenberg who recognized that a low-velocity layer would cause raypaths to bend steeply downward, creating a shadow zone, a region at the surface of the Earth where arrivals are not recorded.

key for natural hazard mitigation. Large-scale plate tectonic convection and consequently multiple plate tectonic cycles constructed continents and also ocean basins, which hold water at the free surface, both important factors for our life on the planet. Plate tectonic processes have resulted in large-scale mass transfer between the solid Earth and atmosphere through geologic time. Yet free surface water and a hydrosphere have been preserved over billions of years, making the planet favorable for life above and below water.

1. History of the LAB

The concepts of lithosphere and asthenosphere were first developed to explain the existence of Earth's surface topography. These models of Earth's isostatic compensation used a strong outer shell, or lithosphere, which could resist shear stress, that was underlain by a weaker layer, the asthenosphere, which deformed in response to the lithospheric loading (Barrell, 1914; Daly, 1940). Given that seismic wave velocities are also sensitive to the strength of the Earth, albeit at a much shorter timescale, a series of seismic wave observations were also interpreted accordingly, particularly by Beno Gutenberg. Gutenberg observed a strong decrease in *P* wave amplitudes from shallow earthquakes over a certain distance range, a shadow zone, interpreted it as an asthenospheric low-velocity zone (LVZ) at 75 km depth (Figure 2) (Gutenberg, 1926; as summarized by Gutenberg, 1959). Gutenberg continued to investigate the LVZ in a variety of locations including South America and California (Gutenberg & Richter, 1939) and using a variety of observables also including *S* wave shadow zones and guided waves, concluding, “There is no clear evidence that the asthenosphere channel is

missing in any of the larger units of the earth's subcrustal layers" (Gutenberg, 1955). As a result of this early work by Gutenberg the seismic velocity discontinuities detected at the top of the LVZ, particularly beneath the oceans, are frequently referred to as the Gutenberg discontinuity or G-discontinuity (Gaherty et al., 1996; Schmerr, 2012).

Many other studies supported the existence of a sub-lithospheric LVZ such as that proposed by Gutenberg. Teleseismic Rayleigh wave dispersion curves supported the existence of a LVZ (Ewing & Press, 1954, 1959; Takeuchi et al., 1959). Rayleigh wave observations were also used to support the notion of a global low LVZ where the lithosphere decoupled from the asthenosphere (Press, 1959).

Inga Lehmann also played an important role in detecting and constraining the LVZ beneath the lithosphere. She considered body wave arrival times and also found evidence for an LVZ beneath Europe (Lehmann, 1961, 1964). In this work she also found evidence for an abrupt velocity increase with depth around 220 km depth that she interpreted as the base of the LVZ, which was later named the Lehmann discontinuity. This was another important constraint in terms of understanding lithosphere-asthenosphere interactions, and we will also discuss the depth and character of the base of the LVZ in subsequent sections.

However, interestingly, the early 1-D global seismic reference model, which was based on observations of body wave arrival times from 1930 to 1939, did not include a LVZ (Jeffreys & Bullen, 1940). Instead, seismic velocity monotonically increased with depth through the crust and mantle. This contrast was an early example of discrepancies among models regarding the pervasiveness of an LVZ. The relationship between the LVZ and the lithosphere-asthenosphere boundary (LAB) and the nature and location of the LAB itself have remained elusive ever since.

Variations in the thickness of the lithosphere with tectonic environment were suggested based on body wave travel times, and the LAB was interpreted as being centered at depths ranging from 45 to 120 km (Vesanen et al., 1959). Dorman et al. (1960) further clarified tectonic variation, suggesting that the LVZ was shallower and more pronounced beneath the oceans than the continents, based on a compilation of 11 velocity profiles from other studies.

Plate tectonic theory was developing, based on observations of magnetic lineations (Vine & Matthews, 1963), hot spot tracks (Morgan, 1971), and seafloor bathymetry (Heezen et al., 1959; Hess, 1962; Mckenzie, 1967; Parker & Oldenburg, 1973; Parsons & Sclater, 1977; Wilson, 1965). The half-space cooling (HSC) model was developed, in which the LAB was determined thermally by the geotherm-adiabat intersection, that is, the depth at which the temperature of the Earth is no longer determined by conductive cooling, which deepened according to the square root of age (Mckenzie, 1967; Parker & Oldenburg, 1973; Parsons & Sclater, 1977). Overall, the HSC model matched observations such as subsidence of the seafloor and heat flow and therefore was generally accepted as the first-order definition of the LAB.

Interpretation of seismic results evolved, including the concept of individual plates being formed at mid-ocean ridges, maturing over millions of years according to HSC in the oceans, meeting their demise at opposite plate margins by subducting into the weaker asthenosphere, and showing distinct characteristics related to tectonic history in the continents. For instance, a zone of relatively low attenuation and high seismic velocity was interpreted as descending lithosphere at the Tonga subduction zone (Oliver & Isacks, 1967). Surface wave dispersion curves for paths through oceans, shields, and tectonically active regions suggested variable shear velocity structure according to the classifications (Dziewonski, 1971; Kanamori, 1970; Toksoz & Anderson, 1966; Toksoz et al., 1967), and this was interpreted as variations in lithospheric thickness, for instance, from about 70 km beneath oceans to twice that beneath shields (Kanamori & Press, 1970). However, as is still the case today and further described in subsequent sections, there was a wide range in the reported values of lithospheric thickness. Free oscillation results and body wave travel times were used to argue for a much thicker layer, 400 km or even up to 700 km thick, that transfers coherently beneath continental interiors (Jordan, 1975). Finer classification (oceans, rifts, shields, mountains, and continental aseismic) similarly gave variable shear velocity structures, and it was suggested that in some cases (e.g., beneath shields and mountains) a decrease in velocity beneath the lithosphere may not be present at all (Knopoff, 1972). Surface wave dispersion was used to show ocean lithosphere also

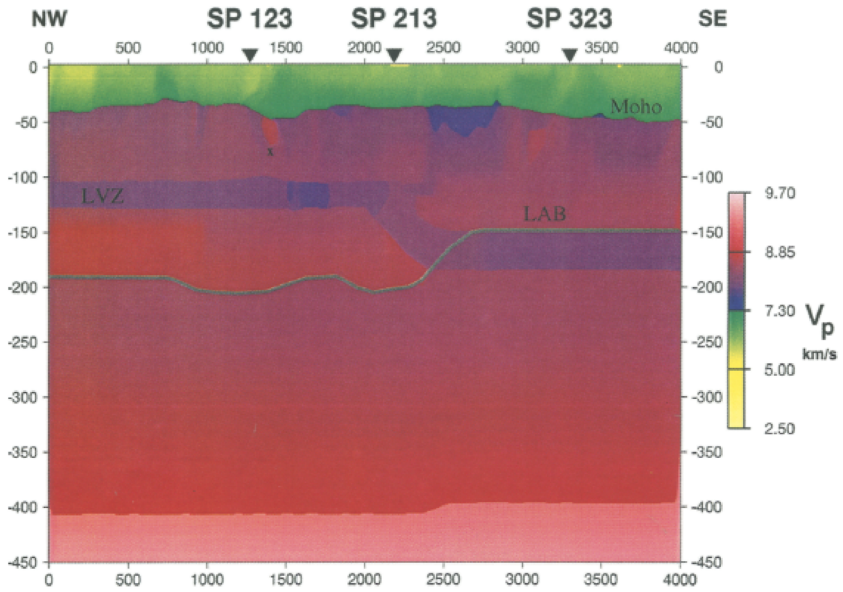

Figure 3. An example of a LAB interpretation (Ryberg et al., 1996). The profiles cross the East European Platform (0–1,200 km), the Urals around 1,500 km, the Western Siberian Platform (1,600–3,200 km), and the Altai-Sayan Folded Region (3,200–4,000 km). The LAB interpretation is drawn as a green line, with the low-velocity zone (LVZ) indicated in purple. The LVZ beneath the European platform is in the depth range of many reported midlithospheric discontinuities.

increased in seismic velocity and thickness with age, which agreed with thermal predictions from the HSC model (Forsyth, 1975).

A number of other observations, besides seismic, also supported a thick lithosphere beneath the continents. For instance, heat flow beneath cratonic continental interiors is generally low (e.g., Mareschal & Jaupart, 2004; Pollack et al., 1993; Rudnick & Nyblade, 1999). Geochemical constraints on the pressure-temperature conditions of the origin depths of xenoliths also suggested cold temperatures to great depths beneath the continents (e.g., Griffin et al., 1999; Lee et al., 2011). The continents were also shown to be resistive to deeper depths than the oceans (Hirth et al., 2000; Jones, 1999; Lizarralde et al., 1995; Schultz et al., 1993). Finally, diamonds are only stable at relatively cool temperatures. The fact they have been found in xenoliths that are billions of years old, originating from great depths beneath continental interiors was also explained by a relatively thick, rigid, and unconvecting lithosphere (Pearson et al., 1995).

Some early *S*-to-*P* (*Sp*) conversion studies, primarily sensitive to relatively sharp velocity drops in comparison to other methods, detected a velocity drop interpreted as the LAB at 400 km depth beneath South America (Sacks & Snoke, 1977) and 250 km depth beneath the Baltic Shield (Sacks et al., 1979). It was noted that the boundary was sharp, velocity decreasing by 5% over only a few kilometers depth interval (Sacks & Snoke, 1977). However, exactly how such a sharp drop in velocity could be reconciled with the typical gradual variation from the lithosphere to the asthenosphere predicted for a thermally defined plate, such as that of the HSC model was not addressed. It was also noted that if a seismic discontinuity related to the LAB exists, its depth must vary laterally, given the lack of evidence for any upper mantle discontinuity shallower than 410 km in long-period global body wave stacks (Shearer, 1991).

A number of active source seismic experiments, sensitive to only the sharpest velocity discontinuities, detected deep discontinuities that were discussed in light of the LAB. For instance, passive nuclear explosions were used to image a discontinuity at 150 km depth in parts of northern Eurasia, deepening to 200–220 km beneath the Urals and interpreted as the LAB (Morozova et al., 2000; Ryberg et al., 1996). Interestingly, a shallower feature was interpreted as a midlithospheric discontinuity, similar to those frequently imaged and similarly interpreted beneath continental interiors today (Figure 3) (Ford et al., 2010) (Ryberg et al., 1996). It was also recognized that the velocity gradients of deeper discontinuities near LAB

depths were sharp, occurring over 1–4 km, and that they might not be related to the thermal LAB (Steer, Knapp, Brown, Echtler, et al., 1998). Therefore, the discontinuities imaged beneath the Urals and also at 75 km beneath the North Sea were also interpreted as frozen-in features such as subduction-related scars, mafic intrusions, or rheological layering (Knapp et al., 1996; MONA-LISA Working Group, 1997; Steer, Knapp, & Brown, 1998; Steer, Knapp, Brown, Echtler, et al., 1998). The MONA LISA Working Group (1997) stated, "For the first time, sub-horizontal reflections have been recorded on two perpendicular profiles at 20–24 s [two way travel time] which is also the expected travel time for reflections from the lithosphere–asthenosphere boundary. However, the reflections are sharper than expected for a thermal–rheological transition which suggests that the deep reflectors are tectonic interfaces or lithological boundaries." Analyses of several long offset data sets from North America and Eurasia found evidence for a change in the character of arrivals from a certain distance range, consistent with a LVZ at 100 km depth, which was not necessarily equated with the LAB, but was interpreted as a pervasive layer of melt within continental regions (Thybo, 2006; Thybo & Perchuc, 1997). Also, *P*-to-*S* (*Ps*) imaging of a feature dipping from 170 to 230 km depth toward the interior of the Slave Craton was interpreted as a frozen-in slab emplaced during craton formation (Bostock, 1998).

In the next decade much more passive-source seismic data were available, both from temporary seismometer deployments and also a growing global seismic database. This was particularly helpful for improved imaging with receiver functions, and in particular for *Sp* receiver functions. *Sp* has advantages over *Ps*, since the *Ps* LAB can be masked by reverberations from shallower structure. However, *Sp* arrives within the coda of the earthquake, typically requiring more events to eliminate noise by stacking. Discontinuities imaged by teleseismic *Sp* and *Ps* converted phases again began to be interpreted as the LAB, particularly beneath ocean islands including Hawaii, Iceland, Greenland, and Jan Mayen at 40–120 km depth (Collins et al., 2002; Kumar, Kind, et al., 2005; Li et al., 2004) but also beneath Tien Shan at 90 km (Oreshin et al., 2002). The ocean island LAB depths were sometimes consistent with predictions for the ocean lithosphere (e.g., 100–110 km beneath 90–100 Myr old lithosphere near the Big Island of Hawaii (Li et al., 2004) but were also interpreted as plume related thinning of the lithosphere (50–60 km) beneath Kauai (Li et al., 2004), although the explanation for the required sharpness of the velocity gradient, in comparison to thermal predictions, was not typically addressed.

Waveform modeling of receiver functions showed that a strong, sharp velocity drop (5–10% over <10 km) was required at 90–110 km depth beneath eastern North America (Rychert et al., 2005, 2007). The discontinuity was within the gradual drop in velocity at the base of the plate in the regional surface wave model (Li, 2003). The sharpness of the discontinuity required an additional property or process besides temperature, such as an increase with depth in the presence of partial melt or hydration combined with a change in anisotropy (Rychert et al., 2007). Melt and hydration also weaken the mantle at geologic timescales (Hirth et al., 1996; Hirth & Kohlstedt, 1995; Jackson et al., 2006). Therefore, it was suggested that the LAB was defined by hydration or melt (Rychert et al., 2005, 2007). However, it was unclear if the LAB was sharp because of the unique location at the edge of the continental keel, where, for instance, mantle might upwell along the base of the keel, forming a small amount of partial melt, or whether it was a global phenomenon. If not global, then exactly how or why the LAB definition varied with tectonic environment remained unclear.

Many more receiver function results were soon interpreted as the LAB. Waveform modeling of discontinuities imaged with *Ps* confirmed a similarly sharp boundary (3–7% velocity drop over <10 km depth) beneath the Tanlu Fault Zone (Chen et al., 2006). *Ps* and *Sp* receiver functions imaged a strong (7–8%), sharp (over <15 km depth) velocity drop at increasing depth with seafloor age beneath the Pacific that was interpreted as the result of layered melt in the asthenosphere (Kawakatsu et al., 2009). A global *Ps* imaging study found a discontinuity typically within the 60–110 km depth range at all stations where there were large amounts of data and also a simple crustal structure, so that real discontinuities could be distinguished from crustal reverberations. The average depth of the discontinuity also varied according to tectonic environment, thickening toward continental interiors: oceans (70 km), tectonically altered regions (81 km), and Precambrian Shields and Platforms (95 km) (Rychert & Shearer, 2009). Therefore, it was suggested that the LAB was strong and sharp everywhere. Beneath continental interiors the depth of discontinuities was too shallow to be consistent with the thickness of the seismically fast lithosphere, for instance, from surface wave anomalies that

extend to at least 200 or 250 km depth (Nettles & Dziewonski, 2008), and therefore, it was recognized that these could be frozen-in features within the lithosphere, possibly related to variations in anisotropy (Rychert & Shearer, 2009). In the next decade many more discontinuities were imaged and attributed to the LAB, whereas shallow discontinuities at ~60–110 km beneath continental interiors were primarily interpreted as midlithospheric discontinuities (MLDs) (Ford et al., 2010).

Many of the LAB results were interpreted as requiring partial melt. Melt offered a more straightforward explanation for a range of observations with different sensitivities and resolutions. This was underscored by geodynamic modeling using a composite diffusion dislocation creep rheology that included grain size evolution (Austin & Evans, 2007) with hydration as a defect, which could not explain observed strong velocity drops beneath old ocean lithosphere without higher, possibly supersolidus temperatures (Behn et al., 2009). Similarly, low-resistivity anomalies could not be explained by hydration, since the hydration required would also depress the solidus enough to result in melting (Naif et al., 2013). Thus, a melt channel was interpreted beneath the Cocos Plate before subduction (Naif et al., 2013). LAB melt channels about 10 km thick were also interpreted beneath the Pacific Plate subducting beneath New Zealand (Stern et al., 2015), beneath 40 and 70 Myr old lithosphere near the Mid-Atlantic Ridge (Mehouachi & Singh, 2018), and beneath 0 to 30 Myr old lithosphere near the Mid-Atlantic Ridge (Wang et al., 2020).

In response to these observations and interpretations, a variety of other subsolidus models were proposed to explain observed sharp velocity discontinuities and/or slow seismic velocity anomalies, either LAB or MLD. These include grain size (Faul & Jackson, 2005), elastically accommodated grain boundary sliding (Karato et al., 2015), an enhanced reduction of seismic velocity at near solidus conditions (Yamauchi & Takei, 2016), anisotropy (Auer et al., 2015; Beghein et al., 2014), the oxidation state of the mantle (Cline et al., 2018), and bulk chemistry (Rader et al., 2015; Selway et al., 2015). In other words, the debate over whether or not melt can exist in the mantle over length and timescales so as to be seismically imageable continues. The following sections describe the more recent observations and interpretations.

2. Recent Observational Constraints on the Depth and Sharpness of the LAB

2.1. Seismic and Isotropic

Surface wave tomography provides comprehensive 3-D resolution of the absolute shear wave velocity structure of the seismically fast lithosphere and the slower asthenosphere. The long periods of the waveforms (>20 s) mean that they have relatively broad lateral resolution at the base of the plate, at the scale of ~100 km for regional-scale studies and ~1,000 km for global studies. Averaging global surface wave models (French et al., 2013) by the age of the overriding continental crust according to CRUST1.0 (Laske et al., 2013), and the age of the seafloor (R. D. Muller et al., 2008) shows that lithosphere gets faster and thicker with age from the youngest oceans to the oldest continents (Figure 4). We applied a *k*-means cluster to the Rayleigh wave phase velocities (Ekstrom, 2011) and find a very similar trend (Figure 4). This shows that the tectonic trend is robust, existing regardless of the assumptions made during the inversion of the phase velocities for shear wave velocities. The trend is also visible in surface wave models that are translated to thickness assuming a thermal model of the plate (Figure 5) (e.g., Steinberger & Becker, 2018).

Despite robust tectonic trends, prescribing an exact lithospheric thickness from surface wave seismic velocity models is challenging. First, the exact shapes of the shear wave velocity-depth profiles depend on smoothing, damping, regularization, crustal assumptions, the types of data included, and the parameterization. For instance, the slowest seismic velocity occurs at depths of 25 to 75 km for young and old lithosphere in the SEMum2 model (French et al., 2013) in comparison to 54 to 144 km (Figure 6; Nishimura & Forsyth, 1989). Beneath continental interiors some models include a drop in velocity at the base of the plate (Figure 4) (French et al., 2013), while others show no drop in seismic velocity at all (Pedersen et al., 2009). Second, surface waves have broad depth sensitivity kernels resulting in gradual velocity drops in depth and therefore LAB depth depends on how the LAB is selected along a smooth model (Figure 6). One could consider the sharpest part of the velocity drop (Nishimura & Forsyth, 1989; Tharimena, Rychert, & Harmon, 2017), the mean of the depth of the negative velocity gradient, the depth of the slowest velocity (Tharimena, Rychert, Harmon, & White, 2017), an isovelocity surface, the top and bottom of the drop assuming a gradual

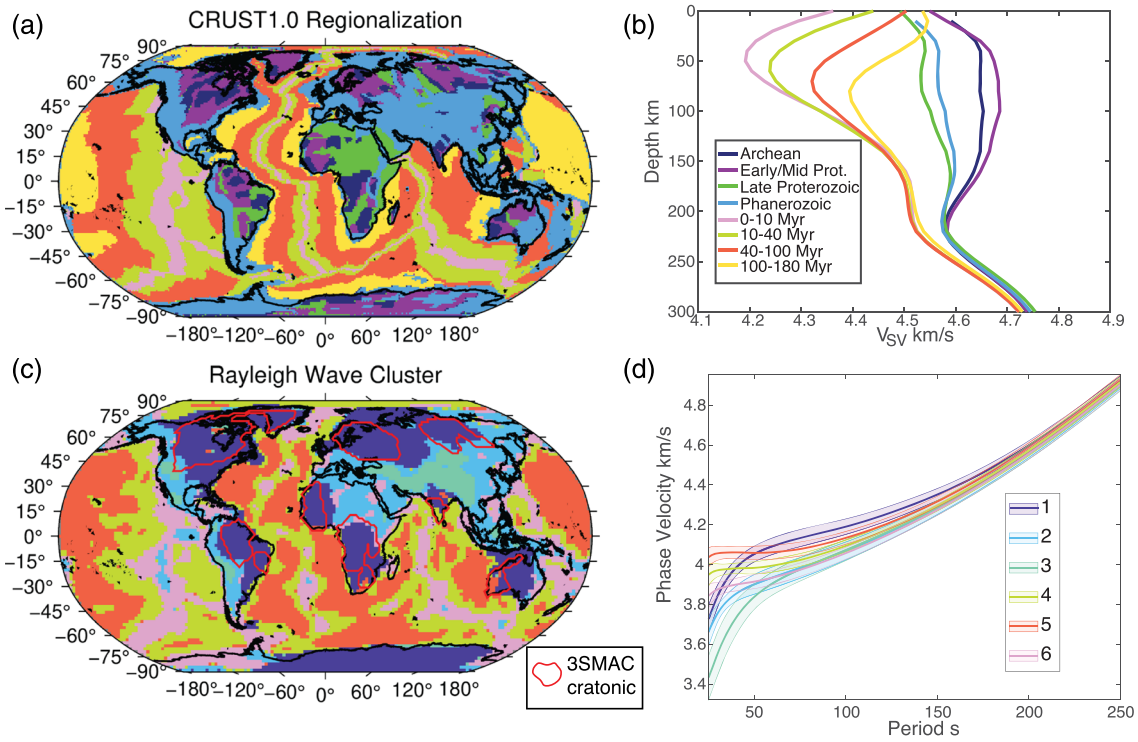

Figure 4. Regionalization. (a) Map view of crustal ages based on the model of CRUST1.0 (Laske et al., 2013). (b) Average shear wave velocity profiles from the SEMum2 model averaged according to crustal ages from CRUST1.0 (French et al., 2013). (c) Results of the *k*-means clustering applied to phase velocities of (Ekstrom, 2011). The 3SMAC cratonic regions are outlined in red (Nataf & Ricard, 1996). (d) Phase velocities (solid) and 95% confidence regions (transparent) for the clustered regions shown in (c) using the same color scale.

transition (Yoshizawa, 2014), or the depth where oceanic and continental velocity profiles converge (Jordan & Paulson, 2013). Other approaches include using a constant anomaly value (Conrad & Lithgow-Bertelloni, 2006), the integrated velocity anomaly over 400 km depth (Bird et al., 2008), or inverting phase velocities for the best fitting shear wave velocity thickness of only three layers—the crust, lithosphere, and asthenosphere (Pasyanos, 2010). Another approach is to compare surface wave velocities to thermal predictions (e.g., Ritzwoller et al., 2004), developing empirical relationships, assuming the thermal model of the plate (Figure 5) (Priestley & McKenzie, 2006; Steinberger & Becker, 2018), and/or including calibrations based on xenolith observations (Plank & Forsyth, 2016; Priestley & McKenzie, 2006). The absolute depths based on different assumptions are variable. For instance, in the SEMum2 model the thickness of the continental lithosphere based on the maximum negative gradient would vary from 155 to 175 km. The thickness based on lowest shear wave velocity would be ~220 km (Figure 4). The thickness from the depth of convergence of the profiles could be 350 km or more. Third, although the age-averaged profiles result in smooth, monotonic variations with age as predicted by thermal models, individual transects show greater variability (Figures 7 and 8; French et al., 2013). This could be caused by an artifact of the resolution of the tomography, or it could be caused by real lateral variability. Regional surface wave imaging at the equatorial Mid-Atlantic Ridge supports the latter, finding evidence for both a gradual age-depth progression of the LAB in one location and an undulating LAB in another, the result of punctuated upwellings (Harmon et al., 2020).

Scattered waves from teleseismic or regional earthquakes such as *Ps* and *Sp* converted phase receiver functions and also underside reflections such as *SS* precursors are useful for imaging and constraining velocity discontinuities that could occur at the LAB. *Ps* and *Sp* receiver functions detect discontinuities in seismic shear wave velocity. They contain higher frequencies than surface waves with dominant periods of, for example, 1–4 s for *P* waves and 7–14 s for *S* waves (Rychert et al., 2007). The lateral sensitivity, or Fresnel zone diameter, of these waves at conversion points at the base of the plate is on the order of ~20–80 km. They provide information from the region beneath a seismic station, being converted at a radius of ~20–40 km (*Ps*) or ~100–200 km (*Sp*) at LAB depths. *Sp* has the advantage that it does not suffer from

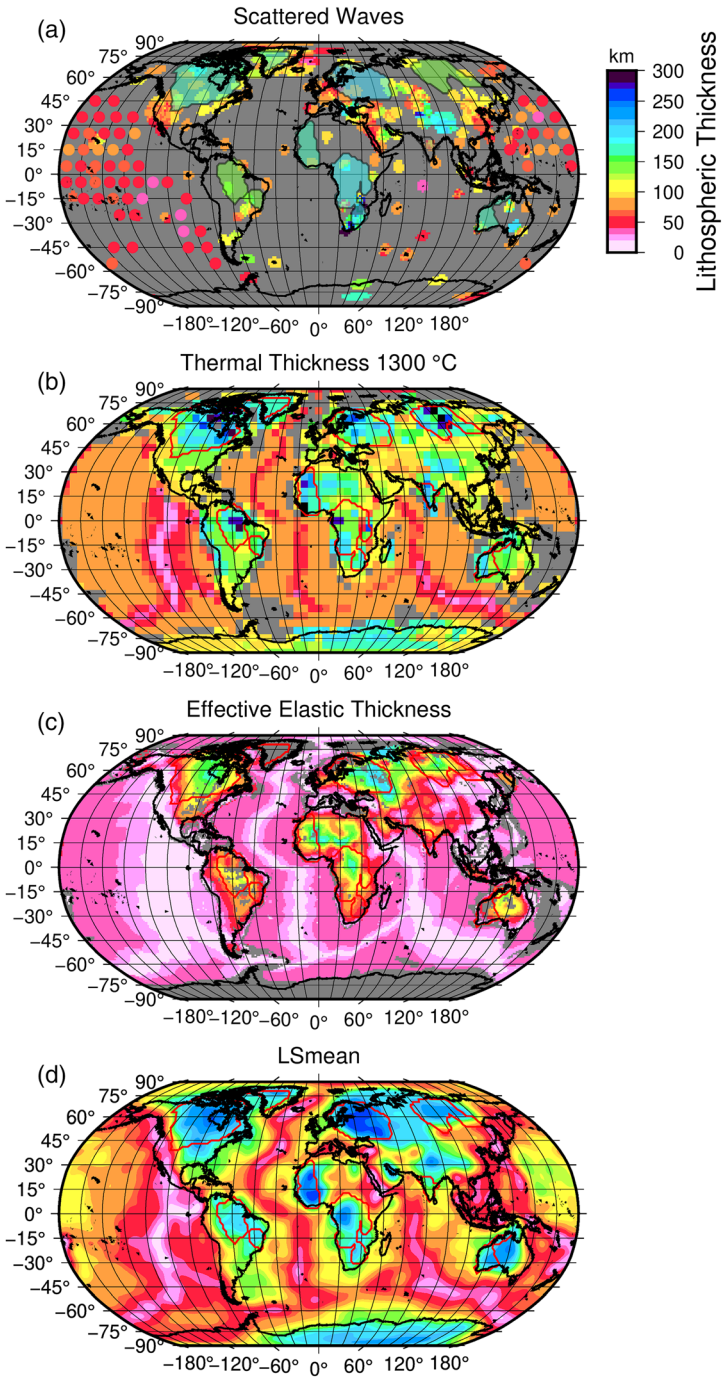

Figure 5. Lithospheric thickness estimates. (a) A compilation of results from *SS* precursors (large translucent regions outlined in black on the continents) (Tharimena, Rychert, & Harmon, 2017) and circles across the oceans (Tharimena, Rychert, Harmon, & White, 2017) and receiver functions (smaller, opaque irregular shapes primarily on continents and ocean islands) (Rychert & Shearer, 2009; Rychert et al., 2010, and references therein). (b) Lithospheric thickness determined by the depth of the 1300°C isotherm, which is based on geotherms calculated to fit borehole heat flow measurements beneath the continents (Artemieva, 2006) and based on a plate model (Stein & Stein, 1992) assuming a 90 km thick plate and 1350°C potential temperature beneath the oceans (Hasterok, 2013). (c) Effective elastic thickness determined by the coherence between topography and gravity beneath the continents (Audet & Burgman, 2011) and the predicted depth of the 600°C isotherm of the plate model as in (b) beneath the oceans (Burov & Diament, 1995; Watts et al., 2013). (d) Lithospheric thickness based on global seismic tomography anomalies relative to a thermal model (Steinberger & Becker, 2018). The 3SMAC continent boundaries are outlined in red or black (panel a) (Nataf & Ricard, 1996).

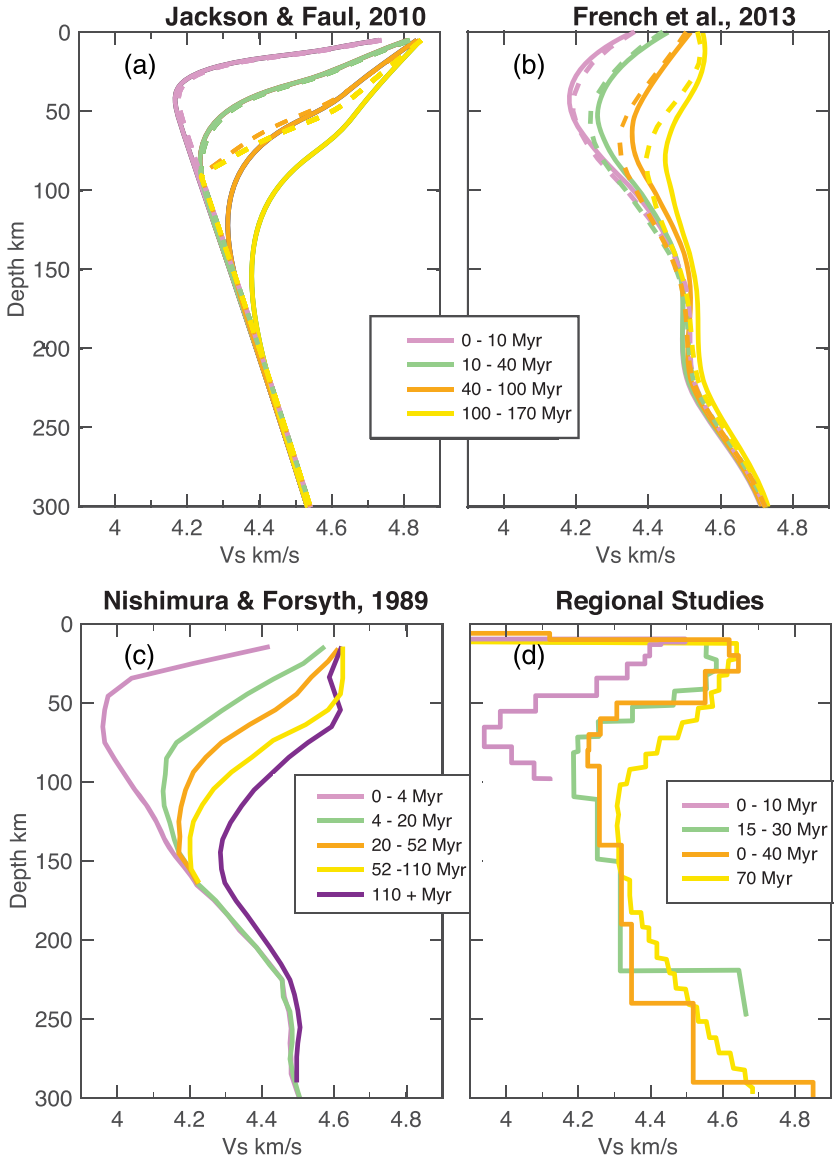

Figure 6. Comparison of 1-D velocity structure of the oceanic lithosphere. (a) Predictions for the half-space cooling (HSC; solid) and plate model with a 90 km thick plate (dashed) assuming grain size = 1 mm at 5, 25, 70, and 135 Myr. (b) Global seismic velocity model SEMum2 averaged across the Pacific for V_{SV} (dashed) and V_{Voigt} (solid). (c) Surface wave velocities (V_{SV}) averaged over the Pacific (Nishimura & Forsyth, 1989). (d) Average profiles from regional-scale studies: 0–10 Myr old Pacific lithosphere (Harmon et al., 2009); 15–30 Myr old lithosphere in the Shikoku Basin (Takeo et al., 2013); 0–40 Myr old lithosphere near the Mid-Atlantic Ridge (Harmon et al., 2020); and 70 Myr Pacific lithosphere (Lin et al., 2016).

reverberations caused by shallow structure that can obscure LAB phases in *Ps*. Given that most seismic stations are located on land, the results are mostly continental. The discontinuities must also be relatively horizontal for detection with typical methodologies (Lekic & Fischer, 2017). Receiver function imaging of features like thin low-velocity channels on the order of 10 km or thinner are typically hampered by destructive interference between conversions from the top and the bottom of the channel (Rychert & Harmon, 2018). These types of conversions are only detectable when the seismic velocity gradient in depth is relatively sharp, typically occurring over <30 km depth (Rychert et al., 2007, 2010), but they can also provide tight constraints on velocity gradients. The observations sometimes require gradients that are even sharper, for instance, 5–10% over <11 km (Rychert et al., 2007) or 7–8% over <10–15 km (Figure 9; Kawakatsu et al., 2009). *SS* precursors are used to image seismic shear wave velocity and/or density

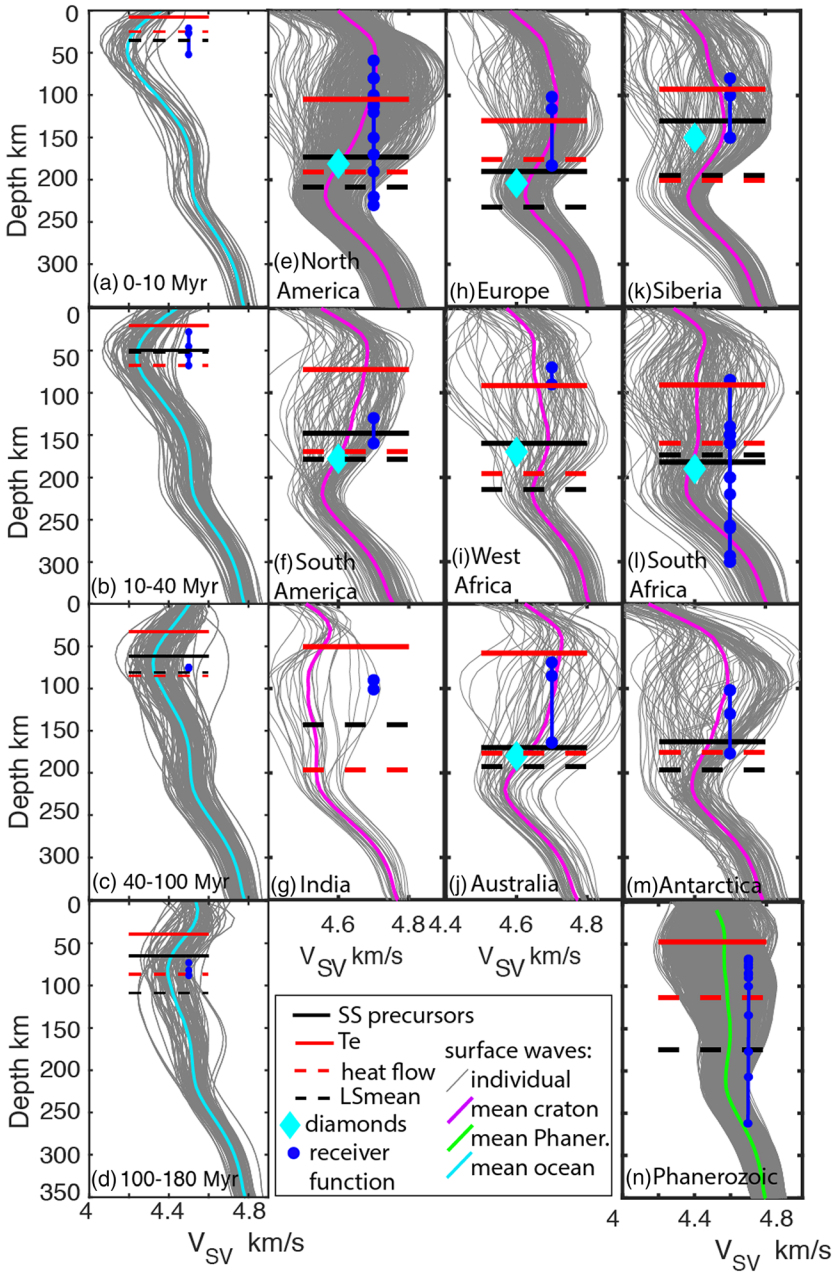

Figure 7. Comparison of velocity profiles and various lithospheric thickness estimates from oceans and cratons. Individual (thin gray) and average oceanic (thick cyan), Phanerozoic (thick green), and cratonic (thick magenta) velocity profiles from the SEMum2 model are compared to a variety of other estimates. (a–d) Profiles from the Pacific shown for four bins divided by seafloor age (R. D. Muller et al., 2008) as labeled. (e–m) Profiles from individual cratons using limits from 3SMAC (Nataf & Ricard, 1996) as labeled. (n) Profiles from Phanerozoic regions. These are compared to estimates for effective elastic thickness (*Te*) based on gravity and topography (Audet & Burgman, 2011) and the predicted depth of the 600°C isotherm (Burov & Diament, 1995) (red lines), depths of negative discontinuities from inversions of *SS* precursors stacks beneath each craton (Tharimena, Rychert, & Harmon, 2017) and from averaging the 10° bin results from the Pacific according to age (Tharimena, Rychert, Harmon, & White, 2017) (black lines), depths derived from surface wave anomalies relative to predictions for a thermal model (LSmean) (Steinberger & Becker, 2018) (black dashed lines), depth to the 1300°C isotherm based on borehole heat flow measurements (Artemieva, 2006) or the based on a plate model (Stein & Stein, 1992) assuming a 90 km thick plate beneath the oceans (Hasterok, 2013) (red dashed lines), the deepest origin depth of diamonds (cyan diamond) (Tharimena, Rychert, & Harmon, 2017, and references therein), and negative discontinuities from receiver functions (Tharimena, Rychert, & Harmon, 2017, and references therein, and Rychert et al., 2010, and references therein), and receiver function results from normal oceanic lithosphere shown in Figure 10 (blue dots connected by blue lines).

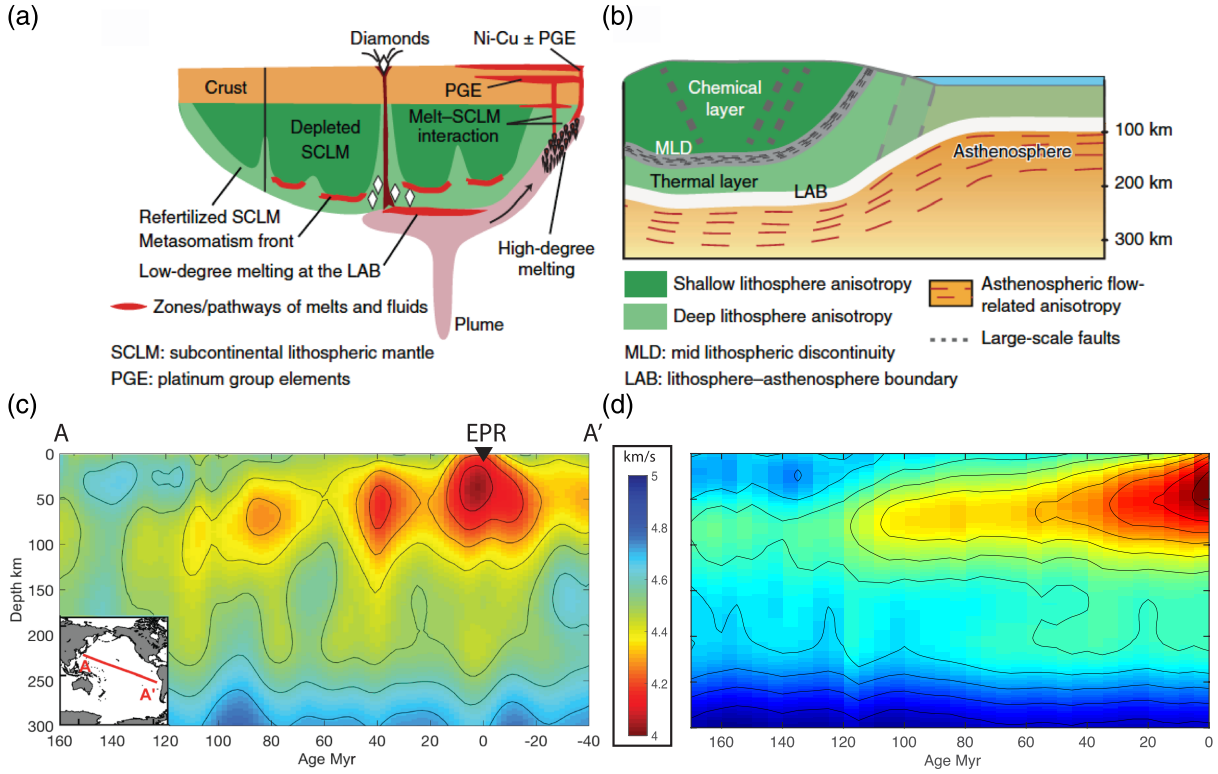

Figure 8. The shape of the lithosphere. The continental lithosphere as inferred from (a) geochemistry and (b) surface wavetomography, originally from Griffin et al. (1999) and Yuan and Romanowicz (2010), and here, after Yuan and Romanowicz (2018). The oceanic lithosphere from (c) a single Pacific transect through the SEMum2 model (French et al., 2013) and (d) the SEMum2 model in the Pacific, averaged by age of the seafloor, after Rychert, Harmon, and Tharimena (2018b).

discontinuities midway between the station and the receiver and therefore have sensitivity in locations where station coverage is sparse. These waveforms have dominant periods ~10 s and have good depth resolution but relatively large lateral sensitivity with an approximately 10° wide saddle shaped Fresnel zone. Waveform modeling of *SS* waves constrains negative velocity discontinuities that are typically 7–9% over a 14–52 km depth interval beneath continental interiors (Tharimena, Rychert, & Harmon, 2017) and 4–15% over 0–22 km thick depth interval beneath the oceans (Tharimena, Rychert, Harmon, & White, 2017). The velocity discontinuities imaged with these methods tightly constrain the LAB in the cases where they fall within the gradual velocity drop in velocity from surface waves. Large-amplitude, high-frequency (>2 Hz) coda waves called P_O/S_O or P_n/S_n have also been observed and interpreted as the result of scattering owing to laterally elongated heterogeneities, providing rare insight into the internal structure of old oceanic and continental lithosphere (Kennett et al., 2014, 2017; Kennett & Furumura, 2015; Shito et al., 2015, 2013). Modeling the waves provides a constraint on the depth extent of the heterogeneities, which has been interpreted as the LAB particularly beneath the oceans (Shito et al., 2015, 2013). These studies typically assume a sharp LAB and depth resolution depends on the number of model thicknesses tested, typically every 20 km owing to computational cost (Shito et al., 2015).

The discontinuity depths imaged by receiver functions and underside reflections such as *SS* precursors increase in depth with increasing seafloor age beneath normal oceanic seafloor at least out to 36 ± 4 Myr (Figure 10). The discontinuity depths beneath older seafloor and also seafloor on or nearby hot spots are centered around 64 ± 11 km depth with a wider range of depths reported (Figure 10). Scattered waves frequently image discontinuities beneath Phanerozoic crust, primarily within the 60–110 km depth range. However, Phanerozoic crust encompasses a wide range of tectonic regimes, and therefore, the total reported range of depths is much larger. Beneath some areas of rifting regions such as the Afar, the lack of a strong LAB phase has been interpreted as a very thin (<10 km thick) or nonexistent mantle lithosphere

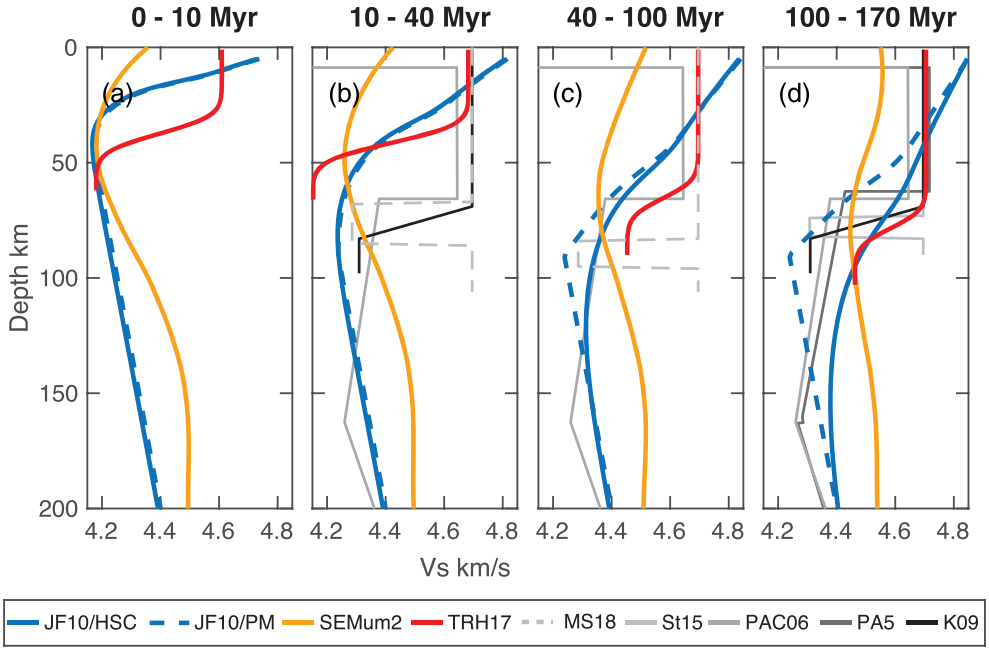

Figure 9. (a–d) Sharpness of the oceanic LAB at different ages. Comparison of seismic velocity gradients from a variety of methods. Velocity gradients are predicted using Jackson and Faul (2010) (JF10) for half-space cooling (HSC; solid blue) and plate models (PM) (dashed blue) assuming potential temperature 1350°C, plate thickness 90 km, and grain size 1 mm. These are compared to Voigt average velocity from surface waves (SEMum2; gold) (French et al., 2013), *SS* precursors (TRH17; red) (Tharimena, Rychert, Harmon, & White, 2017), multiple *S* bounces alone or combined with *ScS* and surface waves (PA5; PAC06; gray) (Gaherty et al., 1996; Tan & Helmberger, 2007), receiver functions (K09; black) (Kawakatsu et al., 2009), and active source reflection (MS18; light gray dashed and S15; lightest gray) (Mehouachi & Singh, 2018; Stern et al., 2015). *SS* velocity gradients are shown for four example bins nearest the center of the age bin. Since *SS* can only constrain changes in velocity, the profiles are calibrated to align with shallow velocity from PA06 and PA05. Depths are plotted with respect to the seafloor.

(Lavayssiere et al., 2018; Rychert, Hammond, et al., 2012), whereas beneath mountain ranges such as the Tibetan Plateau LAB phases have been interpreted at 200 km or deeper (Kumar, Yuan, et al., 2005; Kumar et al., 2007; Zhao et al., 2011). Beneath the oldest Archean cratons a large range of depths have been reported, with shallow phases at 60–110 km depth often interpreted as MLDs possibly related to strong compositional variations (Ford et al., 2010; Rader et al., 2015; Selway et al., 2015). *SS* precursors find discontinuities at 130–190 km depth interpreted as the LAB (Figures 5 and 7). Deeper discontinuities (>150 km) are sometimes imaged with these methods beneath cratons and interpreted as the LAB (Kumar et al., 2007; Vinnik & Farra, 2002), whereas other studies report a lack of conversions from sharp discontinuities beneath cratons (Abt et al., 2010; Ford et al., 2010; Mancinelli et al., 2017).

Active source seismic reflection studies image discontinuities in compressional velocity and/or density, and these studies sometimes approach or reach LAB depths. These studies are typically done at very high frequencies (tens to hundreds of hertz). They have lateral resolution of 0.1–3.0 km at LAB depths, and they have very high depth resolution, <1 km. The two active source studies that have reached LAB depths found lithospheric thicknesses of 68, 84, and 73 km beneath 40, 70, and 120 Myr old seafloor, respectively (Figures 9 and 10) (Mehouachi & Singh, 2018; Stern et al., 2015). The discontinuities were very sharp, 8–10% over <1 km. The studies also imaged equally large and sharp accompanying velocity increases 10–18 km deeper than the LAB discontinuities (Mehouachi & Singh, 2018; Stern et al., 2015). The discontinuity pairs were interpreted as the top and bottom of melt-rich LAB channels. Active source studies are very limited in spatial area globally, given that imaging to LAB depths in a marine environment, where the LAB is thought to be relatively shallow, requires large synthetic sources and long streamers that are not typically available to academics. Active source imaging of deeper contintental LABs requires larger sources than typically available, such as nuclear explosions.

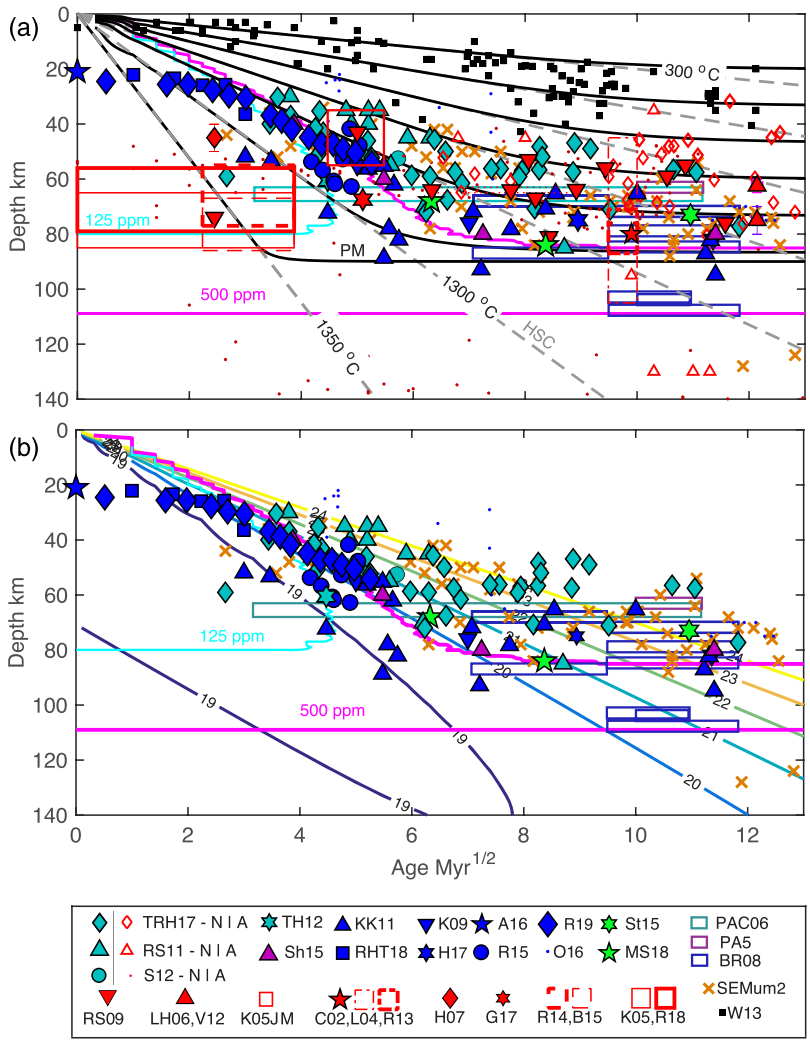

Figure 10. Discontinuity depths from scattered waves compared to *Te*, surface waves, and model predictions. (a) Thermal contours are plotted for the half-space cooling model (HSC; gray dashed lines) and the plate model assuming a 90 km thick plate (PM; black lines) at 200°C interval and also a contour very close to the potential temperature, 1350°C. The solidi for a mildly hydrated mantle are shown for 125 ppm (cyan) and 500 ppm (pink) water assuming a plate model and 90 km plate thickness (Katz et al., 2003). Depths are plotted relative to the seafloor with results that were reported from the sea surface corrected by the amount listed, if any. *SS* precursor results from the entire Pacific including TRH17 (Tharimena, Rychert, Harmon, & White, 2017), RS11 (Rychert & Shearer, 2011), and S12 (Schmerr, 2012) are sorted into normal lithosphere (N; cyan) and anomalous (A; red) lithosphere affected by hotpots (Korenaga & Korenaga, 2008). Depths from a *SS* precursor result, TH12 (cyan star; Tonegawa & Helffrich, 2012), and a P_O/S_O result, Sh15 (purple triangles; Shito et al., 2015), are shown. Receiver function results (solid blue symbols) include RHT18 (Rychert et al., 2018a; −3km), R15 (Reeves et al., 2015; −3 km), O16 (Olugboji et al., 2016), KK11 (Kumar & Kawakatsu, 2011), K09 (Kawakatsu et al., 2009), H17 (Hannemann et al., 2017), and A16 (Audet, 2016). Transect studies that encompass a range of ages are shown as boxes with fixed thickness (5 km), including PAC06 (Tan & Helmberger, 2007), PA5 (Gaherty et al., 1996; −5 km), and BR08 (Bagley & Revenaugh, 2008; −4 km). Active source studies (solid green symbols) include MS18 (Mehouachi & Singh, 2018; −4 km) and St15 (Stern et al., 2015). The depth of the minimum velocity in the low-velocity zone beneath the Pacific from surface wave model SEMum2 (French et al., 2013; −4 km) is shown as orange x's. Oceanic effective elastic thickness estimates are shown by black squares (Watts et al., 2013). Receiver function studies from ocean island hot spot studies are shown as solid red symbols or red boxes where the studies encompass a range of ages or depths, with −5 km depth correction applied to island studies: LH06 (Lodge & Helffrich, 2006), V12 (Vinnik et al., 2012), K05JM (Kumar, Kind, et al., 2005), L04 (Li et al., 2004), H07 (Heit et al., 2007), G17 (Geissler et al., 2017), R14 (Rychert, Harmon, & Ebinger, 2014), B15 (Byrnes et al., 2015), K05 (Kumar, Kind, et al., 2005), and the listed amount applied to submarine studies R13 (Rychert et al., 2013; −4 km) and C02 (Collins et al., 2002; 0 km). (b) Same as (a) except that ocean island results, *SS* precursor results from anomalous lithosphere, and effective elastic thickness results are excluded and background contours show log viscosity predictions in Pa s (labeled colored contours; Behn et al., 2009).

2.2. Seismic and Anisotropic

A change in seismic anisotropy with depth is another way of quantifying the LAB. Anisotropy refers to variability in seismic wave speeds that depend on the direction of propagation and/or the direction of polarization of the vibrations. Azimuthal anisotropy refers to variations with azimuth, whereas radial anisotropy refers to the difference between vertical and horizontal polarization or propagation direction. The mantle is made in large part of the highly anisotropic mineral olivine, which aligns according to the direction of shear strain when it is in the dislocation creep regime, which is predicted for much of the upper mantle (Hirth & Kohlstedt, 1995; Karato & Wu, 1993). Mantle observations of seismic azimuthal anisotropy are typically interpreted as olivine fast-axis alignment in the direction of shear strain caused by plate motions (Hess, 1964). The shear strain could either have occurred in the past, with anisotropy currently frozen-in to the lithosphere (fossil anisotropy) or the strain and associated anisotropy could be currently accumulating, potentially reflecting present-day absolute plate motion (APM).

The transition with depth from one fast direction to another could be considered the LAB. However, resolving the exact depth of the transition is challenging given that most depth constraints come from surface waves, with the broad depth sensitivity and dependence on parameterization choices discussed above. Anisotropy is also a higher-order effect and a smaller signal compared to isotropic velocity changes, resulting in comparatively lower resolution and trade-off with isotropic variation. Global surface wave anisotropy models find a general transition from fossil directions at lithospheric depths to APM directions deeper and also that the depth of the transition occurs deeper beneath older seafloor (Maggi et al., 2006). The depth at which the direction of azimuthal anisotropy correlates with APM similarly suggests an increase from <50 km beneath young Pacific lithosphere to 125 km beneath older lithosphere (Burgos et al., 2014). This has been interpreted as the LAB, with scattered wave observations explained by a shallower and frozen-in change in radial anisotropy (Auer et al., 2015; Burgos et al., 2014). Similarly, two peaks in depth in the maximum gradient in the direction of azimuthal anisotropy beneath cratonic North America were interpreted as the result of two lithospheric layers with frozen-in orientations above an asthenospheric layer with APM orientation beginning beneath the second peak, at 180 to 240 km depth (Figure 8) (Yuan & Romanowicz, 2010). Alternatively, it has been proposed that a change in azimuthal anisotropy with depth is frozen-in and unrelated to the LAB (Beghein et al., 2014) and that the peak in radial anisotropy at 75–125 km depth represents the flowing asthenosphere at the base of the plate (Gung et al., 2003; Montagner, 2002).

Overall, anisotropic structure may be more complex even in relatively simple oceanic settings. For instance, detailed regional studies have also found anisotropic fast directions that are not in the direction of APM in the asthenosphere (Eilon & Forsyth, 2020; Lin et al., 2016; Russell et al., 2019; Takeo et al., 2018). This could be explained by either by pressure gradient-driven flow or small-scale convection. In addition, many regional studies of oceanic lithosphere do not necessarily support simple fossil spreading orientations in the subcrustal lithosphere (Dunn et al., 2005; Eilon & Forsyth, 2020; Russell et al., 2019; Shintaku et al., 2014; Takeo et al., 2016, 2018; Toomey et al., 2007; VanderBeek & Toomey, 2017). If these results reflect frozen-in olivine alignment via dislocation, then it could instead reflect ancient APM (rather than fossil spreading) (Takeo et al., 2016), more complex near-ridge mantle flow than simple passive upwelling, and/or an alternate E-type fabric type (Karato et al., 2008; Katayama et al., 2004; Russell et al., 2019). Alternatively, it could be caused by serpentine layering in the shallow mantle lithosphere (Faccenda et al., 2008), exotic mineralogies, or the influence of a different deformation mechanism at shallow depths (<1000°C), that is, low-temperature plasticity rather than dislocation creep (Mei et al., 2010). Precise quantification of low-temperature plasticity and its effects on crystallographic alignment are still an actively evolving area of research. Future work is needed to incorporate this deformation mechanism into accurate numerical models (e.g., Blackman et al., 2017) of shear strain and subsequent anisotropic fabric development in the uppermost mantle. In addition, more observational constraints are required to fully understand the implications of anisotropy constraints for the LAB even for the relatively simple case of oceanic lithosphere (Kawakatsu & Utada, 2017).

Resolving the sharpness of the changes in seismic anisotropy is challenging. Anisotropic variations could be sharp, if a shear zone exists, where the mantle is suddenly weaker, possibly owing to the presence of hydration or melt. Strong anisotropy observed by an active source study has been interpreted as a frozen-in, past shear zone beneath the oceanic Moho (Kodaira et al., 2014). Sharp anisotropic changes have been proposed

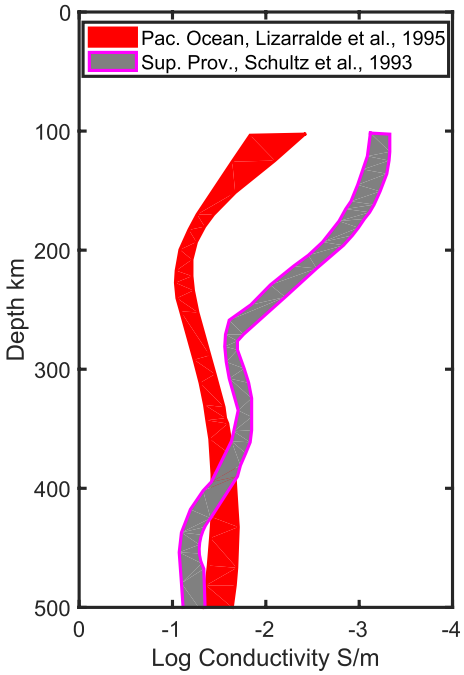

Figure 11. Electrical conductivity profile examples. The result from Superior Province is shown by the purple lines (Schultz et al., 1993), and the result from the Pacific Ocean is shown by the red line (Lizarralde et al., 1995).

to explain scattered wave observations (Auer et al., 2015; Beghein et al., 2014), which we discuss further in subsequent sections. However, there has not yet been a tight observational constraint on the sharpness of anisotropic changes at LAB depths, in particular because comprehensive imaging comes from surface waves, with previously discussed broad depth sensitivity.

2.3. Magnetotelluric Imaging

Magnetotelluric (MT) imaging provides 2-D and 3-D imaging of Earth's more resistive lithosphere and less resistive asthenosphere owing to its sensitivity to electrical resistivity differences related to temperature and conductive fluids. The MT method is particularly sensitive to locations of strong conductors, such as melts or partial melts which are able to indicate the transition from resistive lithosphere to conductive asthenosphere (Heinson, 1999; Praus et al., 1990). The method can resolve relatively thin conductive layers such as those that might be associated with melt accumulated in LAB channels (Parker & Whaler, 1981). However, the method can suffer from trade-off between anomalies that are strong and localized in depth and those that are weaker but distributed over broader depths (so-called conductance equivalence). As a consequence, MT data can be satisfied by either smooth or sharp gradients in depth, although most inversion schemes favor smooth models due to the reduction of nonuniqueness, for example, Occam-type inversions (Constable et al., 1987). MT resolution is confined by the diffusion feature of electromagnetic fields, which is different from seismic wave propagation. The value of MT imaging is that it provides additional constraints on melts, partial melts or volatiles (such as H_2O and CO_2), and viscosity and also has distinguishable sensitivity to such electrical properties from cold and resistive materials (Heinson, 1999; Liu & Hasterok, 2016; Naif et al., 2013; Wang et al., 2020) and therefore may be used in conjunction with seismic imaging to unambiguously determine the physical and chemical properties of the Earth. In particular, the partial addition of fluids, either hydrous or silicate melts, affects the electrical properties of a rock by an order of magnitude or more, a much stronger response than for seismic properties. Temperature and salinity of hydrous fluids, while invisible to the seismic method, have an impact on electrical resistivity that can be imaged using the MT method. Pore and/or grain boundary geometry can create an electrical anisotropy that can be detected in MT data and provide useful constraints on deformation. Thus, for example, Naif et al. (2013) used MT data to detect enhanced conductivity in the plate-motion direction for partial melts at the LAB, interpreted as shearing. Chesley et al. (2019) observed a similar anisotropy in subsolidus lithospheric mantle using a related electrical method (controlled-source sounding), and Wang et al. (2020) estimated melt fraction at the LAB beneath Mid-Atlantic Ridge using MT data.

Resistivity models indicate a similar pattern to the other lithospheric thickness estimates, with the continents being more resistive to deeper depths than the oceans (Figure 11) (Hirth et al., 2000; Jones, 1999; Lizarralde et al., 1995; Schultz et al., 1993). Estimates for the resistive lithospheric lid thickness from MT data in continents range from ~50–400 km depth, for example, ~60–170 km beneath the Eastern Great Basin and Colorado Plateau (Liu & Hasterok, 2016; Wannamaker et al., 2008), <50–300 km beneath the Yellowstone hot spot area (Kelbert et al., 2012; Zhdanov et al., 2011), ~100–300 km beneath the northern Canada (Jones et al., 2003; Jones et al., 2005), and ~160–250 km beneath cratons in southern Africa (Evans et al., 2011; M. R. Muller et al., 2009). Korja (2007) summarized that the electrical lithospheric lid varies from 45–400 km in Europe, such as 45–100 km thick under the extensional Pannonian Basin (Ádám & Wesztergom, 2001; Cerv et al., 2001) and 150–350 km thick beneath the Fennoscandia (Hjelt et al., 2006; Smirnov & Pedersen, 2009). The electrical LAB is estimated to be 50–80 km in northeastern China (Wei et al., 2008) and 80–120 km in the Qiangtang Terrane, central Tibet (Vozar et al., 2014). Beneath young seafloor estimates for the resistive lithospheric lid are thin, <80 km, near the East Pacific Rise, ~17°S (Baba et al., 2006; Evans et al., 1999) and 9°N (Key et al., 2013), beneath the area near the Mid-Atlantic Ridge ~2°S (Wang

et al., 2020), beneath the area near the ultraslow-spreading Mohns Ridge (Johansen et al., 2019), and beneath the region offshore Nicoya Peninsula, Costa Rica ~9°N (Worzewski et al., 2011). A conductive LAB channel was reported beginning at 45 km depth beneath 30–40 Myr seafloor off central America (Naif et al., 2013) and beneath <30 Myr seafloor at Mid-Atlantic Ridge (Wang et al., 2020). Beneath older seafloor in the Pacific the lithosphere could be as thick as 100 km (Hirth et al., 2000) (Figure 11). Although broad-scale age progression is supported by MT, imaging at the Mid-Atlantic Ridge found evidence for a smooth age-depth progression of the LAB in one location and an undulating LAB, underlain by punctuated conductivity anomalies in another location (Wang et al., 2020). The anomalies could be caused by local upwellings, and the result suggests that in detail structure is likely more variable.

Studies show that the relation of the electrical LAB obtained through MT data and the seismic LAB obtained from a variety of methodologies is still elusive due to different data sensitivity. Beneath 70 Myr old Pacific lithosphere, there is general agreement between the 1-D seismic velocity profile and the 1-D resistivity profile, where the LVZ is characterized by a small volume of interconnected melt (Selway & O'Donnell, 2019). Beneath young seafloor near the equatorial Mid-Atlantic Ridge there is good agreement between the location of the slowest seismic velocity anomalies and the lowest resistivity anomalies, which also generally occur beneath the strongest LAB phases in Sp imaging (Harmon et al., 2020; Rychert et al., 2019; Wang et al., 2020). Beneath the Piedmont and Coastal Plain in the southeastern United States, the electrical LAB is ~50 km deeper than the seismic LAB obtained from seismic tomography (Murphy & Egbert, 2019). In Precambrian Europe the electric LAB is ~75 km deeper than the seismic LAB resolved by receiver functions, while Phanerozoic Europe shows a consistent LAB from the two (Jones et al., 2010). A low-velocity anomaly was also observed deeper than conductive anomaly at about LAB depths beneath the Yellowstone hot spot area (Kelbert et al., 2012). Although the seismic and MT sometimes agree, apparent discrepancies are not surprising, likely caused by the different sensitivities of the methodologies to Earth properties. Thus, more information is necessary to detail the relationships between the electrical LAB and seismic LAB, especially beneath continents and in particular cratons (Eaton et al., 2009).

2.4. Other Observations

Heat flow measurements are used to calculate geotherms in an attempt to estimate the depth of the geotherm-adiabat intersection, that is, the depth extent of colder lithosphere, characterized by conductive heat transfer to Earth's surface assuming a thermally defined plate. This approach requires that the heat flow-derived geotherm estimates are corrected to account for radiogenic heat production, which is done by calibrating with xenolith pressures and temperatures (Artemieva, 2006; Hasterok & Chapman, 2011) and/or electromagnetic profiles (Artemieva, 2006). In the best fitting models of heat flow the LAB deepens with age beneath young lithosphere from 0 to 90 km depth, with very little further deepening beneath older seafloor according to the plate or Chablis models (Doin & Fleitout, 1996; Hasterok, 2013; Stein & Stein, 1992) (Figure 5). Beneath continents there is also a deepening of the adiabat intersection toward continental interiors from 90 to 300 km (Artemieva, 2006) (Figure 5). The LAB is assigned a single depth in these models, although the associated predicted gradient in temperature and also predicted seismic velocity are gradual occurring over 50 km even beneath young seafloor (Figure 6a).

Viscosity estimates based on isostatic readjustment of the crust and mantle after loading and unloading of water or ice or estimates based on postseismic relaxation provide a means to estimate the thickness of the lithosphere that behaves rigidly over geologic timescales. The methods use a viscoelastic model to invert timing and spatial patterns of rebound or subsidence for viscosity, elastic parameters, and density. The lithosphere is associated with the high-viscosity lid, while the asthenosphere is defined by the viscosity minimum below. Glacial isostatic adjustment data have been modeled to understand the viscosity structure of the Earth as well as sea level rise in response to deglaciation, particularly from the Fennoscandia and Hudson Bay data (e.g., Mitrovica & Forte, 2004) and also glacial retreat in places like Iceland (Figure 12; Fleming et al., 2007). These studies find a global average high-viscosity region in the upper 80 km, with a low-viscosity asthenosphere between 100 and 200 km depths. Studies of lake subsidence/rebound after climate or man-made induced lake level changes provide another probe for crustal and mantle viscosity. In the western United States in the Basin and Range studies of Lakes Bonneville and Lahontan estimated relatively thin high-viscosity lithospheres (40 and 80 km, respectively) with low-viscosity asthenosphere extending down to 160 km depth, with minimum values of effective viscosities of 10^{17} to 10^{18} Pa s

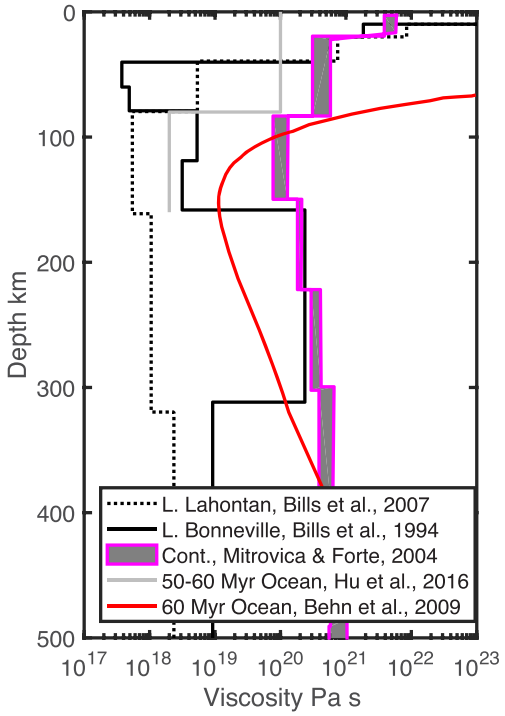

Figure 12. Viscosity profiles. Continental interior viscosity bounds are from the joint inversion of glacial isostatic adjustment data from Fennoscandia and Hudson Bay along with convection constraints based on observations of the geoid and seismic tomography (purple lines) (Mitrovica & Forte, 2004). Continental viscosity estimates for the tectonically active Basin and Range from Lake Bonneville (black dashed line) (Bills et al., 1994) and from Lake Lahontan (black line) (Bills et al., 2007) are from the inversion of variability in paleoshoreline data. The viscosity profile from the Indian Ocean is derived from postseismic relaxation data (gray line) (Hu et al., 2016). Viscosity prediction based on flow laws from laboratory experiments and incorporating grain size evolution (Austin & Evans, 2007) are shown for a 60 Myr old oceanic plate moving at 10 cm/year with potential temperature 1350°C assuming mild hydration (1,000 H/10^6 Si) (red line) (Behn et al., 2009).

(Figure 12). The Basin and Range is a tectonically active rifting region, with Quaternary volcanism, and it was noted that these observations might be close to oceanic type viscosities rather than viscosities estimated from beneath glaciated passive continental regions (Bills et al., 1994, 2007). Studies of submarine earthquakes and their postseismic relaxation via geodetically observed motions provide a means for estimating viscosity beneath the oceans (Hu et al., 2016; James et al., 2009). For instance, a two-layer model in the Indian Ocean found an 80 km thick lithosphere with underlying viscosity estimated to be 10^{18} Pa s (Figure 12) (Hu et al., 2016), while a joint postseismic relaxation and glacial isostatic rebound study estimated asthenospheric viscosities of 10^{18} to 10^{19} Pa s beneath Cascadia (James et al., 2009). A study that modeled GPS responses to seasonal loading estimated that the asthenospheric viscosity could be no lower than 5×10^{17} (Chanard et al., 2018). The sharpness of the viscosity drop varies between the different types of studies. The glacial isostatic adjustment viscosity model is relatively smooth, dropping a maximum of ~1 order of magnitude with change in model depth, which likely reflects the combination choice of Occam inversion as well as relatively modest asthenospheric low viscosities (Mitrovica & Forte, 2004). The lake studies and the postseismic relaxation estimates have stronger drops in viscosity, 2–3 orders of magnitude with a change in model depth. The lake models had no smoothing imposed, although the authors chose relatively coarse parameterizations (Bills et al., 1994, 2007), while the postseismic relaxation models are also coarse. Overall, sharp drops in viscosity, 2–3 orders of magnitude, are possible at the LAB based on these models.

Effective elastic thickness (*Te*), or the depth to which the lithosphere responds elastically when loaded, for instance, by glaciers and/or topography is sometimes related to the LAB. The estimates involve calculating the coherence and admittance between gravity and topography (Forsyth, 1985). Alternatively, estimates of *Te* can be made based on models of crustal and mantle structure, composition, and material properties (Tesauro et al., 2012) or by fitting the shape of bending plates at subduction zones (Levitt & Sandwell, 1995) or numerical modeling of rheological properties to fit bathymetry (Zhong & Watts, 2013). *Te* estimates provide information about the strength of the plate in response to vertical loading given an elastic or viscoelastic response, primarily sensitive to Young's modulus. The rheological LAB reflects the viscous response to shearing of the mantle. Therefore, although *Te* may have a relationship to the LAB, given that temperature influences both the depth of the elastic response to vertical loading and the viscous response to shearing, this depth is not necessarily the same thing as the LAB. Nevertheless, we present it and discuss it as well, for comparison purposes. *Te* is frequently calculated globally on the continents, albeit with broad spatial resolution and regionally beneath oceans where estimates are primarily limited to the locations of seamounts or trenches. Beneath the oceans the maximum extent of *Te* results increase with age according to the predicted depth of the ~600°C isotherm, which is thought to be the brittle ductile transition (Figures 5 and 10) (Burov & Diament, 1995; Watts, 2001). Beneath the continents *Te* increases toward continental interiors, where it reaches 200 km (Figure 5) (Audet, 2014; Audet & Burgman, 2011). Models of *Te* implicitly have a sharp rheological contrast built into them, as the elastic plate overlies an inviscid fluid.

3. Resolution—Sharp Discontinuities and Channels Versus a Gradual LAB

Here we compare the resolution of receiver function, surface wave, and MT data to two structures, including a sharp and a smooth drop in seismic velocity and resistivity (Figure 13). In the sharp velocity model, the lowest velocities are ~4.05 km/s in the mantle, with a 15% velocity drop beneath the fast lid, while the smooth model reaches a minimum of 4.28 km/s. We assume a constant *Vp*/*Vs* ratio in the seismic models.

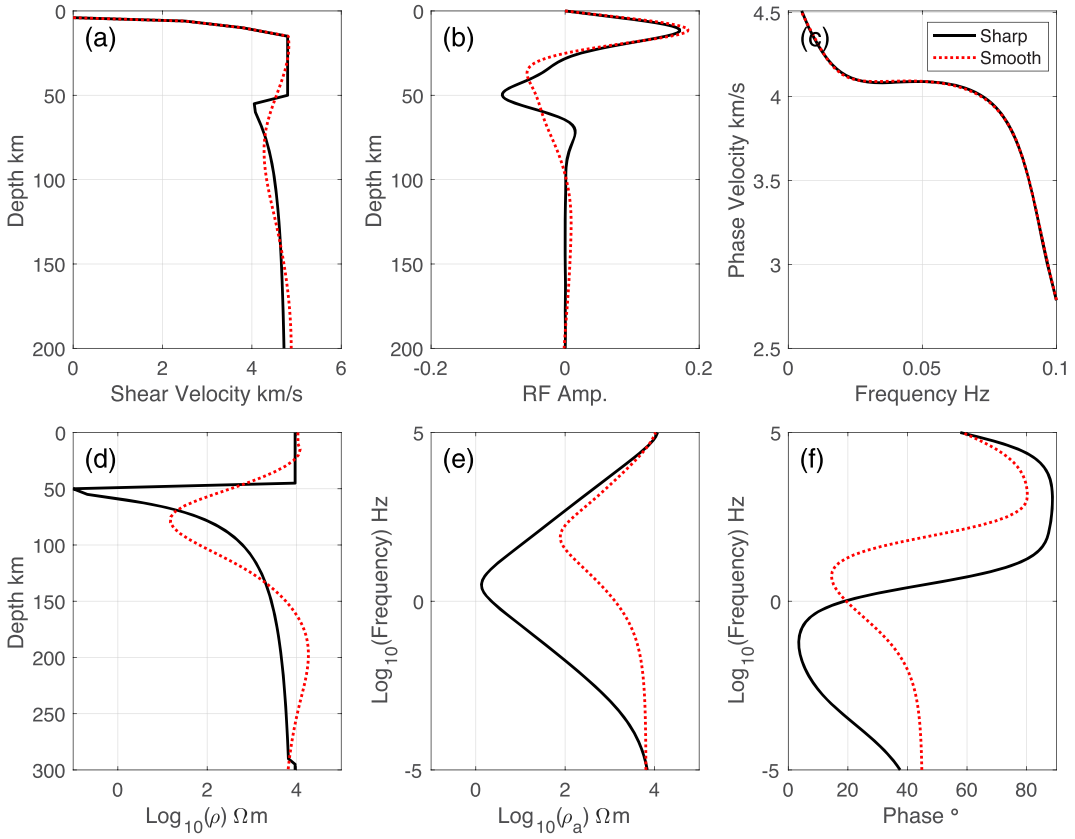

Figure 13. Resolution demonstration. Here we demonstrate seismic and magnetotelluric imaging techniques for two different 1-D profiles. (a) Seismic velocity profiles tested include a sharp (black) and a smooth (red dashed) drop with depth. (b) The corresponding *Sp* receiver functions show that only the model with the sharp drop gives a large negative converted phase. (c) The surface wave phase velocities are indistinguishable for both the sharp and the gradual drops. (d) A profile corresponding to an exponential relationship between resistivity and shear wave velocity profile in (a). (e) The corresponding apparent resistivity amplitude and (f) phase for the models in (d). The difference between the sharp and smooth models would be easily resolved in the resistivity and receiver functions but not resolvable in the surface wave data alone. Similarly, if sharp velocity decreases are required by scattered waves, surface wave data can typically be satisfied with such a structure, and therefore, the velocity decrease is very likely sharp in such locations.

The shear wave velocities and velocity drops are roughly consistent with minima observed in several oceanic studies. To relate the seismic velocity to resistivity, we use an exponential relationship, which yields resistivity <1 $\log_{10}$ Ω m for shear wave velocities <4.2 km/s and resistivity ~4 $\log_{10}$ Ω m for shear wave velocities above 4.5 km/s. This again yields a similar range as the resistivity observed in the ocean basins in some locations. We use a 1-D forward calculation for MT apparent resistivity and phase.

The smooth drop does not produce a conversion in the receiver functions and also gives a weaker resistivity anomaly with a minimum of ~1.87 $\log_{10}$ Ω m. In addition, the phase is substantially different between the sharp and smooth models, with almost 90° total range in the sharp, compared with 60°. The sharp drop gives a strong, negative receiver function phase and a lower resistivity anomaly of ~0.13 $\log_{10}$ Ω m. However, the surface wave data is fit equally well by both models, with differences in the fundamental mode of Rayleigh wave dispersion <0.01 km/s, well within typical observational errors.

MT need not match the seismic results given that the two have different sensitivity to Earth properties. However, velocity profiles from receiver functions and surface waves should be somewhat comparable. Therefore, we further investigate the degree to which surface wave data could be consistent with different velocity structures, including sharp velocity gradients.

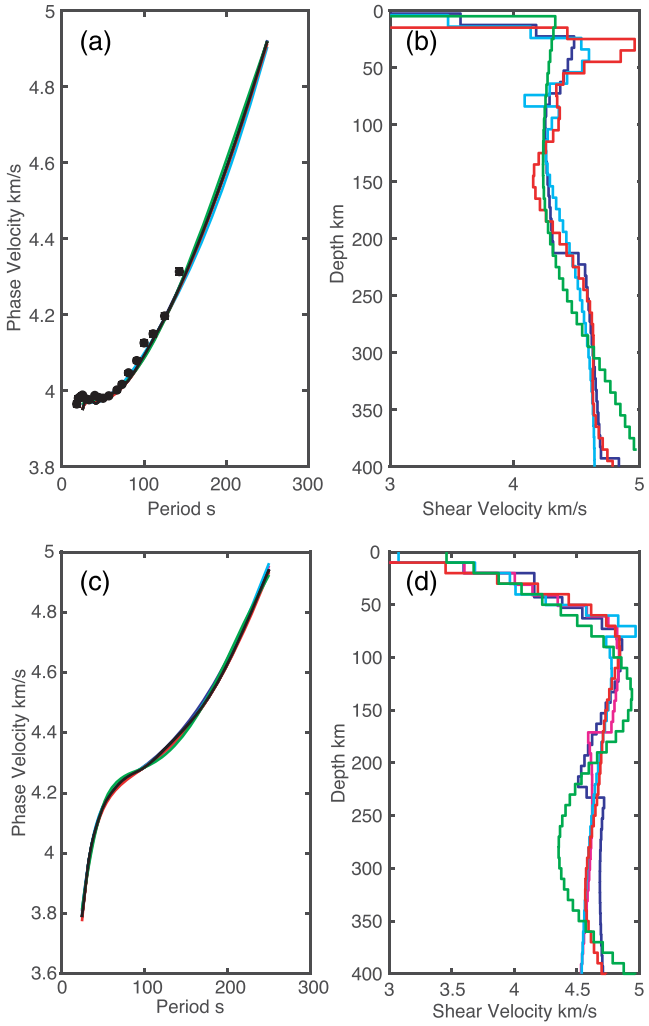

Figure 14. Examples of possible variations in 1-D shear velocity structure that satisfy surface wave dispersion. (a) One-dimensional phase velocities at the equatorial Mid-Atlantic Ridge from a global model (solid, black) (Ekstrom, 2011) and the in situ regional study (dots) (Harmon et al., 2020) compared to synthetic fits corresponding to the shear velocities in (b). (c) One-dimensional phase velocities from the cratonic region of North America according to the 3SMAC model from a global model (solid, black) (Ekstrom, 2011) compared to synthetic fits corresponding to the shear velocities in (d). All shear synthetic phase velocity profiles fit the data within error, within 0.05 km/s.

For oceanic lithosphere at the equatorial Mid-Atlantic, we find that the average 1-D phase velocity profile from surface waves can be fit within error (±0.05 km/s) with a variety of 1-D shear wave velocity profiles, including the case with a sharp 8% drop at 50 km depth (Figure 14). Similarly, the 10–18 km thick channels imaged by active source studies (Mehouachi & Singh, 2018; Stern et al., 2015) can be accommodated in surface wave models (Figure 14). No channel result has been colocated with a scattered wave report of a single negative discontinuity, so it is not clear if the two need to be reconciled. One possibility is that melt channels are transient or not laterally pervasive. Another possibility is that active source studies resolve the shallowest melt channel, and multiple, finely spaced melt channels exist at depth, with a gradual decrease in the amount of melt with depth (Rychert & Harmon, 2018), similar to layered melt models (Kawakatsu et al., 2009).

Beneath continental interiors most receiver function imaging finds discontinuities shallower (60–110 km) than the gradual surface wave velocity drops, and these are often interpreted as midlithospheric and caused by strong changes in composition (Ford et al., 2010; Rader et al., 2015; Selway et al., 2015). We show midlithospheric discontinuities of 5–6% can be consistent within error of phase velocities determined from surface waves (Figure 14). *SS* precursor imaging found discontinuities at 130–190 km attributed to the base of the plate (Tharimena, Rychert, & Harmon, 2017). We show that beneath cratonic North America a moderate velocity drop (~4%), at the lower limit of the *SS* result, can be accommodated by the surface wave phase velocities. This suggests that sharp discontinuities at the base of the continents as imaged by *SS* are also not necessarily inconsistent with the surface waves.

4. Comparisons

In light of the previously discussed resolution tests, we proceed making comparisons among studies, assuming that where scattered waves image sharp discontinuities, this reflects the real Earth structure. In all cases besides the very shallow MLDs beneath cratonic interiors, we assume that these also represent the LAB. We make some comparisons among methods to evaluate the significance of the differences and similarities of lithospheric thicknesses from a variety of models. The overall agreement among a variety of independent observables regarding lithospheric thickening with age from the youngest oceans to the oldest continents suggests that to first-order temperature dictates the thickness of the plate. However, there is also a fair amount of variability among methods and also among individual profiles included in age averages of a single method that may also be important.

4.1. Oceans

Heat flow, *Te*, and seismic imaging all support an age progression in lithospheric thickness between the youngest and the oldest seafloor (Figures 5 and 10). *Te* is much shallower than the others probably owing to its different sensitivity as described above. Beneath the youngest seafloor (<10 Myr) scattered wave depths are consistently deeper than the HSC and plate model isotherms beneath the youngest seafloor (<10 Myr) (Figure 10). This can be explained by differences in spreading rate. In 2-D models lateral cooling is predicted to thicken the lithosphere at intermediate and slow spreading ridges, in comparison to faster spreading centers, which better resemble HSC (Morgan et al., 1987). The scattered wave results from young seafloor in the compilation in Figure 10 come from the intermediate spreading Gorda and Juan de Fuca Ridges and the slow-spreading Mid-Atlantic Ridge. Beneath older seafloor scattered wave images are in good general

agreement with age-averaged surface waves, that is, at depths within the gradual surface wave velocity drop and/or generally at the depth of the minimum surface wave velocity in depth (orange x's, Figure 10). General agreement between the scattered wave depths and surface waves combined with the fact that sharp gradients are required by scattered waves suggests that the base of the plate includes a sharp drop in velocity at least in the many locations where scattered waves have imaged the LAB. The result suggests an oceanic LAB around the depth of the 1100°C isotherm predicted by the plate-cooling model with a wider range of depths reported at older ages, >36 Myr, and in hotpot affected regions (Figure 10). These variations suggest that ocean LAB depths are likely more variable than the simple smooth thermal models predict (Harmon et al., 2020).

The depth of the 1100°C isotherm is predicted to be much shallower than the depth of the 1350°C isotherm that would be expected for the classical thermal model, but 1100°C is a meaningful value for mantle rheology, which is highly temperature dependent. There are several important changes in deformation mechanisms and strength for mantle rocks that occur with increasing temperature and pressure. As discussed earlier, at <600°C, the lithosphere is thought to deform primarily brittlely (Byerlee, 1978) and is commonly understood to be the brittle-ductile transition, or the maximum depth extent of seismicity and also estimated *Te* (Watts et al., 2013). For temperatures > ~600°C, the lithosphere enters the ductile deformation regime. Up to ~1000°C low-temperature plasticity is active (Mei et al., 2010). Strain rates predicted by this mechanism are very low, $\ll 10^{-15}$ s^{-1}, for typical oceanic geotherms and tectonic stresses (<100 MPa) (Mei et al., 2010), indicating that the lithosphere is relatively strong. At temperatures > ~1000°C high-temperature dislocation and diffusion creep become the dominant deformation mechanisms and the predicted strain rates increase rapidly resulting in a strong drop in effective viscosity for tectonic stresses (<100 MPa). For instance, numerical parameterizations of the flow laws including grain size evolution predict a viscosity change from 10^{24} Pa s at low temperatures (~900°C) down to ~10^{19} Pa s near the depth of the 1350°C isotherm of the HSC model (Figure 10b; Behn et al., 2009). We find good agreement between the depths of the discontinuities from scattered waves and the predicted center of the gradient in viscosity from the numerical parameterization, near 10^{21} Pa s, which also falls very close to the depth of the 1100°C isotherm predicted by HSC (Figure 7). We also note that the minimum viscosity from the laboratory calibrated flow laws (Behn et al., 2009) is similar but still 1–2 orders of magnitude greater than the minimum estimates of viscosity from observations (Figure 12). For example, beneath the Basin and Range region, estimates of viscosity structure in the asthenosphere ranged from 10^{17} to 10^{18}. This suggests that another mechanism beyond dislocation creep may be needed.

Partial melt is another factor that could be important at depths near the predicted 1100°C isotherm. For instance, beneath young seafloor (<16 Myr) the predicted solidus for a mildly hydrated mantle falls very close to the predicted 1100°C isotherm (Katz et al., 2003) suggesting partial melt could be stable in the mantle beneath (Figure 10). At older ages if we assume a 90 km thick plate model, as suggested by the best fit to heat flow data (Hasterok, 2013), melt is predicted to be stable at temperatures above 1280°C, that is, over wide swaths of the mantle assuming a moderately hydrated mantle (500 ppm) (area within the pink lines (solidi), Figure 10). The addition of carbonatitic melts could also make melt stable at cooler temperatures and shallower depths and potentially cause deeper melts to form (Hirschmann, 2010).

A high degree of depth variability at any single age from surface waves and scattered waves could be consistent with lateral heterogeneity. Age-averaged surface waves show a smooth increase in LAB depth, which is a good reflection of overall properties (Figures 4–6 and 8), whereas individual 1-D profiles and also individual transects show more variability (Figures 7 and 8). Of course, lateral variability in the surface wave profiles could be an artifact of resolution. Similarly, scattered wave variability could be the result of varying assumptions, methodologies, and resolutions. However, another possibility is that the variability is real. This notion would also be consistent with *SS* precursor imaging that found lateral variability in the character of the velocity gradients not necessarily related to age, with about half the Pacific characterized by two negative discontinuities in depth (Tharimena, Rychert, Harmon, & White, 2017). The result could also be explained by LAB depth variations that occur within the bin size or Fresnel zone of the waves, suggesting that the scatter in the compilation may be real. Overall, it suggests that an overarching process such as temperature controls the average thickness of the plate; other processes are responsible for deviations.

The many sharp discontinuities imaged beneath the ocean suggest that the oceanic LAB is sharp, at least in the several locations where it has been sampled. In fact, active source estimates are as sharp as 1 km or less

(Mehouachi & Singh, 2018; Stern et al., 2015). Of course high-resolution imaging of the LAB beneath the oceans is far from comprehensive, and it may be that in some cases the gradient is gradual, and underlying seismic and conductivity anomalies are less intense. For instance, the resistivity anomaly beneath 70 Myr old lithosphere in the NoMelt region is only moderate (~1.7 $\log_{10}$ Ω m) and interpreted as not necessarily requiring anything but trace amounts of melt (<0.1%) (Sarafian et al., 2015). Variability in the presence of melt could be explained by local or regional mantle dynamics; if, for instance, the mantle is upwelling or downwelling in a particular area as part of a small-scale convective system, it could sharpen thermal contours and/or cause decompression melting, which will be discussed further in later sections.

4.2. Continents

Heat flow, *Te*, and seismic imaging all support a rough increase in lithospheric thickness from the Phanerozoic to the oldest Proterozoic and Archean continental interiors (Figure 5). The youngest parts of the continents-the Phanerozoic, made up of mobile belts, accreted terranes, and so forth, are generally characterized by thinner lithosphere, mostly ranging from 60–110 km. Older (>500 Myr) continental interiors have thickness estimates that range from 130 to >350 km depending on the choice of observable and assumptions used to relate it to lithospheric thickness. While the division between generally thinner Phanerozoic and thicker Proterozoic/Archean lithosphere is robust, there is not a simple monotonic thickening with age. A large amount of variability is observed across Phanerozoic regions and continental interiors and continental interiors.

Phanerozoic continental lithosphere encompasses a wide variety of tectonic structures from mountain belts, rifts, and passive accreted terranes. Averaging over this variability results in a 1-D average profile without a clear LAB (Figures 4 and 7). However, several individual regional studies find sharp discontinuities in Phanerozoic regions that fall within the gradual surface wave velocity drops (Fischer, 2015; Fischer et al., 2010; Rychert et al., 2010, and references therein). This suggests that in these regions the LAB in Phanerozoic regions is sharp and not defined by temperature alone.

Comparison of the average shear wave velocity profiles of individual cratons differ from one another, suggesting structural variability in addition to variations in thickness (Figure 7). At an even finer level, within a given craton there is a lot of variability among individual 1-D profiles (Figure 7). Schematics of the continents based on seismic wave observations are typically smooth because global surface wave models have lateral resolution on the order of >500 km, reflecting average properties (Figure 8), whereas more complex LAB topography is interpreted when geochemical analyses of xenoliths origin depths are considered, which has resolution at the individual kimberlite scale (Figure 8; Griffin et al., 1999).

Interestingly, while the maximum depth extent of the continental signature is frequently highlighted and discussed, the deepest depth is only reached over a small portion of the tectonic regime in the models shown here. For example, lithospheric thickness from the LSmean (Steinberger & Becker, 2018) model reaches >250 km over <6% of the area of any individual continental interior defined by the 3SMAC model (Nataf & Ricard, 1996). Similarly, the thickest (>250 km) areas from the heat flow model are realized over <14% of the area of any of individual 3SMAC continental interior (Artemieva, 2006). If we instead average lithospheric thickness from heat flow or surface waves over the "Archean craton" regions from 3SMAC (Nataf & Ricard, 1996), the average thickness for the cratons ranges from 150–200 km, similar to the 130–190 km depth range based on *SS* precursors and the deepest origin depths of diamonds (Figures 5, 7, and 8; Tharimena, Rychert, & Harmon, 2017). Overall, this suggests that although there is a lot of emphasis on the deepest depths of continental interiors, there may also be strong lateral variations in the thickness of continental interiors. On average continental thicknesses are generally moderate (130–200 km), with smaller regions of extreme thickness. One possible explanation for the thickening could be local downwellings related to small-scale convection.

Whether or not sharp discontinuities exist at deep depths (>150 km) beneath the cratons is debated. Reports from receiver functions are rare (Kumar et al., 2007; Vinnik & Farra, 2002) and some report the absence of discontinuities (Abt et al., 2010; Ford et al., 2010; Mancinelli et al., 2017), whereas *SS* precursor studies detect discontinuities with a range of sharpness (7–9% over 14–52 km depth) at 130–190 km beneath all continental interiors besides India (Tharimena, Rychert, & Harmon, 2017). This may be explained by differences in resolution and sensitivity. *SS* negative discontinuities could be preferentially enhanced by a decrease in density

or an increase in radial anisotropy with depth (Rychert & Harmon, 2017), although neither is necessarily expected. The continents are thought to be low in density (Jordan, 1988), and radial anisotropy is observed to decrease with depth in the 130–190 km depth range (French et al., 2013; Tharimena, Rychert, & Harmon, 2017). Alternatively, a more complex structure, such as that implied by geochemistry, where the cratonic LAB varies laterally in thickness (Figures 1 and 8a), could explain the apparent discrepancy between singular, strong discontinuities imaged by *SS* precursors and the sporadic imaging by receiver functions. *SS* has broad lateral resolution (~10°) and would be sensitive to generally pervasive discontinuities, even in the presence of smaller-scale variations, whereas laterally variable LAB depths could prevent consistent imaging by Sp receiver functions (Mancinelli et al., 2017), which have smaller lateral sensitivity, a couple of degrees, and also have difficulty imaging sloping discontinuities (Lekic & Fischer, 2017). Of course, if a sharp change in density (decrease) or anisotropy (increase) did exist at these depths (Rychert & Harmon, 2017), for instance, if melt is trapped at the base of a permeability boundary or if strong flow or melt layering exists beneath the *SS* discontinuity, not only would these enhance an *SS* reflection, but they would also likely represent the base of the plate. Similarly, upwellings associated with small-scale convection could tighten thermal contours, reduce lithospheric thickness in some locations, and also result in decompression melting.

5. Definition of the LAB

Sharp discontinuities that fall within the gradual drops in velocity from surface waves and also the predicted gradual drop from HSC or plate models of the ocean add support that these are related to the LAB. As we have already discussed, sharp velocity discontinuities are not necessarily discrepant with the surface waves. However, sharp discontinuities are discrepant with predictions for a purely classical thermal model of the lithosphere. The predicted velocity gradient for the HSC and plate models beneath the oceans, including the effects of attenuation predict gradual gradients (Figure 6a). These cannot explain the sharp gradients required by reflected and converted waves (Rychert & Harmon, 2018; Rychert et al., 2018a).

Our result shows that temperature, alone, cannot explain the many LAB observations throughout the oceans and continents. This implies greater complexity than that of the thermal models and the explanation is currently debated. An increase in hydration and/or a decrease in grain size with depth could exist. Both continental and oceanic lithosphere are typically thought to be relatively depleted and dehydrated by past melting events, and their longevity could promote grain growth (Austin & Evans, 2007; Gaherty et al., 1999; Jordan, 1988). However, numerical modeling with grain-size evolution (Austin & Evans, 2007) with hydration as a defect with a composite diffusion dislocation creep rheology found that even saturated water conditions or extreme grain-size variation cannot explain even small 3% velocity contrasts at 70 km depth beneath 100 Myr old seafloor (Behn et al., 2009). Recent forced oscillation experiments at seismic frequencies on undersaturated olivine found no sensitivity to hydration, instead finding a dependence on mantle redox conditions (Cline et al., 2018). However, this would predict that detections of sharp discontinuities from scattered wave observations would be limited to large redox areas such as subduction zones, which has not necessarily been implied by observations. It has been proposed that elastically accommodated grain boundary sliding would increase the impact of hydration on seismic waves and create an apparent seismic velocity discontinuity at 70 km beneath the oceans that may not necessarily be related to the base of the plate (Karato et al., 2015). However, several predictions of the model, such as the sharpening at older ages are not consistently observed (Rychert et al., 2018a). It has been suggested there is a stronger decrease in seismic velocities at near-solidus conditions (Yamauchi & Takei, 2016), although the expected depths and amplitudes of the conversions are not sufficient to explain all observations (Rychert et al., 2018a).

Depth variation in seismic anisotropy, either radial or azimuthal, has been proposed as an explanation for sharp discontinuity observations without necessarily being the LAB, as discussed in section 2.2. Anisotropy is not a simple explanation for all scattered wave observations. For instance, variations in the polarity of *SS* precursors are expected for a discontinuity defined only by a variation in azimuthal anisotropy (Rychert, Harmon, & Schmerr, 2014; Rychert, Schmerr, & Harmon, 2012), although positive polarity discontinuities are not typically detected by *SS* precursor studies near LAB depths (Tharimena, Rychert, Harmon, & White, 2017). In addition, anisotropy from olivine alignment does not explain highly conductive regions imaged by MT (Yoshino et al., 2006). Finally, neither radial anisotropy caused by compositional layering

nor olivine can explain large apparent velocity discontinuities from receiver functions (Rychert & Harmon, 2017). Overall, while anisotropy is important, and likely influences some constraints, it cannot universally explain the observations of sharp LABs (Rychert & Harmon, 2017).

Finally, a small amount of melt (Rychert et al., 2005, 2007; Tharimena, Rychert, & Harmon, 2017) or melt layers (Kawakatsu et al., 2009) could rapidly reduce seismic velocity beneath the observed discontinuities. Melt provides the simplest explanation for observations of strong anomalies and sharp discontinuities from a variety of independent methods and interpreted as LAB (Kawakatsu et al., 2009; Naif et al., 2013; Stern et al., 2015). There is debate about whether or not melt could exist in the mantle at a time and length scale to be imaged by seismic waves because melt is expected to be buoyant and melt compaction theory suggests it should rapidly rise through the mantle (Mckenzie, 1984). For instance, melt might be expected beneath hot spots, mid-ocean ridges, subduction zones, and/or even areas of general upwelling, for instance, at the edge of a continental keel (Till et al., 2010). However, beneath continental interiors and also older oceans temperatures are predicted to be cold.

One possibility is that the presence of volatiles such as water or carbon lowers the melting temperature and facilitates melting (Hirschmann, 2010). Increased availability of volatiles could be caused by the instability of hydrous phases in mantle peridotite (Green et al., 2010) or a sharp decrease in the solubility of water in nominally anhydrous minerals in the asthenosphere (Mierdel et al., 2007). Melt could also exist if there are local or regional upwellings, perturbing the thickness of the thermal lithosphere, sharpening thermal gradients, and also causing decompression melting. The melt may exist at a depth of neutral buoyancy, which could be relatively constant at old ages (Sakamaki et al., 2013) or ponded beneath a permeability boundary (Sparks & Parmentier, 1991). The amount of melt required to explain the seismic observations ($\leq$1%) (Chantel et al., 2016; Hammond & Humphreys, 2000) or more (Clark & Lesher, 2017) would also significantly reduce the viscosity of the mantle and allow it to shear more easily and likely convect (Hirth & Kohlstedt, 1995; Jackson et al., 2006), thus resulting in a plate base where relative flow becomes nonnegligible. Therefore, the presence of melt would define the plate.

6. Melt in Many Forms

A wide variety of observations suggest that melt may define the plate. Exactly how much melt is required, how it is configured, and where it exists have important implications for our understanding of mantle dynamics. However, there is wide variability among studies as to the character or geometry of the melt.

Partial melt is suggested over a range of length scales and in a variety of shapes beneath ridges based on observational constraints. Melt is interpreted over a broad asymmetrical triangular area (>200 km wide), based on slow surface wave shear velocities at the East Pacific Rise at 17°S (Figure 15) (Forsyth et al., 1998). Melt is interpreted in a narrow (<60 km), symmetric zone just beneath the ridge based on a highly conductive region that is imaged at the 9°N segment of the East Pacific Rise (Key et al., 2013). Asymmetrically distributed melt is interpreted in a narrow area (<50 km) in the upper 30 km near the ridge axis and a wider area (>70 km) at depths >50 km, beneath the Mohns Ridge again based on imaging of a highly conductive region (Johansen et al., 2019). A melt channel is observed as geodynamically predicted at the Mid-Atlantic Ridge at 2°S (Wang et al., 2020).

There is similar variability in interpretations beneath older seafloor and continental regions. *SS* precursor studies of the entire Pacific Plate have interpreted the presence of melt beneath the plate pervasively (Rychert & Shearer, 2011), sporadically (Schmerr, 2012), or relatively pervasively but with laterally variable character beneath the plate (Tharimena, Rychert, Harmon, & White, 2017). As previously discussed in section 4.1 lateral variability in the depth of the melt and/or sporadic existence beneath continental interiors could reconcile apparent discrepancies among studies using a range of methodologies.

The character of the base of the LVZ, low-resistivity layer, and associated partial melting is also interesting and important. Melt could gradually drop off in depth as evidenced by observations of singular negative velocity gradients, unaccompanied by deeper positive phases (Rychert et al., 2018b; Tharimena, Rychert, Harmon, & White, 2017). Gradual dropoffs could be realized within punctuated upwellings from depth (Harmon et al., 2020; Rychert et al., 2019; Wang et al., 2020) and/or by increased spacing of melt-rich layers with depth (Kawakatsu et al., 2009). Or there could be an abrupt dropoff corresponding to the solidus

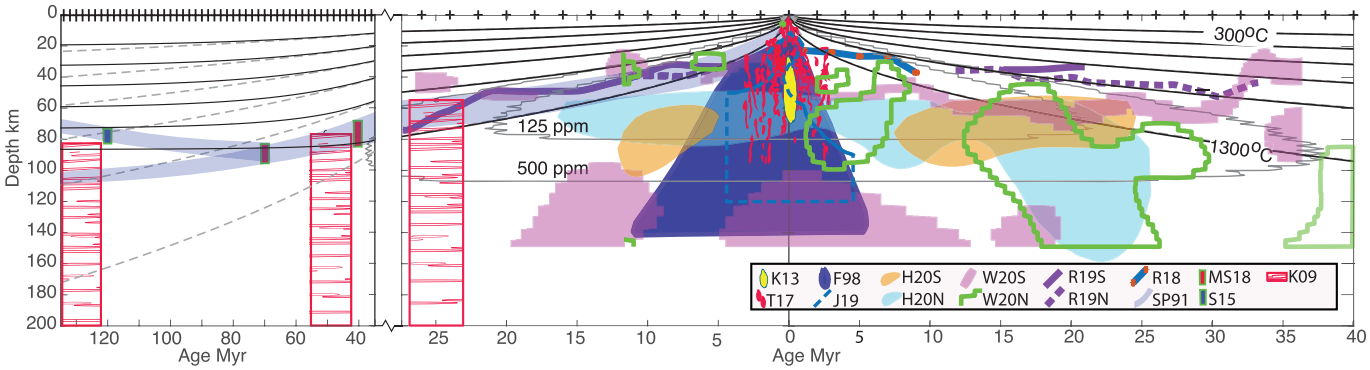

Figure 15. Comparison of melt inferred beneath ocean plates. Melt interpretations are shown based on the following criteria: low resistivity region (<1 $\log_{10}$ Ω m) at 9°N on the EPR (K13, yellow oval) (Key et al., 2013), as predicted by numerical model including two-phase flow (T17, red blobs) (Turner et al., 2017), wide melt triangle in schematic diagram (F98, solid purple triangle) (Forsyth et al., 1998) from slow anomalies in surface and body wave tomography (Forsyth et al., 1998; Toomey et al., 1998), low resistivity region (<1.4 $\log_{10}$ Ω m) beneath Mohns Ridge (J19, blue dashed outline) (Johansen et al., 2019), slow surface wave anomalies and low resistivity region (<1 $\log_{10}$ Ω m) beneath the northern (H20N, light blue and W20N, green outline, respectively) and southern (H20S, orange and W20S, purple, respectively) Mid-Atlantic Ridge segments of the PI-LAB experiment (Harmon et al., 2020; Wang et al., 2020), discontinuity imaged by receiver functions beneath Cascadia (R18, blue line with red circles) (Rychert et al., 2018a), discontinuity imaged by receiver functions near the Mid-Atlantic Ridge from the northern (dashed purple) and southern (solid purple) ridge segments (Rychert et al., 2019), ponding beneath a permeability boundary from numerical modeling (SP91, pale purple) (Sparks & Parmentier, 1991), layered as inferred from receiver function imaging beneath the Philippine and Pacific Plates (K09, red stripes) (Kawakatsu et al., 2009), in a channel that thins with age from active source reflections in two locations near the Mid-Atlantic Ridge (MS18, red rectangles outlined in green) (Mehouachi & Singh, 2018), and beneath the Pacific Plate descending beneath New Zealand (S15, blue rectangle outlined in green) (Stern et al., 2015). Although not shown, melt inferred from receiver functions likely falls off gradually with depth beneath the lines drawn here.

boundary at the base of the melt-rich layer. This is suggested, for instance, by the reflection pairs interpreted as a thin melt channel beneath older seafloor, >40 Myr (Mehouachi & Singh, 2018; Stern et al., 2015). Beneath volcanically active regions, abrupt bases beneath melt-rich regions, again related to the solidus, are interpreted based on receiver functions detections of positive phases. These include the Cobb hot spot in Cascadia (Rychert et al., 2018a), the Afar Rift (Rychert, Hammond, et al., 2012), Galapagos (Rychert, Harmon, & Ebinger, 2014), Iceland (Rychert, Harmon, & Armitage, 2018; Vinnik et al., 2005), and Hawaii (Li et al., 2000; Rychert et al., 2013). Positive phases have been imaged sporadically at deeper depths (>200 km) beneath normal seafloor and continents and often interpreted in terms of a change in anisotropy related to the base of the dislocation regime (Deuss & Woodhouse, 2004; Gaherty & Jordan, 1995).

Melt interpretations beneath some of the oldest seafloor may be associated with subduction dynamics (Figure 16). Melt in a ~25 km thick channel beneath the Cocos Plate just before subduction at the middle America trench is interpreted based on an imaged region of high conductivity (Naif et al., 2013). A very thin (10 km) melt channel beneath the Pacific Plate descending beneath New Zealand is interpreted based on active source reflections (Stern et al., 2015). Layered melt is interpreted beneath the Pacific Plate subducting beneath Japan based on receiver function imaging of a sharp, dipping discontinuity (Kawakatsu et al., 2009). A large zone of ponded melt that has ascended along the base of the slab is interpreted based on body wave tomography beneath Cascadia (Hawley et al., 2016). Intraplate volcanism is observed on the outer rise in some subduction centers such as the Petite hot spot, which may be related to geophysically inferred subslab melt (Hirano et al., 2006; Pilet et al., 2016).

Interestingly, many of these melt interpretations are supported by geodynamic models of melt generation and migration using porous flow approximations (Morgan, 1987) or compaction theory (Mckenzie, 1984) and two-phase flow (e.g., Spiegelman & Mckenzie, 1987). These models predict that melt migration occurs relatively quickly, in comparison to geological timescales, and leaves the system. However, models that allow the melt to be replenished from below in a steady or quasi-steady state predict the existence of partial melt over broad regions, in focused channels, and/or fingers with characteristics that evolve and through time. Melt channels ponding at the base of the lithosphere are proposed to explain focusing of melt toward the ridge from a broad melt triangle (Hebert & Montesi, 2010; Sparks & Parmentier, 1991) and are also suggested as a means of focusing melt from the back arc to the arc (England & Katz, 2010). More complex models of two-phase flow models predict melt originates at depth before rising in intricate vertical and

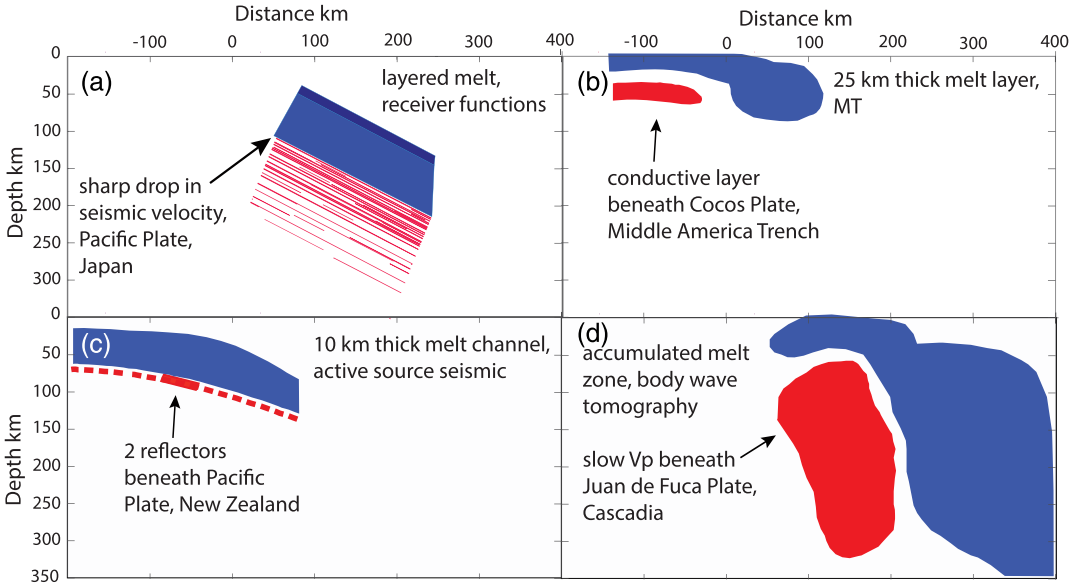

Figure 16. Melt beneath descending slabs. Several studies interpret melt (red) beneath the descending plate (blue) at subduction zones. Here the scale and location of the melt regions are compared with respect to distance from the trench at 0 km. (a) Melt beneath the Pacific Plate descending beneath Japan based on receiver function imaging (Kawakatsu et al., 2009). (b) Melt beneath the Cocos Plate before descending beneath Central America based on a high conductivity anomaly (Naif et al., 2013). (c) Melt in a 10 km thick channel beneath the Pacific Plate subducted beneath New Zealand based on active source reflections, with dashed section showing potential continuation (Stern et al., 2015). (d) Melt as an accumulation from upward flow beneath the Juan de Fuca slab subducting beneath Cascadia based on body wave tomography (Hawley et al., 2016). Subslab melt has also been hypothesized to explain the existence of petit spot volcanism on the Pacific Plate just before it descends beneath Japan, which might resemble, for instance, that in panel (b) or (c), but extending to at least −400 km distance from the trench (Hirano et al., 2006; Pilet et al., 2016).

subvertical melt channel structures beneath the ridge and out to ~4–7 Myr seafloor (Ghods & Arkani-Hamed, 2000; Sim et al., 2020; Turner et al., 2017). In some models with low spreading rates, channelization of melt occurs at the base of the lithosphere, in some cases with multiple channels forming at depth due to porosity waves forming (Ghods & Arkani-Hamed, 2000; Sim et al., 2020). The porosity waves are ephemeral in these models, with melt accumulating gradually, before leaving the system or freezing into the lithosphere. These temporal variations may explain global variations in observations of the amount, scale, location, and existence of melt. Future work will be needed to explore the feasibility of channel formation at older seafloor ages and 3-D geometries will be required to fully explore the geophysical observations.

7. Geodynamic Implications

The existence of plate tectonics and a low-viscosity asthenosphere has important implications for the evolution and dynamics of the Earth as well as planetary habitability. Here we explore these via geodynamic predictions.

The presence of plates and a low-viscosity asthenosphere may allow multiple scales of convection to occur, which is thought to be required to satisfy observations from subduction zones, hot spots, and mid-ocean ridges. Seismic imaging finds velocity anomalies and deflections in mantle transition zone discontinuities that support whole mantle convection at least beneath some subducting slabs and also major hot spots, whereas a lack of associated anomalies and several geochemical arguments suggest mid-ocean ridge upwellings originate from shallower, upper mantle depths. These different convection scales can be reproduced in geodynamic models that incorporate surface plates and temperature dependent viscosities when a low-viscosity asthenosphere is included (Zhong et al., 2000).

The presence of plates and a low-viscosity asthenosphere may also be important for initiating even finer-scale mantle convection, which is also thought to be required to explain many observations. In most geodynamic models small-scale convection arises as gravitational instabilities form at the base of the

cooling lithosphere, which then drip off into the asthenosphere below, which leads to mantle upwelling in response. The convection cells can then be organized by the plate motion into a helical pattern with an axis in the direction of plate motion, creating "Richter Rolls" (Richter, 1973). The net effect of small-scale convection would be to provide a constant heat flux in an average sense to the base of the plate, as suggested in the Chablis model (Doin & Fleitout, 1996). This process could effectively maintain an average thickness plate at a critical thickness that is gravitationally stable, even in the presence of local downwelling where the plate may be thicker or upwellings there may be thinning (Ritzwoller et al., 2004). The onset time for the gravitational instabilities depends on the viscosity contrast between the lithosphere and the asthenosphere and can range from 5 Myr (Buck & Parmentier, 1986) to 60 Myr (Davaille & Jaupart, 1994), with earlier onsets associated with lower viscosities. Upwelling may also enhance mantle melting and may also lead to distinct regions of higher asthenospheric melt content, which may also help explain observations of mantle melt at a wide range of seafloor ages or beneath continents.

The existence of partial melt in the asthenosphere, either intermittent or widespread, especially away from major hot spots, and plate boundaries may be the cause of the numerous intraplate volcanoes that litter the seafloor. Commonly large non–hot spot origin seamounts form on oceanic lithosphere at a wide range of ages such as the petit spot seamounts (Hirano et al., 2006), or the Puka-Puka/Hotu Matua/Sojourn Chain (Harmon et al., 2011), with no clear tectonic explanation. One estimate suggests that to create the total volume of these intraplate seamounts would require extraction of ~0.1% molten asthenosphere (Conrad et al., 2017), and a better understanding of their formation has broad implications. However, the reason that these exist and the processes that create the melt remains the subject of debate. Proposed processes range from small-scale convection (Ballmer et al., 2007; Haxby & Weissel, 1986), shear-driven upwelling (Ballmer et al., 2013; Conrad et al., 2010), ambient melt that is released by thermal cracking (Sandwell & Fialko, 2004), to ponded melt at the base of the plate that is released by bending stresses (Hirano et al., 2006).

The presence of a low-viscosity asthenosphere may have a pivotal role in establishing the plate tectonic style of convection, which has had a large influence on the cooling of the Earth and its evolution through time, given that plate tectonics as we know it began ~1 Gyr into Earth's history (Shirey & Richardson, 2011). Numerical simulations of mantle flow suggest asthenospheric viscosity must be reduced by 2–3 orders of magnitude in comparison to the lithosphere to achieve plate tectonic style convection (Richards et al., 2001). This study imposed the viscosity drop, but as we have shown in the previous section viscosity drops of 2–3 orders of magnitude are predicted from geodynamic models incorporating solid-state mantle flow laws (Behn et al., 2009) and observed in estimates of mantle viscosity as described in section 2.4. Greater degrees of hydration and/or partial melt can further enhance the viscosity reduction, (Hirth et al., 1996; Hirth & Kohlstedt, 1995; Jackson et al., 2006; Karato, 2012; Karato & Wu, 1993) bringing it into better alignment with observational estimates based on lake paleoshorelines (Bills et al., 1994, 2007), postseismic relaxation (Hu et al., 2016), and/or postseismic relaxation together with glacial isostatic rebound (James et al., 2009).

The viscosity of the asthenosphere can also affect the driving forces of plate tectonics. For instance, a low-viscosity asthenosphere can result in different flow fields such as Couette and Poiseuille flow (Turcotte & Schubert, 2002). Couette flow, or moving boundary-driven flow, is caused by plate motions. In other words, the gravitational force of descending slabs into the asthenosphere pulls the rigid plate over the weaker asthenosphere (Forsyth & Uyeda, 1975). In this case the low-viscosity asthenosphere acts as the transition layer of the mantle flow field between the moving plate above and the potentially moving lower mantle below (Turcotte & Schubert, 2002). The asthenosphere effectively decouples motion between the plate and the lower mantle. The maximum velocities occur in the rigid plate, with lower velocities beneath. The gradient in velocity with depth produces the shear strains necessary for the development of olivine anisotropic fabric. Models in which anisotropy varies with depth from the paleo plate motion in the lithosphere to APM in the asthenosphere are based on this type of flow. On the other hand, Poiseuille flow, or pressure gradient-driven flow, might be caused by injection of plume material (Morgan et al., 1995) into the asthenosphere or by lateral temperature gradients (Hoink & Lenardic, 2010). In some ocean basins that are not surrounded by an extensive system of subducting slabs such as the Atlantic, Poiseuille flow could create higher velocities in the asthenosphere which could drive plate tectonics locally (Hoink & Lenardic, 2010). In addition, in regions of vigorous mantle plumes, this type of flow is important for accommodating the influx of plume material into the upper mantle (e.g., Morgan et al., 1995) and may explain geophysical and geochemical anomalies at mid-ocean ridges and intraplate settings away from the main center of the plume. This type

of flow and associated shear strain could also explain observations of asthenospheric anisotropy that are not aligned with APM (Lin et al., 2016; Russell et al., 2019). Global mantle flow derived from seismic tomography, geoid studies and plate motions suggests Poiseuille flow could be important in up to 40% of the Earth's asthenosphere (Natarov & Conrad, 2012).

The presence of volatiles and/or partial melt in the Earth also likely makes the Earth unique and habitable. Volatiles on Earth and in particular the presence of free-surface water are thought to be an important factor in establishing plate tectonics and also associated geohazards such as earthquakes, tsunamis, landslides, and volcanoes, in contrast to the stagnant lid convection exhibited on other similar planets, such as Venus (Kaula, 1990; Landuyt & Bercovici, 2009; Phillips, 1990). This could be because Earth's volatiles directly weaken the lithosphere allowing it crack and deform or because free surface water reduces surface temperatures of the planet which in turn leads to more localized deformation (Bercovici, 1998; Bercovici & Ricard, 2014; Korenaga, 2007, 2020; Landuyt & Bercovici, 2009; Lenardic & Kaula, 1994; Moresi & Solomatov, 1998; Mulyukova & Bercovici, 2019; Regenauer-Lieb et al., 2001; Tozer, 1985). Plate tectonic processes also create mountain chains and continents required for our survival on the planet above water. Plate tectonics forms the ocean basins, the vessels of free surface water, which are similarly crucial to our existence. Plate tectonics contributes to Earth's water cycle bringing hydration into the mantle at subduction zones before releasing it at volcanoes. Thus, Earth's plate tectonics are intricately linked with the presence of water and a low-viscosity asthenosphere. Despite large amounts of mass transfer in these processes the Earth has maintained a stable hydrosphere over billions of years making the planet suitable for life.

8. Conclusions

1. Overall, lithospheric thickening with age is observed beneath the oceans and toward the continental interiors suggesting that temperature plays a first-order role in controlling its thickness. However, within any given tectonic age interval a wide range of lithospheric thicknesses have been reported. This is true even for similar methodologies such as those using scattered waves. Beneath young seafloor (0 to 36 Myr) lithospheric thickness generally increases with age up to 64 km depth. Beneath older seafloor (>36 Myr) thickness ranges mostly between 40 and 90 km but with some outliers. Beneath Phanerozoic continental regions lithospheric thicknesses mostly range from 60 to 110 km, although the total range is much larger owing to thinning at rifts and thickening beneath mountain chains. Beneath continental interiors thicknesses are 130–200 km on average but could reach greater values, up to 250 km or more. Our analyses suggest thicknesses >250 km occur over a very limited area, <6–14% of the area of any individual continental interior. Overall, at least some of the observed lateral variability in thickness within any age or tectonic classification is real. This implies that other factors besides temperature are also important.
2. Scattered waves suggest strong, sharp discontinuities in seismic velocity with depth, and models with sharp discontinuities can also generally satisfy surface wave data and MT observations. There are many areas of agreement, and locations where apparent discrepancies exist can be explained by the different sensitivities of the methodologies. Discontinuities from scattered waves typically require at least 4–5% velocity drops but are as large as 15% in some cases. The velocity drops occur over <30 km, although in most cases even sharper drops are required, <15 km for most receiver function studies and <1 km for most active source studies. Resistivity anomalies (<1 $\log_{10}$ Ω m) and slow seismic velocity anomalies (Vs < 4.2) are also frequently imaged, for instance, by MT studies and surface wave tomography, respectively. Irregular LAB depth variations, sharp anomalies from scattered waves, slow surface wave anomalies, and low resistivities are thought to require another mechanism besides temperature to explain them.
3. Except for the shallow (60–110 km) discontinuities beneath continental interiors, which are classified as MLDs, the depths of the discontinuities from scattered waves coincide with the predicted depth of a strong decrease in viscosity, and also the depth of the solidus for mildly hydrated mantle. A large number of subsolidus properties and models have been proposed to explain observations of sharp discontinuities. However, the most straightforward way to explain all independent global observations of sharp LAB discontinuities, slow seismic velocity anomalies, and high conductivity anomalies is a small amount of partial melt in the asthenosphere.
4. Melt has been proposed to occur in a variety of ways: in a focused melt triangle or a much wider triangle beneath spreading ridges, in a thin channel, in multiple layers, at a depth of neutral buoyancy, or beneath a permeability boundary connecting to the ridge. It may exist sporadically or pervasively beneath older

lithosphere and even continental interiors. It may fall off in depth gradually or have a sharp base. Geodynamic models support the notion that melt is dynamic and ephemeral and can take the forms inferred from seismic and MT observations.

5. Volatiles or partial melt in the mantle could reduce asthenospheric viscosities beyond predictions based on laboratory solid-state flow laws. This could provide a better match to the predicted LAB viscosity drop of 3 orders of magnitude based on observational constraints. The presence of volatiles would also promote melting by lowering the melting temperature. At long timescales a low-viscosity asthenosphere caused by volatiles and/or melt may allow multiple scales of convection and result in complex mantle dynamics. Small-scale convection could further enhance melt in locations of upwelling. This convection together with melt dynamics likely moderate lithospheric thickness and could explain thickness variations observed within a given tectonic age interval. Pervasive partial melt in the mantle and/or upwellings related to small-scale convection could explain non–hot spot, intraplate volcanism, and also non-APM asthenospheric anisotropy observations. At short timescales the low-viscosity asthenosphere and nature of the LAB play a role in influencing deformations such those following deglaciations and earthquakes. This is important for our understanding of climate change in the geologic record and natural hazard mitigation.
6. Overall, our synthesis suggests that the LAB is dynamic and variations in melt generation and migration define the plate. This dynamic lithosphere-asthenosphere system has likely promoted plate tectonic style convection on the Earth and also dictated the driving forces of the plates. Plate tectonics in turn has shaped the planet for billions of years and continues today, presenting a major source of geohazards. These processes have also formed the continents and ocean basins necessarily for our existence on land and also preserved a hydrosphere over billions of years, promoting planetary habitability.

Data Availability Statement

No original data were used in this manuscript. The data on which this article is based are available in Artemieva (2006), Harmon et al. (2009), Audet and Burgman (2011), Ekstrom (2011), French et al. (2013), Kumar and Kawakatsu (2011), Schmerr (2012), Steinberger and Becker (2018), Rychert and Shearer (2009, 2011), Tharimena, Rychert, and Harmon (2017), Tharimena, Rychert, Harmon, and White (2017), Rychert et al. (2018b, and references therein), Harmon et al. (2020), Wang et al. (2020), Watts et al. (2013), Shito et al. (2015), Forsyth et al. (1998), Hawley et al. (2016), Kawakatsu et al. (2009), Lin et al. (2016), Takeo et al. (2013), Gaherty et al. (1996), Tan and Helmberger (2007), Mehouachi and Singh (2018), Stern et al. (2015), Lizarralde et al. (1995), Schultz et al. (1993), Bills et al. (1994, 2007), Behn et al. (2009), Mitrovica and Forte (2004), Hu et al. (2016), Key et al. (2013), Naif et al. (2013), Turner et al. (2017), and Johansen et al. (2019).

Acknowledgments

C.A.R. and N.H. were funded by the Natural Environment Research Council (NE/M003507/1) (PI-LAB) and the H2020 European Research Council (GA 638665) (EURO-LAB). S.C. was funded by the National Science Foundation (OCE-1536400). We thank reviewers Donna Blackman, Clint Conrad, the Associate Editor, and Editor for excellent and insightful comments and suggestions. We thank P. Audet for providing the continental elastic thickness model. We thank G. Ekstrom and C. Dalton for providing phase velocity maps. We thank T. Becker and B. Steinberger for providing the LSmean model. We thank I. Artemieva for providing the lithospheric thickness map from heat flow. We thank A. B. Watts for providing the oceanic *Te* compilation.

References

Abt, D. L., Fischer, K. M., French, S. W., Ford, H. A., Yuan, H. Y., & Romanowicz, B. (2010). North American lithospheric discontinuity structure imaged by *Ps* and *Sp* receiver functions. *Journal of Geophysical Research*, *115*, B09301. https://doi.org/10.1029/2009JB006914

Ádám, A., & Wesztergom, V. (2001). An attempt to map the depth of the electrical asthenosphere by deep magnetotelluric measurements in the Pannonian Basin (Hungary). *Acta Geologica Hungarica*, *44*(2–3), 167–192.

Artemieva, I. M. (2006). Global 1° × 1° thermal model TC1 for the continental lithosphere: Implications for lithosphere secular evolution. *Tectonophysics*, *416*(1–4), 245–277. https://doi.org/10.1016/j.tecto.2005.11.022

Audet, P. (2014). Toward mapping the effective elastic thickness of planetary lithospheres from a spherical wavelet analysis of gravity and topography. *Physics of the Earth and Planetary Interiors*, *226*, 48–82. https://doi.org/10.1016/j.pepi.2013.09.011

Audet, P. (2016). Receiver functions using OBS data: Promises and limitations from numerical modelling and examples from the Cascadia Initiative. *Geophysical Journal International*, *205*(3), 1740–1755. https://doi.org/10.1093/gji/ggw111

Audet, P., & Burgman (2011). Dominant role of tectonic inheritance in supercontinent cycles. *Nature Geoscience*, *4*. https://doi.org/10.1038/NGEO1080

Auer, L., Becker, T., Boschi, L., & Schmerr, N. (2015). Thermal structure, radial anisotropy, and dynamics of oceanic boundary layers. *Geophysical Research Letters*, *42*, 9740–9749. https://doi.org/10.1002/2015GL066246

Austin, N., & Evans, R. (2007). Paleowattmeters: A scaling relation for dynamically recrystallized grain size. *Geology*, *35*, 343–346. https://doi.org/10.1130/g23244a.1

Baba, K., Chave, A. D., Evans, R. L., Hirth, G., & Mackie, R. L. (2006). Mantle dynamics beneath the East Pacific Rise at 17°S: Insights from the Mantle Electromagnetic and Tomography (MELT) experiment. *Journal of Geophysical Research*, *111*, B02101. https://doi.org/10.1029/2004JB003598

Bagley, B., & Revenaugh, J. (2008). Upper mantle seismic shear discontinuities of the Pacific. *Journal of Geophysical Research*, *113*, B12301. https://doi.org/10.1029/2008JB005692

Ballmer, M. D., Conrad, C. P., Smith, E. I., & Harmon, N. (2013). Non-hotspot volcano chains produced by migration of shear-driven upwelling toward the East Pacific Rise. *Geology*, *41*(4), 479–482. https://doi.org/10.1130/G33804.1

Ballmer, M. D., van Hunen, J., Ito, G., Tackley, P. J., & Bianco, T. A. (2007). Non-hotspot volcano chains originating from small-scale sublithospheric convection. *Geophysical Research Letters*, *34*, L23310. https://doi.org/10.1029/2007gl031636

Barrell, J. (1914). The strength of the Earth's crust. *Journal of Geology*, 22–23. https://doi.org/10.1086/622189

Beghein, C., Yuan, K. Q., Schmerr, N., & Xing, Z. (2014). Changes in seismic anisotropy shed light on the nature of the Gutenberg Discontinuity. *Science*, *343*(6176), 1237–1240. https://doi.org/10.1126/science.1246724

Behn, M. D., Hirth, G., & Elsenbeck, J. R. (2009). Implications of grain size evolution on the seismic structure of the oceanic upper mantle. *Earth and Planetary Science Letters*, *282*(1–4), 178–189. https://doi.org/10.1016/J.Epsl.2009.03.014

Bercovici, D. (1998). Generation of plate tectonics from lithosphere-mantle flow and void-volatile self-lubrication. *Earth and Planetary Science Letters*, *154*(1–4), 139–151. https://doi.org/10.1016/S0012-821x(97)00182-9

Bercovici, D., & Ricard, Y. (2014). Plate tectonics, damage and inheritance. *Nature*, *508*(7497), 513. https://doi.org/10.1038/nature13072

Bills, B. G., Adams, K. D., & Wesnousky, S. G. (2007). Viscosity structure of the crust and upper mantle in western Nevada from isostatic rebound patterns of the late Pleistocene Lake Lahontan high shoreline. *Journal of Geophysical Research*, *112*, B06405. https://doi.org/10.1029/2005JB003941

Bills, B. G., Currey, D. R., & Marshall, G. A. (1994). Viscosity estimates for the crust and upper-mantle from patterns of lacustrine shoreline deformation in the eastern Great-Basin. *Journal of Geophysical Research*, *99*(B11), 22,059–22,086. https://doi.org/10.1029/94JB01192

Bird, P., Liu, Z., & Rucker, W. K. (2008). Stresses that drive the plates from below: Definitions, computational path, model optimization, and error analysis. *Journal of Geophysical Research*, *113*, B11406. https://doi.org/10.1029/2007JB005460

Blackman, D. K., Boyce, D. E., Castelnau, O., Dawson, P. R., & Laske, G. (2017). Effects of crystal preferred orientation on upper-mantle flow near plate boundaries: Rheologic feedbacks and seismic anisotropy. *Geophysical Journal International*, *210*(3), 1481–1493. https://doi.org/10.1093/gji/ggx251

Bostock, M. G. (1998). Mantle stratigraphy and evolution of the Slave province. *Journal of Geophysical Research*, *103*(B9), 21,183–21,200. https://doi.org/10.1029/98JB01069

Buck, W. R., & Parmentier, E. M. (1986). Convection beneath young oceanic lithosphere—Implications for thermal structure and gravity. *Journal of Geophysical Research*, *91*(B2), 1961–1974. https://doi.org/10.1029/JB091ib02p01961

Burgos, G., Montagner, J. P., Beucler, E., Capdeville, Y., Mocquet, A., & Drilleau, M. (2014). Oceanic lithosphere-asthenosphere boundary from surface wave dispersion data. *Journal of Geophysical Research: Solid Earth*, *119*, 1079–1093. https://doi.org/10.1002/2013JB010528

Burov, E. B., & Diament, M. (1995). The effective elastic thickness (T_e) of continental lithosphere—What does it really mean? *Journal of Geophysical Research*, *100*(B3), 3905–3927. https://doi.org/10.1029/94JB02770

Byerlee, J. (1978). Friction of rocks. *Pure and Applied Geophysics*, *116*(4–5), 615–626. https://doi.org/10.1007/Bf00876528

Byrnes, J. S., Hooft, E. E. E., Toomey, D. R., Villagomez, D. R., Geist, D. J., & Solomon, S. C. (2015). An upper mantle seismic discontinuity beneath the Galapagos Archipelago and its implications for studies of the lithosphere-asthenosphere boundary. *Geochemistry, Geophysics, Geosystems*, *16*, 1070–1088. https://doi.org/10.1002/2014GC005694

Cerv, V., Kovacikova, S., Pek, J., Pecova, J., & Praus, O. (2001). Geoelectrical structure across the Bohemian Massif and the transition zone to the West Carpathians. *Tectonophysics*, *332*(1–2), 201–210. https://doi.org/10.1016/S0040-1951(00)00257-2

Chanard, K., Fleitout, L., Calais, E., Barbot, S., & Avouac, J. P. (2018). Constraints on transient viscoelastic rheology of the asthenosphere from seasonal deformation. *Geophysical Research Letters*, *45*, 2328–2338. https://doi.org/10.1002/2017GL076451

Chantel, J., Manthilake, G., Andrault, D., Novella, D., Yu, T., & Wang, Y. B. (2016). Experimental evidence supports mantle partial melting in the asthenosphere. *Science Advances*, *2*(5), e1600246. https://doi.org/10.1126/sciadv.1600246

Chen, L., Zheng, T. Y., & Xu, W. W. (2006). A thinned lithospheric image of the Tanlu Fault Zone, eastern China: Constructed from wave equation based receiver function migration. *Journal of Geophysical Research*, *111*, B09312. https://doi.org/10.01029/02005JB003974

Chesley, C., Key, K., Constable, S., Behrens, J., & MacGregor, L. (2019). Crustal cracks and frozen flow in oceanic lithosphere inferred from electrical anisotropy. *Geochemistry, Geophysics, Geosystems*, *20*, 5979–5999. https://doi.org/10.1029/2019GC008628

Clark, A. N., & Lesher, C. E. (2017). Elastic properties of silicate melts: Implications for low velocity zones at the lithosphere-asthenosphere boundary. *Science Advances*, *3*(12), e1701312. https://doi.org/10.1126/sciadv.1701312

Cline, C. J., Faul, U. H., David, E. C., Berry, A. J., & Jackson, I. (2018). Redox-influenced seismic properties of uppermantle olivine. *Nature*, *555*(7696), 355–358. https://doi.org/10.1038/nature25764

Collins, J. A., Vernon, F. L., Orcutt, J. A., & Stephen, R. A. (2002). Upper mantle structure beneath the Hawaiian swell: Constraints from the ocean seismic network pilot experiment. *Geophysical Research Letters*, *29*(11), 1522. https://doi.org/10.1029/2001GL013302

Conrad, C. P., & Lithgow-Bertelloni, C. (2006). Influence of continental roots and asthenosphere on plate-mantle coupling. *Geophysical Research Letters*, *33*, L05312. https://doi.org/10.1029/2005GL025621

Conrad, C. P., Selway, K., Hirschmann, M. M., Ballmer, M. D., & Wessel, P. (2017). Constraints on volumes and patterns of asthenospheric melt from the space-time distribution of seamounts. *Geophysical Research Letters*, *44*, 7203–7210. https://doi.org/10.1002/2017gl074098

Conrad, C. P., Wu, B. J., Smith, E. I., Bianco, T. A., & Tibbetts, A. (2010). Shear-driven upwrelling induced by lateral viscosity variations and asthenospheric shear: A mechanism for intraplate volcanism. *Physics of the Earth and Planetary Interiors*, *178*(3–4), 162–175. https://doi.org/10.1016/j.pepi.2009.10.001

Constable, S. C., Parker, R. L., & Constable, C. G. (1987). Occams inversion—A practical algorithm for generating smooth models from electromagnetic sounding data. *Geophysics*, *52*(3), 289–300.

Daly, R. A. (1940). *Strength and structure of the Earth* (p. 434). New York: Prentince Hall.

Davaille, A., & Jaupart, C. (1994). Onset of thermal-convection in fluids with temperature-dependent viscosity—Application to the oceanic mantle. *Journal of Geophysical Research*, *99*(B10), 19,853–19,866. https://doi.org/10.1029/94JB01405

Deuss, A., & Woodhouse, J. H. (2004). The nature of the Lehmann discontinuity from its seismological Clapeyron slopes. *Earth and Planetary Science Letters*, *225*(3–4), 295–304. https://doi.org/10.1016/j.epsl.2004.06.021

Doin, M. P., & Fleitout, L. (1996). Thermal evolution of the oceanic lithosphere: An alternative view. *Earth and Planetary Science Letters*, *142*(1–2), 121–136. https://doi.org/10.1016/0012-821x(96)00082-9

Dorman, J., Ewing, M., & Oliver, J. (1960). Study of shearp-velocity distribution in the upper mantle by mantle Rayleigh waves. *Bulletin of the Seismological Society of America*, *50*(1), 87–115.

Dunn, R. A., Lekic, V., Detrick, R. S., & Toomey, D. R. (2005). Three-dimensional seismic structure of the Mid-Atlantic Ridge (35°N): Evidence for focused melt supply and lower crustal dike injection. *Journal of Geophysical Research*, *110*, B09101. https://doi.org/10.1029/2004JB003473

Dziewonski, A. M. (1971). Upper mantle models from pure-path dispersion data. *Journal of Geophysical Research*, *76*(11), 2587. https://doi.org/10.1029/JB076i011p02587

Eaton, D. W., Darbyshire, F., Evans, R. L., Grutter, H., Jones, A. G., & Yuan, X. H. (2009). The elusive lithosphere-asthenosphere boundary (LAB) beneath cratons. *Lithos*, *109*(1–2), 1–22. https://doi.org/10.1016/j.lithos.2008.05.009

Eilon, Z., & Forsyth, D. (2020). Depth-dependent azimuthal anisotropy beneath Juan de Fuca Plate system. *Journal of Geophysical Research: Solid Earth*, *125*, e2020JB019477. https://doi.org/10.1029/2020JB019477

Ekstrom, G. (2011). A global model of Love and Rayleigh surface wave dispersion and anisotropy, 25–250 s. *Geophysical Journal International*, *187*, 1668–1686. https://doi.org/10.1111/j.1365-246X.2011.05225.x

England, P. C., & Katz, R. F. (2010). Melting above the anhydrous solidus controls the location of volcanic arcs. *Nature*, *467*(7316), 700–U784. https://doi.org/10.1038/nature09417

Evans, R. L., Jones, A. G., Garcia, X., Muller, M., Hamilton, M., Evans, S., et al. (2011). Electrical lithosphere beneath the Kaapvaal craton, southern Africa. *Journal of Geophysical Research*, *116*, B04105. https://doi.org/10.1029/2010JB007883

Evans, R. L., Tarits, P., Chave, A. D., White, A., Heinson, G., Filloux, J. H., et al. (1999). Asymmetric electrical structure in the mantle beneath the East Pacific rise at 17°S. *Science*, *286*(5440), 752–756. https://doi.org/10.1126/science.286.5440.752

Ewing, M., & Press, F. (1954). An investigation of mantle Rayleigh waves. *Bulletin of the Seismological Society of America*, *44*(2A), 127–147.

Ewing, M., & Press, F. (1959). Determination of crustal structure from phase velocity of Rayleigh Waves. *Bulletin Geological Society of America*, *70*, 229–244. https://doi.org/10.1130/0016-7606(1959)70[229:DOCSFP]2.0.CO;2

Faccenda, M., Burlini, L., Gerya, T. V., & Mainprice, D. (2008). Fault-induced seismic anisotropy by hydration in subducting oceanic plates. *Nature*, *455*(7216), 1097–U1098. https://doi.org/10.1038/nature07376

Faul, U. H., & Jackson, I. (2005). The seismological signature of temperature and grain size variations in the upper mantle. *Earth and Planetary Science Letters*, *234*(1–2), 119–134. https://doi.org/10.1016/j.epsl.2005.02.008

Fischer, K. (2015). Crust and lithospheric structure—Seismological constraints on the lithosphere-asthenosphere boundary. In *Treatise on geophysics* (pp. 587–612). Amsterdam, The Netherlands: Elsevier. https://doi.org/10.1016/B978-0-444-53802-4.00026-9

Fischer, K. M., Ford, H. A., Abt, D. L., & Rychert, C. A. (2010). The lithosphere-asthenosphere boundary. *Annual Review of Earth and Planetary Sciences*, *38*(38), 551–575. https://doi.org/10.1146/Annurev-Earth-040809-152438

Fleming, K., Martinec, Z., & Wolf, D. (2007). Glacial-isostatic adjustment and the viscosity structure underlying the Vatnajokull Ice Cap, Iceland. *Pure and Applied Geophysics*, *164*(4), 751–768. https://doi.org/10.1007/s00024-007-0187-6

Ford, H. A., Fischer, K. M., Abt, D. L., Rychert, C. A., & Elkins-Tanton, L. T. (2010). The lithosphere-asthenosphere boundary and cratonic lithospheric layering beneath Australia from Sp wave imaging. *Earth and Planetary Science Letters*, *300*. https://doi.org/10.1016/j.epsl.2010.1010.1007

Forsyth, D., & Uyeda, S. (1975). On the relative importance of the driving forces of plate motion. *Geophysical Journal International*, *43*(1), 163–200. https://doi.org/10.1111/j.1365-246X.1975.tb00631.x

Forsyth, D. W. (1975). The early structural evolution and anisotropy of the oceanic upper mantle. *Geophys. J. Roy. Ast. Soc.*, *43*, 103–162. https://doi.org/10.1111/j.1365-246x.1975.tb00630.x

Forsyth, D. W. (1985). Subsurface loading and estimates of the flexural rigidity of continental lithosphere. *Journal of Geophysical Research*, *90*(B14), 2623–2632. https://doi.org/10.1029/JB090iB14p12623

Forsyth, D. W., Scheirer, D. S., Webb, S. C., Dorman, L. M., Orcutt, J. A., Harding, A. J., et al. (1998). Imaging the deep seismic structure beneath a mid-ocean ridge: The MELT experiment. *Science*, *280*(5367), 1215–1218.

French, S. W., Lekic, V., & Romanowicz, B. (2013). Waveform tomography reveals channeled flow at the base of the oceanic asthenosphere. *Science*, *342*(6155), 227–230. https://doi.org/10.1126/science.1241514

Gaherty, J. B., & Jordan, T. H. (1995). Lehmann discontinuity as the base of an anisotropic layer beneath continents. *Science*, *268*(5216), 1468–1471. https://doi.org/10.1126/science.268.5216.1468

Gaherty, J. B., Jordan, T. H., & Gee, L. S. (1996). Seismic structure of the upper mantle in a central Pacific corridor. *Journal of Geophysical Research*, *101*(B10), 22,291–222,309.

Gaherty, J. B., Kato, M., & Jordan, T. H. (1999). Seismological structure of the upper mantle: a regional comparison of seismic layering. *Physics of the Earth and Planetary Interiors*, *110*(1–2), 21–41. https://doi.org/10.1016/S0031-9201(98)00132-0

Geissler, W. H., Jokat, W., Jegen, M., & Baba, K. (2017). Thickness of the oceanic crust, the lithosphere, and the mantle transition zone in the vicinity of the Tristan da Cunha hot spot estimated from ocean-bottom and ocean-island seismometer receiver functions. *Tectonophysics*, *716*, 33–51. https://doi.org/10.1016/j.tecto.2016.12.013

Ghods, A., & Arkani-Hamed, J. (2000). Melt migration beneath mid-ocean ridges. *Geophysical Journal International*, *140*(3), 687–697. https://doi.org/10.1046/j.1365-246X.2000.00032.x

Green, D. H., Hibberson, W. O., Kovacs, I., & Rosenthal, A. (2010). Water and its influence on the lithosphere-asthenosphere boundary. *Nature*, *467*(7314), 448–451. https://doi.org/10.1038/Nature09369

Griffin, W. L., Doyle, B. J., Ryan, C. G., Pearson, N. J., O'Reilly, S. Y., Davies, R., et al. (1999). Layered mantle lithosphere in the Lac de Gras area, Slave Craton: Composition, structure and origin. *Journal of Petrology*, *40*(5), 705–727.

Gung, Y. C., Panning, M., & Romanowicz, B. (2003). Global anisotropy and the thickness of continents. *Nature*, *422*(6933), 707–711. https://doi.org/10.1038/nature01559

Gutenberg, B. (1926). Untersuclmngen zur Frage, bis zu welcher Tiefe die Tirde kristallinist. *Zeitschr Geopbys*, *2*, 24–29.

Gutenberg, B. (1948). On the layer of relatively low wave velocity at a depth of about 80 kilometers. *Bulletin of the Seismological Society of America*, *38*, 121–148.

Gutenberg, B. (1955). Channel waves in the Earth's crust. *Geophysics*, *20*, 283–294. https://doi.org/10.1190/1.1438141

Gutenberg, B. (1959). The asthenosphere low velocity layer. *Annals of Geophysics*, *12*(4), 439–460.

Gutenberg, B., & Richter, C. F. (1939). New evidence for a change in pliysical conditions at depths near 100 kilometers. *Bulletin of the Seismological Society of America*, *29*, 531–539.

Hammond, W. C., & Humphreys, E. D. (2000). Upper mantle seismic wave velocity: Effects of realistic partial melt geometries. *Journal of Geophysical Research*, *105*(B5), 10,975–10,986. https://doi.org/10.1029/2000JB900041

Hannemann, K., Kruger, F., Dahm, T., & Lange, D. (2017). Structure of the oceanic lithosphere and upper mantle north of the Gloria Fault in the eastern mid-Atlantic by receiver function analysis. *Journal of Geophysical Research: Solid Earth*, *122*, 7927–7950. https://doi.org/10.1002/2016JB013582

Harmon, N., Forsyth, D. W., & Weeraratne, D. S. (2009). Thickening of young Pacific lithosphere from high-resolution Rayleigh wave tomography: A test of the conductive cooling model. *Earth and Planetary Science Letters*, *278*(1-2), 96–106. https://doi.org/10.1016/J.Epsl.2008.11.025

Harmon, N., Forsyth, D. W., Weeraratne, D. S., Yang, Y. J., & Webb, S. C. (2011). Mantle heterogeneity and off axis volcanism on young Pacific lithosphere. *Earth and Planetary Science Letters*, *311*(3–4), 306–315. https://doi.org/10.1016/j.epsl.2011.09.038

Harmon, N., Rychert, C., Kendall, J., Tharimena, S., Bogiatzis, P., & Agius, M. (2020). Evolution of the oceanic lithosphere in the equatorial Atlantic from Rayleigh Wave tomography, evidence for small-scale convection from the PI-LAB experiment. *Geochemistry, Geophysics, Geosystems*, *21*, e2020GC009174. https://doi.org/10.1029/2020GC009174

Hasterok, D. (2013). A heat flow based cooling model for tectonic plates. *Earth and Planetary Science Letters*, *361*, 34–43. https://doi.org/10.1016/j.epsl.2012.10.036

Hasterok, D., & Chapman, D. S. (2011). Heat production and geotherms for the continental lithosphere. *Earth and Planetary Science Letters*, *307*(1–2), 59–70. https://doi.org/10.1016/j.epsl.2011.04.034

Hawley, W. B., Allen, R. M., & Richards, M. A. (2016). Tomography reveals buoyant asthenosphere accumulating beneath the Juan de Fuca plate. *Science*, *353*(6306), 1406–1408. https://doi.org/10.1126/science.aad8104

Haxby, W. F., & Weissel, J. K. (1986). Evidence for small-scale mantle convection from Seasat altimeter data. *Journal of Geophysical Research*, *91*(B3), 3507–3520. https://doi.org/10.1029/JB091iB03p03507

Hebert, L. B., & Montesi, L. G. J. (2010). Generation of permeability barriers during melt extraction at mid-ocean ridges. *Geochemistry, Geophysics, Geosystems*, *11*, Q12008. https://doi.org/10.1029/2010gc003270

Heezen, B. C., Tharpe, M., & Ewing, M. (1959). The floors of the oceans. I. The North Atlantic. Text to accompany the physiographic diagram of the North Atlantic. (Vol. Special Paper 65). Geological Society of America.

Heinson, G. (1999). Electromagnetic studies of the lithosphere and asthenosphere. *Surveys in Geophysics*, *20*(3-4), 229–255. https://doi.org/10.1023/A:1006689521329

Heit, B., Sodoudi, F., Yuan, X., Bianchi, M., & Kind, R. (2007). An S receiver function analysis of the lithospheric structure in South America. *Geophysical Research Letters*, *34*, L14307. https://doi.org/10.1029/2007GL030317

Hess, H. (1964). Seismic anisotorpy of the uppermost mantle under oceans. *Nature*, *203*(4945), 629–631. https://doi.org/10.1038/203629a0

Hess, H. H. (1962). *History of ocean basins*. Boulder, CO: Geological Society of America.

Hirano, N., Takahashi, E., Yamamoto, J., Abe, N., Ingle, S. P., Kaneoka, I., et al. (2006). Volcanism in response to plate flexure. *Science*, *313*(5792), 1426–1428. https://doi.org/10.1126/Science.1128235

Hirschmann, M. M. (2010). Partial melt in the oceanic low velocity zone. *Physics of the Earth and Planetary Interiors*, *179*(1–2), 60–71. https://doi.org/10.1016/J.Pepi.2009.12.003

Hirth, G., Evans, R. L., & Chave, A. D. (2000). Comparison of continental and oceanic mantle electrical conductivity: Is the Archean lithosphere dry? *Geochemistry, Geophysics, Geosystems*, *1*. https://doi.org/10.1029/1200GC00048

Hirth, G., Kohlstedt, & D. (1996). Water in the oceanic upper mantle; implications for rheology, melt extraction and the evolution of the lithosphere. *Earth and Planetary Science Letters*, *144*(1–2), 93–108.

Hirth, G., & Kohlstedt, D. L. (1995). Experimental constraints on the dynamics of the partially molten upper-mantle: 2. Deformation in the dislocation creep regime. *Journal of Geophysical Research*, *100*(B8), 15,441–15,449.

Hjelt, S. E., Korja, T., Kozlovskaya, E., Lahti, I., Yliniemi, J., & Bear, S. S. T. W. G. (2006). Electrical conductivity and seismic velocity structures of the lithosphere beneath the Fennoscandian Shield. *Geological Society, London, Memoirs*, *32*(1), 541–559. https://doi.org/10.1144/GSL.MEM.2006.032.01.33

Hoink, T., & Lenardic, A. (2010). Long wavelength convection, Poiseuille-Couette flow in the low-viscosity asthenosphere and the strength of plate margins. *Geophysical Journal International*, *180*(1), 23–33. https://doi.org/10.1111/j.1365-246X.2009.04404.x

Hu, Y., Burgmann, R., Banerjee, P., Feng, L. J., Hill, E. M., Ito, T., et al. (2016). Asthenosphere rheology inferred from observations of the 2012 Indian Ocean earthquake. *Nature*, *538*(7625), 368–372. https://doi.org/10.1038/nature19787

Jackson, I., & Faul, U. H. (2010). Grainsize-sensitive viscoelastic relaxation in olivine: Towards a robust laboratory-based model for seismological application. *Physics of the Earth and Planetary Interiors*, *183*(1–2), 151–163. https://doi.org/10.1016/j.pepi.2010.09.005

Jackson, I., Faul, U. H., Fitz Gerald, J. D., & Morris, S. J. S. (2006). Contrasting viscoelastic behavior of melt-free and melt-bearing olivine: Implications for the nature of grain-boundary sliding. *Materials Science and Engineering a-Structural Materials Properties Microstructure and Processing*, *442*(1–2), 170–174. https://doi.org/10.1016/J.Msea.2006.01.136

James, T. S., Gowan, E. J., Wada, I., & Wang, K. L. (2009). Viscosity of the asthenosphere from glacial isostatic adjustment and subduction dynamics at the northern Cascadia subduction zone, British Columbia, Canada. *Journal of Geophysical Research*, *114*, B04405. https://doi.org/10.1029/2008JB006077

Jeffreys, H., & Bullen, K. E. (1940). Seismological tables. *British Science Association*, *48*.

Johansen, S. E., Panzner, M., Mittet, R., Amundsen, H. E. F., Lim, A., Vik, E., et al. (2019). Deep electrical imaging of the ultraslow-spreading Mohns Ridge. *Nature*, *567*(7748), 379–383. https://doi.org/10.1038/s41586-019-1010-0

Jones, A. G. (1999). Imaging the continental upper mantle using electromagnetic methods. *Lithos*, *48*(1–4), 57–80. https://doi.org/10.1016/S0024-4937(99)00022-5

Jones, A. G., Ledo, J., Ferguson, I. J., Farquharson, C., Garcia, X., Grant, N., et al. (2005). The electrical resistivity structure of Archean to Tertiary lithosphere along 3200 km of SNORCLE profiles, northwestern Canada. *Canadian Journal of Earth Sciences*, *42*(6), 1257–1275. https://doi.org/10.1139/E05-080

Jones, A. G., Lezaeta, P., Ferguson, I. J., Chave, A. D., Evans, R. L., Garcia, X., & Spratt, J. (2003). The electrical structure of the Slave craton. *Lithos*, *71*(2–4), 505–527. https://doi.org/10.1016/j.lithos.2003.08.001

Jones, A. G., Plomerova, J., Korja, T., Sodoudi, F., & Spakman, W. (2010). Europe from the bottom up: A statistical examination of the central and northern European lithosphere-asthenosphere boundary from comparing seismological and electromagnetic observations. *Lithos*, *120*(1–2), 14–29. https://doi.org/10.1016/j.lithos.2010.07.013

Jordan, T. H. (1975). Continental tectosphere. *Reviews of Geophysics*, *13*(3), 1–12. https://doi.org/10.1029/rg013i003p00001

Jordan, T. H. (1988). Structure and formation of the continental tectosphere. *Journal of Petrology*, Special_Volume, *1*, 11–37. https://doi.org/10.1093/petrology/Special_Volume.1.11

Jordan, T. H., & Paulson, E. M. (2013). Convergence depths of tectonic regions from an ensemble of global tomographic models. *Journal of Geophysical Research: Solid Earth*, *118*, 4196–4225. https://doi.org/10.1002/jgrb.50263

Kanamori, H. (1970). Seismological evidence for heterogeneity of mantle. *Journal of Geomagnetism and Geoelectricity*, *22*(1–2), 53. https://doi.org/10.5636/jgg.22.53

Kanamori, H., & Press, F. (1970). How thick is lithosphere. *Nature*, *226*(5243), 330–331. https://doi.org/10.1038/226330a0
Karato, S., Jung, H., Katayama, I., & Skemer, P. (2008). Geodynamic significance of seismic anisotropy of the upper mantle: New insights from laboratory studies. *Annual Review of Earth and Planetary Sciences*, *36*, 59–95. https://doi.org/10.1146/annurev.earth.36.031207.124120
Karato, S., & Wu, P. (1993). Rheology of the upper mantle—A synthesis. *Science*, *260*(5109), 771–778. https://doi.org/10.1126/science.260.5109.771
Karato, S.-I. (2012). On the origin of the asthenosphere. *Earth and Planetary Science Letters*, *321–322*, 95–103. https://doi.org/10.1016/j.epsl.2012.01.001
Karato, S. I., Olugboji, T., & Park, J. (2015). Mechanisms and geologic significance of the mid-lithosphere discontinuity in the continents. *Nature Geoscience*, *8*(7), 509–514. https://doi.org/10.1038/Ngeo2462
Katayama, I., Jung, H., & Karato, S. I. (2004). New type of olivine fabric from deformation experiments at modest water content and low stress. *Geology*, *32*(12), 1045–1048. https://doi.org/10.1130/G20805.1
Katz, R. F., Spiegelman, M., & Langmuir, C. H. (2003). A new parameterization of hydrous mantle melting. *Geochemistry, Geophysics, Geosystems*, *4*(9), 1073. https://doi.org/10.1029/2002GC000433
Kaula, W. M. (1990). Mantle convection and crustal evolution on Venus. *Geophysical Research Letters*, *17*(9), 1401–1403. https://doi.org/10.1029/GL017i009p01401
Kawakatsu, H., Kumar, P., Takei, Y., Shinohara, M., Kanazawa, T., Araki, E., & Suyehiro, K. (2009). Seismic evidence for sharp lithosphere-asthenosphere boundaries of oceanic plates. *Science*, *324*(5926), 499–502. https://doi.org/10.1126/science.1169499
Kawakatsu, H., & Utada, H. (2017). Seismic and electrical signatures of the lithosphere-asthenosphere system of the normal oceanic mantle. *Annual Review of Earth and Planetary Sciences*, *45*(45), 139–167. https://doi.org/10.1146/annurev-earth-063016-020319
Kelbert, A., Egbert, G. D., & DeGroot-Hedlin, C. (2012). Crust and upper mantle electrical conductivity beneath the Yellowstone Hotspot Track. *Geology*, *40*(5), 447–450. https://doi.org/10.1130/G32655.1
Kennett, B. L. N., & Furumura, T. (2015). Toward the reconciliation of seismological and petrological perspectives on oceanic lithosphere heterogeneity. *Geochemistry, Geophysics, Geosystems*, *16*, 3129–3141. https://doi.org/10.1002/2015GC006017
Kennett, B. L. N., Furumura, T., & Zhao, Y. (2014). High-frequency *Po*/*So* guided waves in the oceanic lithosphere: II—Heterogeneity and attenuation. *Geophysical Journal International*, *199*(1), 614–630. https://doi.org/10.1093/gji/ggu286
Kennett, B. L. N., Yoshizawa, K., & Furumura, T. (2017). Interactions of multi-scale heterogeneity in the lithosphere: Australia. *Tectonophysics*, *717*, 193–213. https://doi.org/10.1016/j.tecto.2017.07.009
Key, K., Constable, S., Liu, L., & Pommier, A. (2013). Electical image of passive mantel upwelling beneath the northern East Pacific Rise. *Nature*, *495*(7442), 499–502. https://doi.org/10.1038/nature11932
Knapp, J. H., Steer, D. N., Brown, L. D., Berzin, R., Suleimanov, A., Stiller, M., et al. (1996). Lithosphere-scale seismic image of the southern Urals from explosion-source reflection profiling. *Science*, *274*(5285), 226–228. https://doi.org/10.1126/science.274.5285.226
Knopoff, L. (1972). Observation and inversion of surface-wave dispersion. *Tectonophysics*, *13*(1–4), 497–519. https://doi.org/10.1016/0040-1951(72)90035-2
Kodaira, S., Fujie, G., Yamashita, M., Sato, T., Takahashi, T., & Takahashi, N. (2014). Seismological evidence of mantle flow driving plate motions at a palaeo-spreading centre. *Nature Geoscience*, *7*(5), 371–375. https://doi.org/10.1038/ngeo2121
Korenaga, J. (2007). Thermal cracking and the deep hydration of oceanic lithosphere: A key to the generation of plate tectonics? *Journal of Geophysical Research*, *112*, B05408. https://doi.org/10.1029/2006JB004502
Korenaga, J. (2020). Plate tectonics and surface environment: Role of the oceanic upper mantle. *Earth-Science Reviews*, *205*(103185). https://doi.org/10.1016/j.earscirev.2020.103185
Korenaga, J., & Karato, S. I. (2008). A new analysis of experimental data on olivine rheology. *Journal of Geophysical Research*, *113*, B02403. https://doi.org/10.1029/2007JB005100
Korenaga, T., & Korenaga, J. (2008). Subsidence of normal oceanic lithosphere, apparent thermal expansivity, and seafloor flattening. *Earth and Planetary Science Letters*, *268*(1–2), 41–51. https://doi.org/10.1016/j.epsl.2007.12.022
Korja, T. (2007). How is the European lithosphere imaged by magnetotellurics? *Surveys in Geophysics*, *28*(2–3), 239–272. https://doi.org/10.1007/s10712-007-9024-9
Kumar, P., & Kawakatsu, H. (2011). Imaging the seismic lithosphere-asthenosphere boundary of the oceanic plate. *Geochemistry, Geophysics, Geosystems*, *12*, Q01006. https://doi.org/10.1029/2010GC003358
Kumar, P., Kind, R., Hanka, W., Wylegalla, K., Reigber, C., Yuan, X., et al. (2005). The lithosphere-asthenosphere boundary in the North-West Atlantic region. *Earth and Planetary Science Letters*, *236*(1–2), 249–257. https://doi.org/10.1016/j.epsl.2005.05.029
Kumar, P., Yuan, X., Kind, R., & Kosarev, G. (2005). The lithosphere-asthenosphere boundary in the Tien Shan-Karakoram region from *S* receiver functions: Evidence for continental subduction. *Geophysical Research Letters*, *32*, L07305. https://doi.org/10.1029/2004GL022291
Kumar, P., Yuan, X. H., Kumar, M. R., Kind, R., Li, X. Q., & Chadha, R. K. (2007). The rapid drift of the Indian tectonic plate. *Nature*, *449*(7164), 894–897. https://doi.org/10.1038/nature06214
Landuyt, W., & Bercovici, D. (2009). Variations in planetary convection via the effect of climate on damage. *Earth and Planetary Science Letters*, *277*(1–2), 29–37. https://doi.org/10.1016/j.epsl.2008.09.034
Laske, G., Masters, G., Ma, Z., & Pasyanos, M. (2013). Update on CRUST1.0—A 1-degree global model of Earth's crust. *Geophysical Research Abstracts*.
Lavayssiere, A., Rychert, C., Harmon, N., Keir, D., Hammond, J. O. S., Kendall, J. M., et al. (2018). Imaging lithospheric discontinuities beneath the northern East African Rift using *S*-to-*P* receiver functions. *Geochemistry, Geophysics, Geosystems*, *19*, 4048–4062. https://doi.org/10.1029/2018GC007463
Lee, C. T. A., Luffi, P., & Chin, E. J. (2011). Building and destroying continental mantle. *Annual Review of Earth and Planetary Sciences*, *39*(39), 59–90. https://doi.org/10.1146/Annurev-Earth-040610-133505
Lehmann, I. (1961). *S* and the structure of the upper mantle. *Geophysical Journal of the Royal Astronomical Society*, *4*(SO), 124–138. https://doi.org/10.1111/j.1365-246X.1961.tb06808.x
Lehmann, I. (1964). On the velocity of *P* in the upper mantle. *Bulletin of the Seismological Society of America*, *54*(4), 1097–1103.
Lekic, V., & Fischer, K. M. (2017). Interpreting spatially stacked *Sp* receiver functions. *Geophysical Journal International*, *210*(2), 874–886. https://doi.org/10.1093/gji/ggx206
Lenardic, A., & Kaula, W. M. (1994). Self-lubricated mantle convection—Two-dimensional models. *Geophysical Research Letters*, *21*(16), 1707–1710. https://doi.org/10.1029/94GL01464
Levitt, D. A., & Sandwell, D. T. (1995). Lithospheric bending at subduction zones based on depth soundings and satellite gravity. *Journal of Geophysical Research*, *100*(B1), 379–400. https://doi.org/10.1029/94JB02468

Li, A. (2003). Shear velocity structure and azimuthal anisotropy beneath eastern North America from Rayleigh wave inversion. *Journal of Geophysical Research*, *108*(B8). https://doi.org/10.1029/2002JB002259
Li, X., Kind, R., Priestley, K., Sobolev, S. V., Tilmann, F., Yuan, X., & Weber, M. (2000). Mapping the Hawaiian plume conduit with converted seismic waves. *Nature*, *405*(6789), 938–941. https://doi.org/10.1038/35016054
Li, X. Q., Kind, R., Yuan, X. H., Wolbern, I., & Hanka, W. (2004). Rejuvenation of the lithosphere by the Hawaiian plume. *Nature*, *427*(6977), 827–829.
Lin, P., Gaherty, J. B., Jin, G., Collins, J., Lizarralde, D., Evans, R. L., & Hirth, G. (2016). High-resolution seismic constraints on flow dynamics in the ocean asthenosphere. *Nature*, *535*, 538–541. https://doi.org/10.1038/nature18012
Liu, L. J., & Hasterok, D. (2016). High-resolution lithosphere viscosity and dynamics revealed by magnetotelluric imaging. *Science*, *353*(6307), 1515–1518. https://doi.org/10.1126/science.aaf6542
Lizarralde, D., Chave, A., Hirth, G., & Schultz, A. (1995). Northeastern Pacific mantle conductivity profile from long-period magnetotelluric sounding using Hawaii-to-California submarine cable data. *Journal of Geophysical Research*, *100*(B9), 17,837–17,854. https://doi.org/10.1029/95JB01244
Lodge, A., & Helffrich, G. (2006). Depleted swell root beneath the Cape Verde Islands. *Geology*, *34*(6), 449–452. https://doi.org/10.1130/g22030.1
Maggi, A., Debayle, E., Priestley, K., & Barruol, G. (2006). Azimuthal anisotropy of the Pacific region. *Earth and Planetary Science Letters*, *250*(1–2), 53–71. https://doi.org/10.1016/J.Epsl.2006.07.010
Mancinelli, N. J., Fischer, K. M., & Dalton, C. A. (2017). How sharp is the cratonic lithosphere-asthenosphere transition? *Geophysical Research Letters*, *44*, 10,189–10,197. https://doi.org/10.1002/2017GL074518
Mareschal, J. C., & Jaupart, C. (2004). Variations of surface heat flow and lithospheric thermal structure. beneath the North American craton. *Earth and Planetary Science Letters*, *223*(1–2), 65–77. https://doi.org/10.1016/j.epsl.2004.04.002
Mckenzie, D. (1967). Some remarks on heat flow and gravity anomalies. *Journal of Geophysical Research*, *72*(24), 6261–6273. https://doi.org/10.1029/JZ072i024p06261
Mckenzie, D. (1984). The generation and compaction of partially molten rock. *Journal of Petrology*, *25*(3), 713–765. https://doi.org/10.1093/petrology/25.3.713
Mehouachi, F., & Singh, S. (2018). Water-rich sublithospheric melt channel in the equatorial Atlantic Ocean. *Nature Geoscience*, *11*, 65–69. https://doi.org/10.1038/s41561-017-0034-z
Mei, S., Suzuki, A. M., Kohlstedt, D. L., Dixon, N. A., & Durham, W. B. (2010). Experimental constraints on the strength of the lithospheric mantle. *Journal of Geophysical Research*, *115*, B08204. https://doi.org/10.1029/2009JB006873
Mierdel, K., Keppler, H., Smyth, J. R., & Langenhorst, F. (2007). Water solubility in aluminous orthopyroxene and the origin of Earth's asthenosphere. *Science*, *315*(5810), 364–368. https://doi.org/10.1126/science.1135422
Mitrovica, J. X., & Forte, A. M. (2004). A new inference of mantle viscosity based upon joint inversion of convection and glacial isostatic adjustment data. *Earth and Planetary Science Letters*, *225*(1–2), 177–189. https://doi.org/10.1016/j.epsl.2004.06.005
MONA-LISA Working Group (1997). MONA LISA—Deep seismic investigations of the lithosphere in the southeastern North Sea. *Tectonophysics*, *269*, 1–19. https://doi.org/10.1016/S0040-1951(96)00111-4
Montagner, J. P. (2002). Upper mantle low anisotropy channels below the Pacific Plate. *Earth and Planetary Science Letters*, *202*(2), 263–274. https://doi.org/10.1016/S0012-821x(02)00791-4
Moresi, L., & Solomatov, V. (1998). Mantle convection with a brittle lithosphere: Thoughts on the global tectonic styles of the Earth and Venus. *Geophysical Journal International*, *133*(3), 669–682. https://doi.org/10.1046/j.1365-246X.1998.00521.x
Morgan, J. P. (1987). Melt migration beneath mid-ocean spreading centers. *Geophysical Research Letters*, *14*(12), 1238–1241. https://doi.org/10.1029/GL014i012p01238
Morgan, J. P., Morgan, W. J., Zhang, Y. S., & Smith, W. H. F. (1995). Observational hints for a plume-fed, suboceanic asthenosphere and its role in mantle convection. *Journal of Geophysical Research*, *100*(B7), 12,753–12,767. https://doi.org/10.1029/95JB00041
Morgan, J. P., Parmentier, E. M., & Lin, J. (1987). Mechanisms for the origin of midocean ridge axial topography—Implications for the thermal and mechanical structure of accreting plate boundaries. *Journal of Geophysical Research*, *92*(B12), 12,823–12,836. https://doi.org/10.1029/JB092iB12p12823
Morgan, W. J. (1971). Convection plumes in lower mantle. *Nature*, *230*(5288), 42–43. https://doi.org/10.1038/230042a0
Morozova, E. A., Morozov, I. B., Smithson, S. B., & Solodilov, L. (2000). Lithospheric boundaries and upper mantle heterogeneity beneath Russian Eurasia: Evidence from the DSS profile QUARTZ. *Tectonophysics*, *329*(1–4), 333–344.
Muller, M. R., Jones, A. G., Evans, R. L., Grutter, H. S., Hatton, C., Garcia, X., et al. (2009). Lithospheric structure, evolution and diamond prospectivity of the Rehoboth Terrane and western Kaapvaal Craton, southern Africa: Constraints from broadband magnetotellurics. *Lithos*, *112*, 93–105. https://doi.org/10.1016/j.lithos.2009.06.023
Muller, R. D., Sdrolias, M., Gaina, C., & Roest, W. R. (2008). Age, spreading rates, and spreading asymmetry of the world's ocean crust. *Geochemistry, Geophysics, Geosystems*, *9*, Q04006. https://doi.org/10.1029/2007GC001743
Mulyukova, E., & Bercovici, D. (2019). The generation of plate tectonics from grains to global scales: A brief review. *Tectonics*, *38*, 4058–4076. https://doi.org/10.1029/2018TC005447
Murphy, B. S., & Egbert, G. D. (2019). Synthesizing seemingly contradictory seismic and magnetotelluric observations in the southeastern United States to image physical properties of the lithosphere. *Geochemistry, Geophysics, Geosystems*, *20*, 2606–2625. https://doi.org/10.1029/2019GC008279
Naif, S., Key, K., Constable, S., & Evans, R. L. (2013). Melt-rich channel observed at the lithosphere-asthenosphere boundary. *Nature*, *495*(7441), 356–359. https://doi.org/10.1038/nature11939
Nataf, H., & Ricard, Y. (1996). 3SMAC: an a priori tomographic model of the upper mantle based on geophysical modeling. *Physics of the Earth and Planetary Interiors*, *95*, 101–121.
Natarov, S. I., & Conrad, C. P. (2012). The role of Poiseuille flow in creating depth-variation of asthenospheric shear. *Geophysical Journal International*, *190*(3), 1297–1310. https://doi.org/10.1111/j.1365-246X.2012.05562.x
Nettles, M., & Dziewonski, A. M. (2008). Radially anisotropic shear velocity structure of the upper mantle globally and beneath North America. *Journal of Geophysical Research*, *113*, B02303. https://doi.org/10.1029/2006JB004819
Nishimura, C. E., & Forsyth, D. W. (1989). The anisotropic structure of the upper mantle in the Pacific. *Geophysical Journal International*, *96*, 203–229. https://doi.org/10.1111/j.1365-246X.1989.tb04446.x
Oliver, J., & Isacks, B. (1967). Deep earthquake zones, anomalous structures in the upper mantle, and the lithosphere. *Journal of Geophysical Research*, *72*(16), 4259–4275. https://doi.org/10.1029/JZ072i016p04259

Olugboji, T. M., Park, J., Karato, S., & Shinohara, M. (2016). Nature of the seismic lithosphere-asthenosphere boundary within normal oceanic mantle from high-resolution receiver functions. *Geochemistry, Geophysics, Geosystems*, *17*, 1265–1282. https://doi.org/10.1002/2015GC006214

Oreshin, S., Vinnik, L., Peregoudov, D., & Roecker, S. (2002). Lithosphere and asthenosphere of the Tien Shan imaged by *S* receiver functions. *Geophysical Research Letters*, *29*, 1191. https://doi.org/10.1029/2001GL014441

Parker, R. L., & Oldenburg, D. W. (1973). Thermal model of ocean ridges. *Nature Physical Science*, *242*(122), 137–139. https://doi.org/10.1038/physci242137a0

Parker, R. L., & Whaler, K. A. (1981). Numerical methods for establishing solutions to the inverse problem of electromagnetic induction. *Journal of Geophysical Research*, *86*, 9574–9584.

Parsons, B., & Sclater, J. G. (1977). Analysis of variation of ocean-floor bathymetry and heat-flow with age. *Journal of Geophysical Research*, *82*(5), 803–827. https://doi.org/10.1029/JB082i005p00803

Pasyanos, M. E. (2010). Lithospheric thickness modeled from long-period surface wave dispersion. *Tectonophysics*, *481*(1–4), 38–50. https://doi.org/10.1016/j.tecto.2009.02.023

Pearson, D. G., Carlson, R. W., Shirey, S. B., Boyd, F. R., & Nixon, P. H. (1995). Stabilization of Archean lithospheric mantle—A Re-Os isotope study of peridotite xenoliths from the Kaapvaal Craton. *Earth and Planetary Science Letters*, *134*(3-4), 341–357. https://doi.org/10.1016/0012-821x(95)00125-V

Pedersen, H. A., Fishwick, S., & Snyder, D. B. (2009). A comparison of cratonic roots through consistent analysis of seismic surface waves. *Lithos*, *109*, 81–95. https://doi.org/10.1016/j.lithos.2008.09.016

Phillips, R. J. (1990). Convection-driven tectonics on Venus. *Journal of Geophysical Research, Planets*, *95*(B2), 1301–1316. https://doi.org/10.1029/JB095iB02p01301

Pilet, S., Abe, N., Rochat, L., Kaczmarek, M. A., Hirano, N., Machida, S., et al. (2016). Pre-subduction metasomatic enrichment of the oceanic lithosphere induced by plate flexure. *Nature Geoscience*, *9*(12), 898–903. https://doi.org/10.1038/Ngeo2825

Plank, T., & Forsyth, D. W. (2016). Thermal structure and melting conditions in the mantle beneath the Basin and Range province from seismology and petrology. *Geochemistry, Geophysics, Geosystems*, *17*, 1312–1338. https://doi.org/10.1002/2015GC006205

Pollack, H. N., Hurter, S. J., & Johnson, J. R. (1993). Heat-flow from the Earths interior—Analysis of the global data set. *Reviews of Geophysics*, *31*(3), 267–280. https://doi.org/10.1029/93RG01249

Praus, O., Pecova, J., Petr, V., Babuska, V., & Plomerova, J. (1990). Magnetotelluric and seismological determination of the lithosphere asthenosphere transition in central-Europe. *Physics of the Earth and Planetary Interiors*, *60*(1-3), 212–228. https://doi.org/10.1016/0031-9201(90)90262-V

Press, F. (1959). Some implications on mantle and crustal structure from G waves and Love waves. *Journal of Geophysical Research*, *64*(5), 565–568. https://doi.org/10.1029/JZ064i005p00565

Priestley, K., & McKenzie, D. (2006). The thermal structure of the lithosphere from shear wave velocities. *Earth and Planetary Science Letters*, *244*(1–2), 285–301. https://doi.org/10.1016/J.Epsl.2006.01.008

Rader, E., Emry, E., Schmerr, N., Frost, D., Cheng, C., Menard, J., et al. (2015). Characterization and petrological constraints of the midlithospheric discontinuity. *Geochemistry, Geophysics, Geosystems*, *16*, 3484–3504. https://doi.org/10.1002/2015GC005943

Reeves, Z., Lekic, V., Schmerr, N., Kohler, M., & Weeraratne, D. (2015). Lithospheric structure across the California Continental Borderland from receiver functions. *Geochemistry, Geophysics, Geosystems*, *16*, 246–266. https://doi.org/10.1002/2014GC005617

Regenauer-Lieb, K., Yuen, D. A., & Branlund, J. (2001). The initiation of subduction: Criticality by addition of water? *Science*, *294*(5542), 578–580. https://doi.org/10.1126/science.1063891

Richards, M. A., Yang, W. S., Baumgardner, J. R., & Bunge, H. P. (2001). Role of a low-viscosity zone in stabilizing plate tectonics: Implications for comparative terrestrial planetology. *Geochemistry, Geophysics, Geosystems*, *2*, 1026. https://doi.org/10.1029/2000GC000115

Richter, F. M. (1973). Convection and large-scale circulation of mantle. *Journal of Geophysical Research*, *78*(35), 8735–8745.

Ritzwoller, M. H., Shapiro, N. M., & Zhong, S. J. (2004). Cooling history of the Pacific lithosphere. *Earth and Planetary Science Letters*, *226*(1–2), 69–84. https://doi.org/10.1016/J.Epsl.2004.07.032

Rudnick, R. L., & Nyblade, A. A. (1999). The thickness and heat production of Archean lithosphere: constraints from xenolith thermobarometry and surface heat flow (Vol. Special Publication 6). The Geochemical Society.

Russell, J. B., Gaherty, J. B., Lin, P. Y. P., Lizarralde, D., Collins, J. A., Hirth, G., & Evans, R. L. (2019). High-resolution constraints on Pacific upper mantle petrofabric inferred from surface-wave anisotropy. *Journal of Geophysical Research: Solid Earth*, *124*, 631–657. https://doi.org/10.1029/2018JB016598

Ryberg, T., Wenzel, F., Mechie, J., Egorkin, A., Fuchs, K., & Solodilov, L. (1996). Two-dimensional velocity structure beneath northern Eurasia derived from the super long-range seismic profile Quartz. *Bulletin of the Seismological Society of America*, *86*(3), 857–867.

Rychert, C., Harmon, N., Constable, S., Kendall, J., Tharimena, S., Wang, S., et al. (2019). A dynamic lithosphere-asthenosphere boundary dictated by variations in melt generation and migration: Results from the PI-LAB Experiment in the Equatorial Mid Atlantic American Geophysical Union, San Francisco, CA, USA.

Rychert, C. A., Fischer, K. M., & Rondenay, S. (2005). A sharp lithosphere-asthenosphere boundary imaged beneath eastern North America. *Nature*, *436*(7050), 542–545. https://doi.org/10.1038/nature03904

Rychert, C. A., Hammond, J. O. S., Harmon, N., Kendall, J. M., Keir, D., Ebinger, C., et al. (2012). Volcanism in the Afar Rift sustained by decompression melting with minimal plume influence. *Nature Geoscience*, *5*(6), 406–409. https://doi.org/10.1038/Ngeo1455

Rychert, C. A., & Harmon, N. (2017). Constraints on the anisotropic contributions to velocity discontinuities at ~60 km depth beneath the Pacific. *Geochemistry, Geophysics, Geosystems*, *18*, 2855–2871. https://doi.org/10.1002/2017GC006850

Rychert, C. A., & Harmon, N. (2018). Predictions and observations for the oceanic lithosphere from S-to-P receiver functions and *SS* precursors. *Geophysical Research Letters*, *45*, 5398–5406. https://doi.org/10.1029/2018GL077675

Rychert, C. A., Harmon, N., & Armitage, J. (2018). Seismic imaging of thickened lithosphere resulting from plume pulsing beneath Iceland. *Geochemistry, Geophysics, Geosystems*, *19*, 1789–1799. https://doi.org/10.1029/2018GC007501

Rychert, C. A., Harmon, N., & Ebinger, C. (2014). Receiver function imaging of lithospheric structure and the onset of melting beneath the Galapagos Archipelago. *Earth and Planetary Science Letters*, *388*, 156–165. https://doi.org/10.1016/J.Epsl.2013.11.027

Rychert, C. A., Harmon, N., & Schmerr, N. (2014). Synthetic waveform modelling of *SS* precursors from anisotropic upper-mantle discontinuities. *Geophysical Journal International*, *196*(3), 1694–1705. https://doi.org/10.1093/gji/ggt474

Rychert, C. A., Harmon, N., & Tharimena, S. (2018a). Scattered wave imaging of the oceanic plate in Cascadia. *Science Advances*, *4*(2), eaao1908. https://doi.org/10.1126/sciadv.aao1908

Rychert, C. A., Harmon, N., & Tharimena, S. (2018b). Seismic imaging of the base of the ocean plates. In H. Yuan (Ed.), *Lithospheric discontinuities*, *AGU Monographs* (pp. 71–87). Hoboken, NJ, and Washington, DC: John Wiley & Sons, Inc., and American Geophysical Union.

Rychert, C. A., Laske, G., Harmon, N., & Shearer, P. M. (2013). Seismic imaging of melt in a displaced Hawaiian plume. *Nature Geoscience*, *6*(8), 657–660. https://doi.org/10.1038/Ngeo1878

Rychert, C. A., Rondenay, S., & Fischer, K. M. (2007). *P*-to-*S* and *S*-to-*P* imaging of a sharp lithosphere-asthenosphere boundary beneath eastern North America. *Journal of Geophysical Research*, *112*, B08314. https://doi.org/10.1029/2006JB004619

Rychert, C. A., Schmerr, N., & Harmon, N. (2012). The Pacific lithosphere-asthenosphere boundary: Seismic imaging and anisotropic constraints from *SS* waveforms. *Geochemistry, Geophysics, Geosystems*, *13*, Q0AK10. https://doi.org/10.1029/2012GC004194

Rychert, C. A., & Shearer, P. M. (2009). A global view of the lithosphere-asthenosphere boundary. *Science*, *324*(5926), 495–498. https://doi.org/10.1126/science.1169754

Rychert, C. A., & Shearer, P. M. (2011). Imaging the lithosphere-asthenosphere boundary beneath the Pacific using *SS* waveform modeling. *Journal of Geophysical Research*, *116*, B07307. https://doi.org/10.1029/2010JB008070

Rychert, C. A., Shearer, P. M., & Fischer, K. M. (2010). Scattered wave imaging of the lithosphere-asthenosphere boundary. *Lithos*, *120*, 173–185. https://doi.org/10.1016/j.lithos.2009.12.006

Sacks, I. S., & Snoke, J. A. (1977). Use of converted phases to infer depth of lithosphere-asthenosphere boundary beneath South-America. *Journal of Geophysical Research*, *82*(14), 2011–2017. https://doi.org/10.1029/JB082i014p02011

Sacks, I. S., Snoke, J. A., & Husebye, E. S. (1979). Lithosphere thickness beneath the Baltic Shield. *Tectonophysics*, *56*(1–2), 101–110. https://doi.org/10.1016/0040-1951(79)90016-7

Sakamaki, T., Suzuki, A., Ohtani, E., Terasaki, H., Urakawa, S., Katayama, Y., et al. (2013). Ponded melt at the boundary between the lithosphere and asthenosphere. *Nature Geoscience*, *6*(12), 1041–1044. https://doi.org/10.1038/Ngeo1982

Sandwell, D., & Fialko, Y. (2004). Warping and cracking of the Pacific plate by thermal contraction. *Journal of Geophysical Research*, *109*, B10411. https://doi.org/10.1029/2004JB003091

Sarafian, E., Evans, R. L., Collins, J. A., Elsenbeck, J., Gaetani, G. A., Gaherty, J. B., et al. (2015). The electrical structure of the central Pacific upper mantle constrained by the NoMelt experiment. *Geochemistry, Geophysics, Geosystems*, *16*, 1115–1132. https://doi.org/10.1002/2014GC005709

Schmerr, N. (2012). The Gutenberg discontinuity: Melt at the lithosphere-asthenosphere boundary. *Science*, *335*(6075), 1480–1483. https://doi.org/10.1126/science.1215433

Schultz, A., Kurtz, R. D., Chave, A. D., & Jones, A. G. (1993). Conductivity discontinuities in the upper-mantle beneath a stable craton. *Geophysical Research Letters*, *20*(24), 2941–2944. https://doi.org/10.1029/93GL02833

Selway, K., Ford, H., & Kelemen, P. (2015). The seismic mid-lithosphere discontinuity. *Earth and Planetary Science Letters*, *414*, 45–57. https://doi.org/10.1016/j.epsl.2014.12.029

Selway, K., & O'Donnell, J. P. (2019). A small, unextractable melt fraction as the cause for the low velocity zone. *Earth and Planetary Science Letters*, *517*, 117–124. https://doi.org/10.1016/j.epsl.2019.04.012

Shearer, P. M. (1991). Constraints on upper mantle discontinuities from observations of long-period reflected and converted phases. *Journal of Geophysical Research*, *96*(B11), 18,147–18,182. https://doi.org/10.1029/91JB01592

Shintaku, N., Forsyth, D. W., Hajewski, C. J., & Weeraratne, D. S. (2014). *Pn* anisotropy in Mesozoic western Pacific lithosphere. *Journal of Geophysical Research: Solid Earth*, *119*, 3050–3063. https://doi.org/10.1002/2013JB010534

Shirey, S. B., & Richardson, S. H. (2011). Start of the Wilson cycle at 3 Ga shown by diamonds from subcontinental mantle. *Science*, *333*(6041), 434–436. https://doi.org/10.1126/science.1206275

Shito, A., Suetsugu, D., & Furumura, T. (2015). Evolution of the oceanic lithosphere inferred from *Po*/*So* waves traveling in the Philippine Sea Plate. *Journal of Geophysical Research: Solid Earth*, *120*, 5238–5248. https://doi.org/10.1002/2014JB011814

Shito, A., Suetsugu, D., Furumura, T., Sugioka, H., & Ito, A. (2013). Small-scale heterogeneities in the oceanic lithosphere inferred from guided waves. *Geophysical Research Letters*, *40*, 1708–1712. https://doi.org/10.1002/grl.50330

Sim, S. J., Spiegelman, M., Stegman, D. R., & Wilson, C. (2020). The influence of spreading rate and permeability on melt focusing beneath mid-ocean ridges. *Physics of the Earth and Planetary Interiors*, *304*, 106486. https://doi.org/10.1016/j.pepi.2020.106486

Smirnov, M. Y., & Pedersen, L. B. (2009). Magnetotelluric measurements across the Sorgenfrei-Tornquist Zone in southern Sweden and Denmark. *Geophysical Journal International*, *176*(2), 443–456. https://doi.org/10.1111/j.1365-246X.2008.03987.x

Sparks, D., & Parmentier, E. (1991). Melt extraction from the mantle beneath spreading centers. *Earth and Planetary Science Letters*, *105*(4), 368–377. https://doi.org/10.1016/0012-821x(91)90178-k

Spiegelman, M., & Mckenzie, D. (1987). Simple 2-D models for melt extraction at midocean ridges and island arcs. *Earth and Planetary Science Letters*, *83*(1–4), 137–152. https://doi.org/10.1016/0012-821x(87)90057-4

Steer, D. N., Knapp, J. H., & Brown, L. D. (1998). Super-deep reflection profiling: Exploring the continental mantle lid. *Tectonophysics*, *286*(1–4), 111–121. https://doi.org/10.1016/S0040-1951(97)00258-8

Steer, D. N., Knapp, J. H., Brown, L. D., Echtler, H. P., Brown, D. L., & Berzin, R. (1998). Deep structure of the continental lithosphere in an unextended orogen: An explosive-source seismic reflection profile in the Urals (Urals Seismic Experiment and Integrated Studies (URSEIS 1995)). *Tectonics*, *17*(2), 143–157. https://doi.org/10.1029/97TC03056

Stein, C. A., & Stein, S. (1992). A model for the global variation in oceanic depth and heat-flow with lithospheric age. *Nature*, *359*(6391), 123–129. https://doi.org/10.1038/359123a0

Steinberger, B., & Becker, T. (2018). A comparison of lithospheric thickness models. *Tectonophysics*, *746*, 335–338. https://doi.org/10.1016/j.tecto.2016.08.001

Stern, T. A., Henrys, S. A., Okaya, D., Louie, J. N., Savage, M. K., Lamb, S., et al. (2015). A seismic reflection image for the base of a tectonic plate. *Nature*, *518*(7537), 85–88. https://doi.org/10.1038/nature14146

Takeo, A., Kawakatsu, H., Isse, T., Nishida, K., Shiobara, H., Sugioka, H., et al. (2018). In situ characterization of the lithosphere-asthenosphere system beneath NW Pacific Ocean via broadband dispersion survey with two OBS arrays. *Geochemistry, Geophysics, Geosystems*, *19*, 3529–3539. https://doi.org/10.1029/2018GC007588

Takeo, A., Kawakatsu, H., Isse, T., Nishida, K., Sugioka, H., Ito, A., et al. (2016). Seismic azimuthal anisotropy in the oceanic lithosphere and asthenosphere from broadband surface wave analysis of OBS array records at 60 Ma seafloor. *Journal of Geophysical Research: Solid Earth*, *121*, 1927–1947. https://doi.org/10.1002/2015JB012429

Takeo, A., Nishida, K., Isse, T., Kawakatsu, H., Shiobara, H., Sugioka, H., & Kanazawa, T. (2013). Radially anisotropic structure beneath the Shikoku Basin from broadband surface wave analysis of ocean bottom seismometer records. *Journal of Geophysical Research: Solid Earth*, *118*, 2878–2892. https://doi.org/10.1002/jgrb.50219

Takeuchi, H., Press, F., & Kobayashi, N. (1959). Rayleigh-wave evidence for the low-velocity zone in the mantle. *Bulletin of the Seismological Society of America*, *49*(4), 355–364.
Tan, Y., & Helmberger, D. V. (2007). Trans-Pacific upper mantle shear velocity structure. *Journal of Geophysical Research*, *112*, B08301. https://doi.org/10.1029/2006JB004853
Tesauro, M., Audet, P., Kaban, M. K., Burgmann, R., & Cloetingh, S. (2012). The effective elastic thickness of the continental lithosphere: Comparison between rheological and inverse approaches. *Geochemistry, Geophysics, Geosystems*, *13*, Q09001. https://doi.org/10.1029/2012GC004162
Tharimena, S., Rychert, C., & Harmon, N. (2017). A unified continental thickness from seismology and diamonds suggests a melt-defined plate. *Science*, *357*(6351), 580–583. https://doi.org/10.1126/science.aan0741
Tharimena, S., Rychert, C., Harmon, N., & White, P. (2017). Imaging Pacific lithosphere seismic discontinuities—Insights from *SS* precursor modeling. *Journal of Geophysical Research: Solid Earth*, *122*, 2131–2152. https://doi.org/10.1002/2016JB013526
Thybo, H. (2006). The heterogeneous upper mantle low velocity zone. *Tectonophysics*, *416*(1–4), 53–79. https://doi.org/10.1016/j.tecto.2005.11.021
Thybo, H., & Perchuc, E. (1997). The seismic 8° discontinuity and partial melting in continental mantle. *Science*, *275*(5306), 1626–1629. https://doi.org/10.1126/science.275.5306.1626
Till, C. B., Elkins-Tanton, L. T., & Fischer, K. M. (2010). A mechanism for low-extent melts at the lithosphere-asthenosphere boundary. *Geochemistry, Geophysics, Geosystems*, *11*, Q10015. https://doi.org/10.1029/2010GC003234
Toksoz, M. N., & Anderson, D. L. (1966). Phase velocities of long-period surface waves and structure of the upper mantle. *Journal of Geophysical Research*, *71*(6), 1649–1658. https://doi.org/10.1029/JZ071i006p01649
Toksoz, M. N., Chinnery, M. A., & Anderson, D. L. (1967). Inhomogeneities in the Earth's mantle. *Geophysical Journal International*, *13*, 31–59. https://doi.org/10.1111/j.1365-246x.1967.tb02145.x
Tonegawa, T., & Helffrich, G. (2012). Basal reflector under the Philippine Sea Plate. *Geophysical Journal International*, *189*, 659–668. https://doi.org/10.1111/j.1365-246X.2012.05386.x
Toomey, D. R., Jousselin, D., Dunn, R. A., Wilcock, W. S. D., & Detrick, R. S. (2007). Skew of mantle upwelling beneath the East Pacific Rise governs segmentation. *Nature*, *446*(7134), 409–414. https://doi.org/10.1038/nature05679
Toomey, D. R., Wilcock, W. S., Solomon, S. C., Hammond, W. C., & Orcutt, J. A. (1998). Mantle seismic structure beneath the MELT region of the East Pacific Rise from *P* and *S* wave tomography. *Science*, *280*(5367), 1224–1227. https://doi.org/10.1126/science.280.5367.1224
Tozer, D. C. (1985). Heat-transfer and planetary evolution. *Geophysical Surveys*, *7*(3), 213–247. https://doi.org/10.1007/Bf01449539
Turcotte, D., & Schubert, G. (2002). *Geodynamics*. Cambridge, UK: Cambridge University Press.
Turner, A. J., Katz, R. F., Behn, M. D., & Keller, T. (2017). Magmatic focusing to mid-ocean ridges: The role of grain-size variability and non-Newtonian viscosity. *Geochemistry, Geophysics, Geosystems*, *18*, 4342–4355. https://doi.org/10.1002/2017GC007048
VanderBeek, B. P., & Toomey, D. R. (2017). Shallow mantle anisotropy beneath the Juan de Fuca Plate. *Geophysical Research Letters*, *44*, 11,382–11,389. https://doi.org/10.1002/2017GL074769
Vesanen, E., Nurmia, M., & Porkka, M. T. (1959). New Evidence for the existence of Gutenberg's asthenosphere channel. *Geophysica*.
Vine, F. J., & Matthews, D. H. (1963). Magnetic anomalies over oceanic ridges. *Nature*, *4897*, 947–949. https://doi.org/10.1038/199947a0
Vinnik, L., & Farra, V. (2002). Subcratonic low-velocity layer and flood basalts. *Geophysical Research Letters*, *29*(4), 1049. https://doi.org/10.1029/2001GL014064
Vinnik, L., Silveira, G., Kiselev, S., Farra, V., Weber, M., & Stutzmann, E. (2012). Cape Verde hotspot from the upper crust to the top of the lower mantle. *Earth and Planetary Science Letters*, *319*, 259–268. https://doi.org/10.1016/j.epsl.2011.12.017
Vinnik, L. P., Foulger, G. R., & Du, Z. (2005). Seismic boundaries in the mantle beneath Iceland: A new constraint on temperature. *Geophysical Journal International*, *160*(2), 533–538. https://doi.org/10.1111/j.1365-246X.2005.02529.x
Vozar, J., Jones, A. G., Fullea, J., Agius, M. R., Lebedev, S., Le Pape, F., & Wei, W. B. (2014). Integrated geophysical-petrological modeling of lithosphere-asthenosphere boundary in central Tibet using electromagnetic and seismic data. *Geochemistry, Geophysics, Geosystems*, *15*, 3965–3988. https://doi.org/10.1002/2014GC005365
Wang, S., Constable, S., Rychert, C., & Harmon, N. (2020). A lithosphere-asthenosphere boundary and partial melt estimated using marine magnetotelluric data at the central Middle Atlantic Ridge. *Geochemistry, Geophysics, Geosystems*, *21*, e2020GC009177. https://doi.org/10.1029/2020GC009177
Wannamaker, P. E., Hasterok, D. P., Johnston, J. M., Stodt, J. A., Hall, D. B., Sodergren, T. L., et al. (2008). Lithospheric dismemberment and magmatic processes of the Great Basin-Colorado Plateau transition, Utah, implied from magnetotellurics. *Geochemistry, Geophysics, Geosystems*, *9*, Q05019. https://doi.org/10.1029/2007GC001886
Watts, A. B. (2001). *Isostasy and flexure of the lithosphere* (1st ed.). Cambridge, UK: Cambridge University Press.
Watts, A. B., Zhong, S. J., & Hunter, J. (2013). The behavior of the lithosphere on seismic to geologic timescales. *Annual Review of Earth and Planetary Sciences*, *41*(1), 443–468. https://doi.org/10.1146/annurev-earth-042711-105457
Wei, W., Ye, G., Jin, S., Deng, M., Jing, J., Peng, Z., et al. (2008). Geoelectric structure of lithosphere beneath eastern North China: Features of thinned lithosphere from magnetotelluric soundings. *Earth Science Frontiers*, *15*(4), 204–216. https://doi.org/10.1016/S1872-5791(08)60055-X
Wilson, J. T. (1965). Convection currents and continental drift. *Philosophical Transactions of the Royal Society A*, *258*(19), 145–167.
Worzewski, T., Jegen, M., Kopp, H., Brasse, H., & Castillo, W. T. (2011). Magnetotelluric image of the fluid cycle in the Costa Rican subduction zone. *Nature Geoscience*, *4*(2), 108–111. https://doi.org/10.1038/Ngeo1041
Yamauchi, H., & Takei, Y. (2016). Polycrystal anelasticity at near-solidus temperatures. *Journal of Geophysical Research: Solid Earth*, *121*, 7790–7820. https://doi.org/10.1002/2016JB013316
Yoshino, T., Matsuzaki, T., Yamashita, S., & Katsura, T. (2006). Hydrous olivine unable to account for conductivity anomaly at the top of the asthenosphere. *Nature*, *443*, 973–976. https://doi.org/10.1038/nature05223
Yoshizawa, K. (2014). Radially anisotropic 3-D shear wave structure of the Australian lithosphere and asthenosphere from multi-mode surface waves. *Physics of the Earth and Planetary Interiors*, *235*, 33–48. https://doi.org/10.1016/j.pepi.2014.07.008
Yuan, H., & Romanowicz, B. (2010). Lithospheric layering in the North American craton. *Nature*, *466*. https://doi.org/10.1038/nature09332
Yuan, H., & Romanowicz, B. (2018). Introduction—Lithospheric discontinuities. In H. Yuan, & B. Romanowicz (Eds.), *Lithospheric discontinuities*, *AGU Monograph* (Vol. 239, pp. 1–4). Hoboken, NJ, and Washington, DC: John Wiley & Sons, Inc., and American Geophysical Union.
Zhao, W. J., Kumar, P., Mechie, J., Kind, R., Meissner, R., Wu, Z. H., et al. (2011). Tibetan plate overriding the Asian plate in central and northern Tibet. *Nature Geoscience*, *4*(12), 870–873. https://doi.org/10.1038/Ngeo1309

Zhdanov, M. S., Smith, R. B., Gribenko, A., Cuma, M., & Green, M. (2011). Three-dimensional inversion of large-scale EarthScope magnetotelluric data based on the integral equation method: Geoelectrical imaging of the Yellowstone conductive mantle plume. *Geophysical Research Letters*, *38*, L08307. https://doi.org/10.1029/2011GL046953

Zhong, S. J., & Watts, A. B. (2013). Lithospheric deformation induced by loading of the Hawaiian Islands and its implications for mantle rheology. *Journal of Geophysical Research: Solid Earth*, *118*, 6025–6048. https://doi.org/10.1002/2013JB010408

Zhong, S. J., Zuber, M. T., Moresi, L., & Gurnis, M. (2000). Role of temperature-dependent viscosity and surface plates in spherical shell models of mantle convection. *Journal of Geophysical Research*, *105*(B5), 11,063–11,082. https://doi.org/10.1029/2000JB900003

Further Reading: 10 Papers in the Last 5 Years

Harmon, N., Rychert, C., Constable, S., Kendall, J., Tharimena, S., Bogiatzis, P., & Agius, M. (2020). Evolution of the oceanic Lithosphere in the equatorial Atlantic from Rayleigh wave tomography, evidence for small-scale convection from the PI-LAB experiment. *Geochemistry, Geophysics, Geosystems*, *21*, e2020GC009174. https://doi.org/10.1029/2020GC009174

Lin, P., Gaherty, J. B., Jin, G., Collins, J., Lizarralde, D., Evans, R. L., & Hirth, G. (2016). High-resolution seismic constraints on flow dynamics in the ocean asthenosphere, *Nature*, *535*, 538–541. https://doi.org/10.1038/nature18012

Liu, L., & Hasterok, D. (2016). High-resolution lithosphere viscosity and dynamics revealed by magnetotelluric imaging. *Science*, *353*(6307), 1515–1519. https://doi.org/10.1126/science.aaf6542

Mehouachi, F. & Singh, S. (2018). Water-rich sublithospheric melt channel in the equatorial Atlantic Ocean, *Nature Geoscience*, *11*, 65–69. https://doi.org/10.1038/s41561-017-0034-z

Rychert, C. A., Harmon, N., & Tharimena, S. (2018a). Scattered wave imaging of the oceanic plate in Cascadia, *Science Advances*, *4*, eaao1908. https://doi.org/10.1126/sciadv.aao1908

Sim, S. J., Spiegelman, M., Stegman, D. R., & Wilson, C. (2020). The influence of spreading rate and permeability on melt focusing beneath mid-ocean ridges, *Physics of the Earth and Planetary Interiors*, *304*. https://doi.org/10.1016/j.pepi.2020.106486

Tharimena, S., Rychert, C. A., & Harmon, N. (2017a). A unified continental thickness from seismology and diamonds suggests a melt-defined plate, *Science*, *357*, 580–583. https://doi.org/10.1126/science.aan0741

Tharimena, S., Rychert, C. A., Harmon, N., & White, P. (2017b). Imaging Pacific lithosphere seismic discontinuities: Insights from *SS* precursor modeling, *Journal of Geophysical Research*, *122*, 2131-2152. https://doi.org/10.1002/2016JB013526

Wang, S., Constable, S., Rychert, C., & Harmon, N. (2020). A lithosphere-asthenosphere boundary and partial melt estimated using marine magnetotelluric data at the central Middle Atlantic Ridge. https://doi.org/10.1029/2020GC009177

Yuan, H & Romanowicz, B., eds., (2018). *Lithospheric discontinuities*, AGU Monographs, Washington DC. https://doi.org/10.1002/9781119249740.ch4